

ANALYSIS OF GEOLOGIC STRUCTURE
FOR OPEN PIT SLOPE DESIGN

by

Richard Drake Call

A Dissertation Submitted to the Faculty of the
DEPARTMENT OF MINING AND GEOLOGICAL ENGINEERING

In Partial Fulfillment of the Requirements
For the Degree of

DOCTOR OF PHILOSOPHY
WITH A MAJOR IN GEOLOGICAL ENGINEERING

In the Graduate College

THE UNIVERSITY OF ARIZONA

1 9 7 2

STATEMENT BY AUTHOR

This dissertation has been submitted in partial fulfillment of requirements for an advanced degree at The University of Arizona and is deposited in the University Library to be made available to borrowers under rules of the Library.

Brief quotations from this dissertation are allowable without special permission, provided that accurate acknowledgment of source is made. Requests for permission for extended quotation from or reproduction of this manuscript in whole or in part may be granted by the head of the major department or the Dean of the Graduate College when in his judgment the proposed use of the material is in the interests of scholarship. In all other instances, however, permission must be obtained from the author.

SIGNED: _____

ACKNOWLEDGMENTS

The author would like to express his appreciation to the management of MIFERMA for the opportunity to conduct this study. A thorough analysis of stability conditions early in the life of an open pit, before difficulties are encountered, is the exception rather than the rule in current mining practice. Jean Audibert, General Manager, and Auguste Nicolas, Assistant to the General Manager, are to be commended for their progressive approach in authorizing this study. The cooperation of the entire MIFERMA organization, without which the study could not have been accomplished, is greatly appreciated.

The author was assisted most ably in field studies by Pierre Jaugey and in the computer data processing by Francois Reeves.

Direct shear testing was performed by Dr. H. Kutter at the Interdepartmental Rock Mechanics Laboratory, Imperial College, London.

The physical testing of the core samples was performed by Dr. G. Herget at the Elliot Lake Research Laboratory, Mining Research Centre of the Canadian Department of Energy, Mines and Resources.

The finite element analysis was performed by Dr. Y. S. Yu, Dr. D. F. Coates, and Mr. N. A. Toews at the Mining Research Centre in Ottawa, Canada.

The petrographic analysis was performed by Dr. G. Bronner and Mr. J. P. Lecorche at the Laboratoires des Science de la Terre, St. Jerome, Marseille.

Mr. Henri Reibell, formerly Head of the Mining Department, MIFERMA, and Dr. Donald F. Coates, Head of the Canadian Mining Research Centre, are due special acknowledgment for their invaluable assistance and advice.

The author is indebted to Dr. Willard Lacy, Head of the Department of Mining and Geological Engineering, Dr. John Abel, the dissertation director, and Dr. William Peters for their advice, assistance, patience and support during the innumerable delays in the preparation of this dissertation.

TABLE OF CONTENTS

	Page
LIST OF ILLUSTRATIONS	viii
LIST OF TABLES	xii
ABSTRACT	xiii
1. INTRODUCTION	1
PART I. PIT SLOPE DESIGN AND GEOLOGIC PARAMETERS	3
2. PIT SLOPE DESIGN	4
Economic Aspects of Pit Slope Angles	4
Slope Failure	5
Uncertainty in Slope Design	10
Slope Monitoring	11
Artificial Support	14
Stability Analysis	18
Classification of Slides	18
Methods of Analysis	23
Organization of a Pit Slope Design Study	27
3. MECHANICAL PROPERTIES OF FRACTURES	30
Geologic Structural Features	31
Properties of Individual Fractures	33
Geometric Parameters	33
Compositional Parameters	38
Properties of Fracture Sets	39
Extent	39
Continuity	40
Mean Attitude	40
Dispersion	41
Spacing	42
Properties of Rock Mass	42
Fabric	42
Unit Rock Block	45
Rock Quality Designation	45
Joint Breakage	46

TABLE OF CONTENTS--Continued

	Page
PART II. TAZADIT PIT SLOPE STUDY	47
4. TAZADIT PIT	48
5. GEOLOGIC INVESTIGATIONS	53
Surface Mapping Methods	53
Magnetic Declination	54
Fracture Set Sampling	54
Detail Line Mapping	58
Compilation of Previous Work	63
Subsurface Investigations	72
Oriented Core	74
Drill Hole Survey	75
Core Samples	76
Previous Drilling	76
Lithology	76
Field Classification	76
Stratigraphy of the Footwall	82
General Geologic Structure	83
Folding	83
Tectonism	84
Fabric	84
Lineation	87
Bedding	92
Jointing	104
Fracture Spacing	108
Bedding	109
Jointing	111
6. ROCK STRENGTH	114
Intact Rock Strength	114
Unconfined Compressive Strength	114
Tensile Strength	118
Confined Compressive Strength	120
Elastic Properties	124
Rock Mass Classification	126
Fracture Strength	127
Tensile Strength	127
Shear Strength	127

TABLE OF CONTENTS--Continued

	Page
7. DESIGN APPLICATIONS	143
Plane Shear Analysis	143
Analysis of the Tazadit Pit Hanging Wall	152
Planar Features Parallel to the Pit Slope	152
Intersections	157
Analysis of the Tazadit Pit Footwall	158
Planar Features Parallel to the Pit Slope	158
Intersections	162
Effect of Ground Water	165
Hydrostatic Uplift	166
Seepage Pressure	166
Reduction of Shear Strength	167
Finite Element Analysis	167
Geologic Section	169
Density	171
Modulus of Deformation	173
Final Pit Slope Angles	175
Hanging Wall	175
Footwall	178
8. CONCLUSIONS AND SUGGESTIONS FOR FURTHER RESEARCH	186
Rock Fabric	186
Mapping Methods	186
Rock Strength	187
Rock Mass	187
Fracture Strength	188
Final Pit Slope Angles	189
Suggestions for Further Research	189
Fracture Spacing	189
Core Orientation	190
Application to Existing Slopes	190
APPENDIX A: DIRECT SHEAR TEST RESULTS	191
REFERENCES	196

LIST OF ILLUSTRATIONS

Figure	Page
1. Effect of Changes in Slope Angle on Stripping Volume .	6
2. Profit Versus Slope Angle for the Steep Rock Open Pit .	8
3. Hypothetical Risk Analysis	12
4. Typical Stability Curves for Incompetent Rock	13
5. Highway Research Board Classification of Landslides . .	20
6. Classification of Pit Slope Failures	21
7. Theoretical Stability Conditions	25
8. Generalized Flow Chart for Pit Slope Design	29
9. Location of the Kedia D'Idjil	49
10. Generalized Geology of the Kedia D'Idjil	50
11. View of the Tazadit Pit Looking Northwest	52
12. Isogonic Map of the Tazadit Pit	55
13. Appearance of Fractures in the Pit Face--with overlay .	57
14. Fracture Mapping Data Sheet	59
15. Geometry of Planar Structural Features	60
16. Detail Line Sample Size Test, Adit Data, Kimbley Pit, Nevada	62
17. Location of Detail Line Samples	64
18. Detail Line 1	65
19. Detail Line 2	66
20. Detail Line 3	67
21. Detail Line 5	68

LIST OF ILLUSTRATIONS--Continued

Figure	Page
22. Detail Line 6	69
23. Detail Line 8	70
24. Detail Line 10	71
25. Location of Diamond Drill Holes	73
26. Footwall Contact Between Ore and Schist	79
27. Quartzite, 586 Level, Footwall	79
28. Folding of Schist and Quartzite, 586 Level, Footwall . .	80
29. Schistose BHQ of the Footwall	80
30. Microfolding of BHQ	81
31. Lineation in the Footwall Quartzite	81
32. Tazadit Pit Simplified Surface Geology in pocket	
33. Tazadit Pit Simplified Geology Section D in pocket	
34. Tazadit Pit Simplified Geology Section H in pocket	
35. Tazadit Pit Simplified Geology Section LL in pocket	
36. Fabric Diagrams of the Structural Features in the Tazadit Area	85
37. Mean Attitude of Lineation and Bedding	89
38. Orientation of Lineation	90
39. Vector Mean Strike of Bedding -- Graphic Plot	95
40. Vector Mean Strike of Bedding -- Numerical Plot	96
41. Residuals -- Observed Strike of Bedding Minus Mean Strike	97
42. Linear Trend Surface of Vector Mean Strike of Bedding -- Graphic Plot	98

LIST OF ILLUSTRATIONS--Continued

Figure	Page
43. Linear Trend Surface of Vector Mean Strike of Bedding -- Numerical Plot	99
44. Linear Residuals -- Observed Strike of Bedding Minus Linear Trend Surface	100
45. Linear Plus Quadratic Trend Surface of Vector Mean Strike of Bedding -- Graphic Plot	101
46. Linear Plus Quadratic Trend Surface of Vector Mean Strike of Bedding -- Numerical Plot	102
47. Linear Plus Quadratic Residuals -- Observed Strike Minus Linear Plus Quadratic Trend Surfaces	103
48. Oriented Core Blind Zones	106
49. Detail Line Blind Zones	107
50. Engineering Classification of Intact Rock, Tazadit Pit .	115
51. Hanging Wall BHQ Mohr Diagram	121
52. Hematite Ore Mohr Diagram	122
53. Quartzite Mohr Diagram	123
54. Stress Strain Curve for Quartzite	125
55. Shear Strength Envelopes for Fractures	128
56. Direct Shear Test Results for Sample 1	132
57. Friction Angles for Rocks and Minerals	136
58. Limiting Equilibrium for a Planar Surface Parallel to the Pit Face	145
59. Cohesion Required on Specified Failure Plane at Limiting Equilibrium	146
60. Cohesion Required on Maximum Shear Plane at Limiting Equilibrium	147
61. Dip of Maximum Shear Plane	148

LIST OF ILLUSTRATIONS--Continued

Figure	Page
62. Graphic Stability Analysis of a Wedge Formed by the Intersection of Two Fractures	150
63. Schmidt Diagram of the Plane Shear Analysis of Hanging Wall Jointing	155
64. Dip Histogram of Hanging Wall Critical Joint Set	156
65. Schmidt Diagram of Footwall Bedding	159
66. Dip Histogram of Footwall Bedding	161
67. Footwall Fracture Intersections	164
68. Simplified Geology of Section D for Finite Element Analysis	170
69. Histograms of RQD Measurements	174
70. Slope Angle Sections for the Tazadit Pit Final Pit	176
71. Schmidt Diagram of Tazadit Final Pit Slope Angles and Critical Structures	177
72. Dip Histogram of Footwall Bedding Observations	179
73. Schematic Cross Section of the Proposed Footwall Final Slope	180
74. Footwall 50° Final Slope -- Section LL	181
75. Footwall 50° Final Slope -- Section H	182
76. Footwall 50° Final Slope -- Section D	183
77. Variable Angle Slope, Section D	184

LIST OF TABLES

Table	Page
1. Decrease in Stripping per Foot of Slope for Change in Slope Angle from 50° to 60°	7
2. Classification of Joint Properties	35
3. Mean Attitude of Lineation	88
4. Mean Attitude of Bedding	93
5. Detail Line Joint Spacing	113
6. Results of Physical Testing of Tazadit Pit Rock Samples	117
7. Brazilian Disc Tensile Strength	119
8. Friction Angle Test Results	134
9. Planarity and Continuity Measurements	139
10. Tazadit Hanging Wall Joint Set Dispersion Values	141
11. Limiting Equilibrium for Plane Shear Failure	154
12. Bedding Observations With Dips Less Than 50 Degrees	163
13. Revised Physical Properties for Finite Element Analysis	172

ABSTRACT

An important and sometimes critical aspect of the design and operation of an open pit mine is the steepness of the pit walls. In general, the steeper the pit wall the lower the stripping cost and, therefore, the greater the profitability of the mine. Thus, slope design consists primarily of determining the maximum angle at which a pit wall will stand without failure.

The maximum angle a pit slope can stand without failure is controlled in large part by the geological structures such as joints, faults, and bedding, which are planes or surfaces of weakness along which failure can occur. The objectives of geologic investigation for slope design are (1) to quantitatively determine the geometric aspects or fabric of a rock mass so that a model of the potential failure geometry can be developed and (2) to describe the structural features and lithologic units in order to estimate the strength characteristics of the rock mass.

Geologic investigation and laboratory testing of rock samples were conducted to estimate the optimum slope angles for the Tazadit open pit, which is in a Precambrian hematite iron ore district located in Mauritania, West Africa.

Detailed surface mapping and data from oriented core establish that the rocks of the pit slopes have the pronounced anisotropic fabric of an isoclinally folded tectonite. The mean orientation and spacial

variation of orientation of the fabric elements are analyzed by equal area fabric diagrams and by trend surface analysis. A comparison of the methods of obtaining structural data is made.

The footwall, consisting of a series of quartzites, schists, and schistose banded hematite quartzites, has a potential failure geometry defined by the bedding which strikes parallel to the pit face and dips into the pit at 63° . The hanging wall, consisting of banded hematite quartzite (BHQ), has several potential failure geometries defined by jointing and the intersection of joint sets.

Tests of core samples establish that the intact rocks of the Tazadit pit have unconfined compressive strengths in excess of 32,000 psi for the BHQ and the quartzite, 10,900 psi for the hematite ore, and less than 15,000 psi for the schist. On the basis of direct shear and triaxial slip test results, the residual friction angles for fractures are estimated to be 26° for the BHQ and for the quartzite, and 22° for the schist when dry and 16° when saturated. The geometry of the fractures is estimated to raise the effective friction angles to between 31° and 36° for joint sets in the hanging wall, and to 23° for bedding planes in the footwall schist.

To develop a model for a two-dimensional plane strain finite element analysis, a simplified geologic cross section is constructed and rock deformation characteristics are established from the results of physical testing and fracture spacing observed in drill core.

Maximum stable slopes are estimated to be 65° for the footwall and 50° for the hanging wall on the basis of a plane shear stability analysis and consideration of mining methods.

CHAPTER 1

INTRODUCTION

An important and sometimes critical aspect of the design and operation of an open pit mine is the angle or steepness of the pit walls. The maximum angle at which a pit wall will stand without failure is controlled, in large part, by geologic features such as faults, joints and bedding which are planes or surfaces of weakness along which failure may occur. Thus, there is a need for methods of investigating the rock mass of an existing or proposed pit wall in order to provide information on geologic features to be used as input for pit slope design. The term design is used here in the general sense of determining slope angles which can range from choosing angles based on experience to a full-fledged mathematical analysis of stress-strength relationships.

A considerable amount of geologic data is collected during the exploration and development of an ore body. However, the primary objective of mineral exploration is the location of potentially minable ore bodies, and geologic investigations are oriented toward the genesis of ore mineralization and favorable structural environments rather than the geomechanical properties of the rock. After locating a potential ore body, additional work is then aimed toward proving the grade and dimensions of the ore and determining the metallurgical characteristics for mill design. As a result, geologic information necessary to determine the optimum slope angles (the geometry and character of geologic

structures, the magnitude and distribution of stresses, and the ground water conditions) is often not obtained or may be buried as incidental details on geologic maps and drill logs.

The purpose of this study is to examine how geologic investigations specifically oriented toward slope design can be utilized, in conjunction with laboratory testing, to provide the information necessary to make a rational analysis of the stability of a pit slope. Although it is generally recognized that geologic data are an essential element of slope analysis, the methods of collecting and quantifying these data are still in the development stage. As stated by Hoek (1970, p. 13) "Advances in our ability to design and control slopes will depend, to a large extent, on our ability to devise more effective structural mapping techniques."

This study is divided into two parts. Part I is background information covering the fundamentals of open pit slope design, description of geologic structural features, and sampling methods. Part II describes the methods and results of a slope design investigation of the Tazadit Open Pit, located in a Precambrium iron ore deposit in Mauritania, West Africa. The deposit is currently being mined by Societe Anonyme des Mines de Fer de Mauritanie (MIFERMA).

PART I

PIT SLOPE DESIGN AND
GEOLOGIC PARAMETERS

CHAPTER 2

PIT SLOPE DESIGN

Determination of slope angles is one aspect of open pit design. As the objective of pit design is a pit geometry which will produce the maximum profit over the life of the mine, the economic aspects of pit slope angles must be considered in pit slope design as well as the mechanical behavior of rock.

Economic Aspects of Pit Slope Angles

The geometry, mineralogy and depth of an ore body are fixed by nature. For any given mining method and set of economic conditions, the chief variable that the planning engineer must determine to establish the geometric limits of the pit and the profitability of the mine is the slope angle. The steeper the slope the lower the stripping ratio, thus the more profitable the mine.

The potentially large economic impact of slope angle changes is well recognized. Coates and Brown (1961) pointed out that a 1° increase in the slope of a pit 4,000 feet by 5,000 feet by 1,000 feet deep represents a decrease in stripping of 20 million tons. Long (1963) gave a figure of 1.2 million tons decrease in stripping for a slope angle change from 35° to 36° in a 15,000 feet diameter by 400 feet deep pit. Black (1964) reiterated Coates and Brown's figures.

The number of cubic yards of material per running foot of pit slope represented by an increase in slope angle is illustrated in Figure 1. Using a density of 12.5 cubic feet per ton, which is the most common value for open pit porphyry copper mines as reported by Michaelson and Hammes (1968, p. 888-889), the relationship expressed in tons per foot is

$$W = \frac{H^2 \sin (b-a)}{25 \sin a \sin b}$$

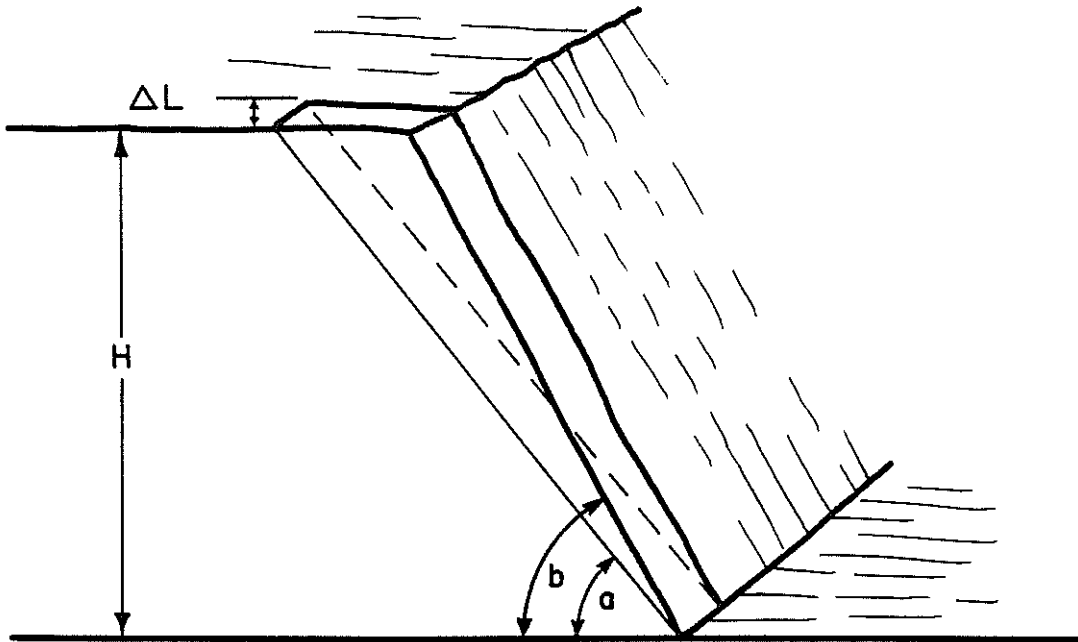
Table 1 is a representation of these relationships. For a slope increment from 50° to 60°, the amount of rock is 10,471 tons per foot of pit wall for a pit 1,000 feet deep. Stripping this material would cost \$3,141 per foot at \$0.30 per ton. For a 3,000 feet long wall the cost would be almost \$10,000,000.

Schottler (1962) has analyzed several cross sections of the Steep Rock deposit to determine the effect of slope angle changes on profit. His results are shown in Figure 2.

Although the economic effect of changes in slope angle is variable and must be computed for each mine and even for each sector of a mine, as a generalization, the steeper the slope the greater the profit. Thus, there is considerable economic incentive to utilize the maximum possible slopes.

Slope Failure

Defining slope failure is not as simple as would appear at first glance. From a theoretical standpoint, if the rock is considered



$$v = \frac{H^2 \sin (b-a)}{54 \sin a \sin b}$$

V = cubic yards per foot of slope length

H = slope height (in feet)

a = initial slope angle

b = final slope angle

Figure 1. Effect of Changes in Slope Angle on Stripping Volume

Table 1. Decrease in Stripping per Foot of Slope for Change in Slope Angle from 50° to 60°

Pit Depth	Yds ³ /Ft	Tons/Ft	Cost Per Foot of Slope		
			@ 20¢/Ton	@ 30¢/Ton	@ 40¢/Ton
100	49	105	\$ 21	\$ 31	\$ 42
500	1212	2618	524	785	1047
1000	4848	10471	2094	3141	4188
1500	10907	23559	4712	7068	9424
2000	19390	41883	8377	12565	16753
2500	30297	65442	13088	19632	26177
3000	43628	94236	18847	28271	37694

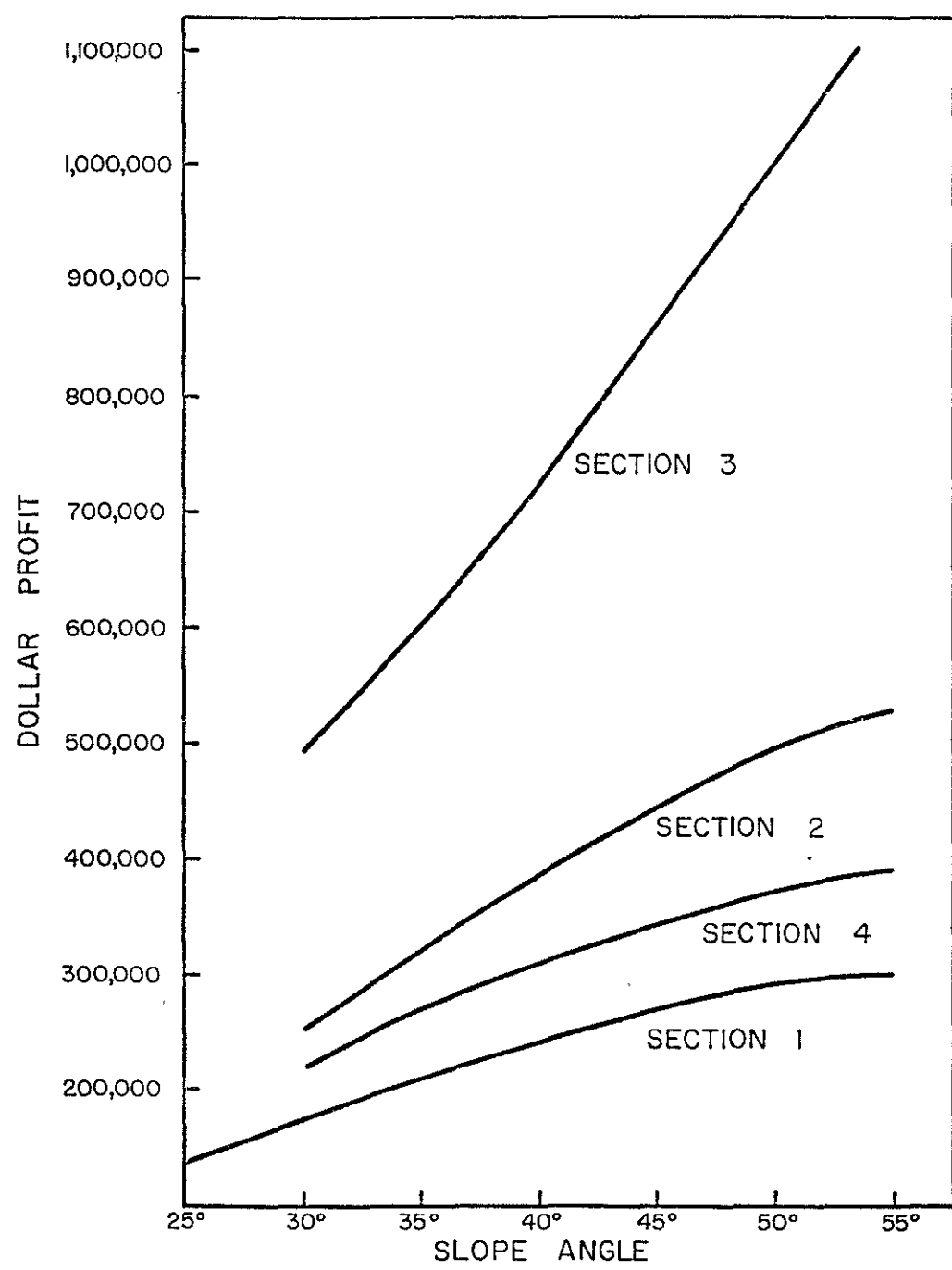


Figure 2. Profit Versus Slope Angle for the Steep Rock Open Pit (After Schottler, 1962)

an elastic material, any displacement beyond recoverable strain constitutes failure. This, however, is not a satisfactory definition for a mine operator who often is successfully mining a pit slope that has "failed" from an elastic standpoint. Displacement of several feet, which would be failure in a mechanical sense, may or may not cause difficulties for a mine operation depending on the rate of movement, the type of mining operation, and the relationship of the moving material to the mining operation.

In a truck and shovel operation which has considerable operational flexibility, a displacement rate of one to two feet per month may present no real problems as material is removed from the mining area at a faster rate and any offsets in the haul roads can be smoothed over by routine maintenance. The real hazard for this type of displacement is not the existing rate of displacement, but the potential of a greatly accelerated rate of movement.

In some cases slow displacement is an economic advantage as it breaks up the rock sufficiently so that drilling and blasting are not necessary. It has been postulated that if there were sufficient understanding of the mechanics of rock movement so that displacement could be controlled, "failure" of this type could be induced which would be a surface equivalent of block caving.

On the other hand, a few inches of displacement of track in a rail pit or in the foundation of a building adjacent to the pit requires extensive realignment and repair. Thus, it is useful to distinguish between "failure" from the theoretical standpoint and what could be

termed "operational failure." When the rate of displacement is greater than the rate at which the slide material can be economically mined, or the movement produces unacceptable damage to a permanent facility, it is an operational failure.

Varnes (1958, p. 20) used a similar economic concept to distinguish between creep and landslides. He restricts the lower limit of the rate of movement of landslide material "...to that actual or potential rate of movement which provokes correction or maintenance."

Uncertainty in Slope Design

Even after accepting a criteria for failure, the maximum slope angle cannot be precisely determined. Two factors contribute to this: (1) the uncertainty in the design technique, and (2) the influence of natural phenomena such as precipitation and earthquakes.

Uncertainty in the design techniques is the result of the large number of factors that influence the stability of a slope, the variability of these factors, and the difficulty in measuring these factors. For example, rock strength, a basic parameter, can vary from an unconfined compressive strength of 30,000 psi for unaltered intact rock to less than 100 psi for a gouge zone a foot or less away. Another factor, the in situ stresses, which can be measured only by expensive and time-consuming strain relief overcoring techniques, have been shown to be significantly different from values calculated for overburden load, and the measured stresses have a high degree of variability in both orientation and magnitude (Coates and Grant 1966). Thus, stability calculations must be based on probabilistic estimates of rock strengths and imposed

stresses. In addition, the construction of a model amenable to mathematical computations requires a number of simplifying assumptions.

The adverse effect of earthquakes and heavy precipitation has been demonstrated both theoretically and by observation of actual slides (Terzaghi 1950, Bjerrum and Jorstad 1964, Hammel 1967). The magnitude of a storm or earthquake and the time of occurrence are governed by such a complex interrelation of factors that it approaches a chance event and the prediction of such an event during the life of a pit can only be a probability of occurrence based on projection of past records.

Considering these uncertainties, it is at least conceptually possible to develop a relationship between slope angle and probability of failure (Figure 3). By relating the curve with the savings resultant from an increase in slope angle, the choice of slope angle could be put on a risk versus profit basis that would be amenable to game theory decision making.

Coates (1970, p. 6-19) presented stability curves for incompetent rock utilizing a similar probability approach (Figure 4) and pointed out that "...even with a moderate variation in strength properties, the slope angle required to eliminate all failures would generally be unacceptably low."

Slope Monitoring

Acceptance of a degree of probability of slope failure carries with it a commitment to slide detection and to safe operation procedures for the protection of lives and equipment. Simple routine inspection for headwall cracking and the monitoring of surface displacement have

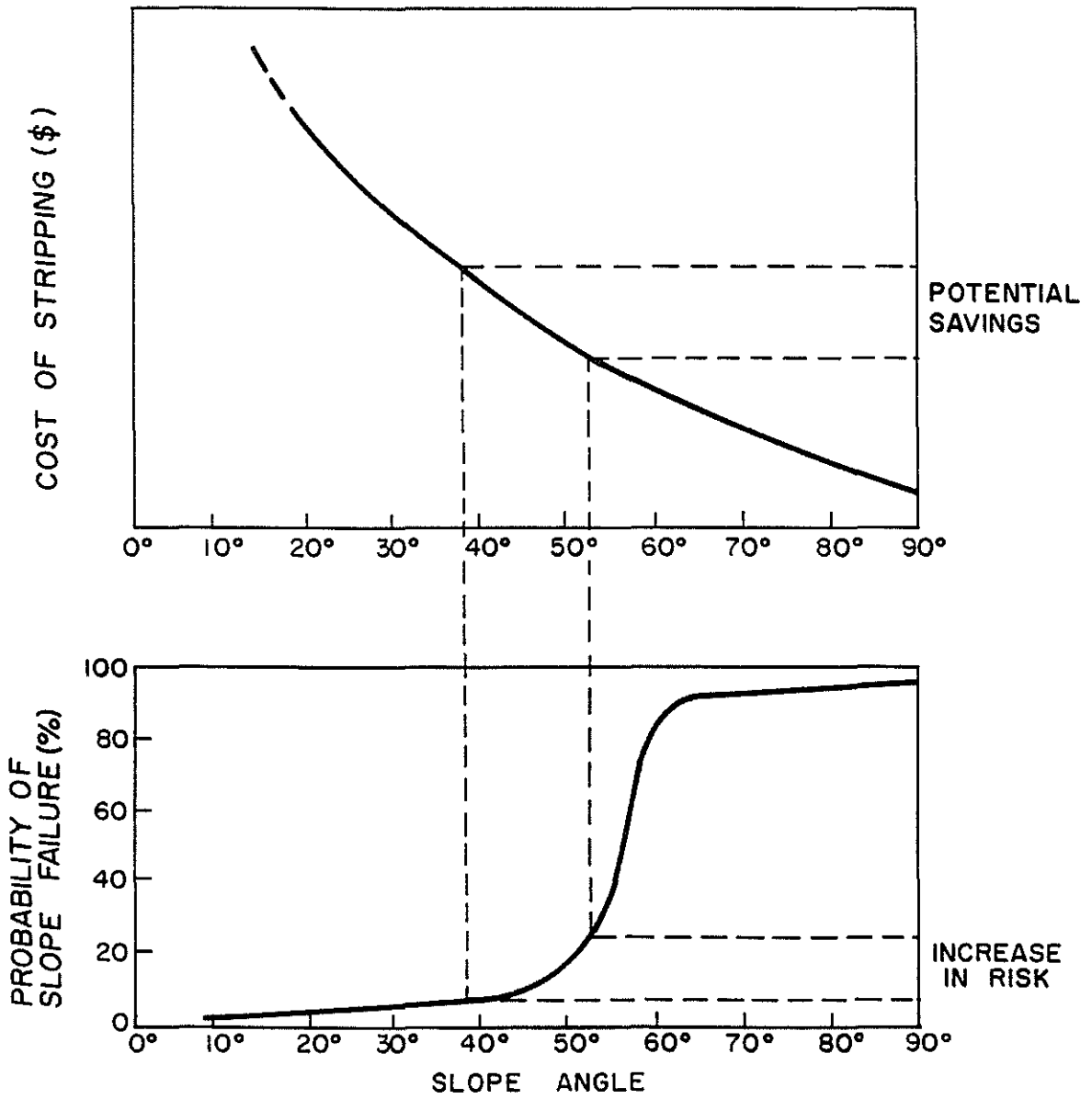


Figure 3. Hypothetical Risk Analysis

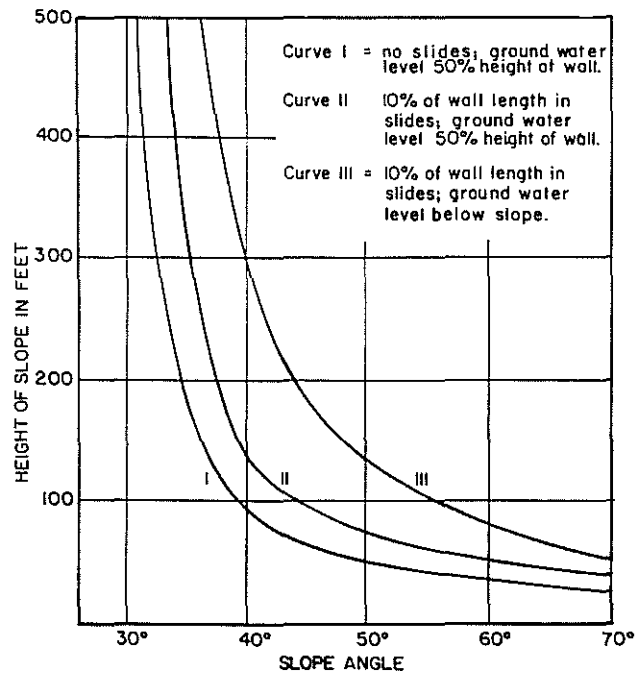


Figure 4. Typical Stability Curves for Incompetent Rock.
(Coates, 1970)

proven to be effective in detecting impending slope failure (Kennedy and Niermyer 1970). More sophisticated techniques such as borehole deflection measurements and microseismic monitoring may be warranted when critical structures such as crushers and conveyor belts are located in or adjacent to a pit.

The cost of safety procedures and the clean up of small slides will reduce the potential savings resulting from slope steepening.

Artificial Support

There exists the possibility of improving the stability of an open slope by artificial means, thereby allowing the slope to be mined at a steeper angle than would be possible with normal mining methods. Artificial support may also be used to increase the stability of an existing slope for reasons of safety. Although artificial support is used in civil construction, its application has been and will be much more limited in open pit mining. The reason for this is the difference in objectives. In civil construction, the objective is to construct a permanent structure such as a highway cut or an excavation for some facility such as a power plant, and excavation is only a means of arriving at this objective. In open pit mining, on the other hand, the objective is the removal of the ore; thus, the excavation is the primary aim and the pit slope is a result, not the objective, of the operation. Long term stability is not required in an open pit slope, and even during the life of a mine, the consequences of slope failure are not as great as in civil construction. Considerable displacement can be tolerated unless a major facility such as a crusher or buildings are involved.

Another factor which reduces the applicability of artificial support to open pit slopes is the uncertainty of the position of the final pit slope. This uncertainty is brought about by imperfect knowledge of the ore body and changing economic conditions. The general trend of increased metal prices and improved technology have resulted in the mining of increasingly lower grade ore at greater depths. Thus, it is quite common during the life of an open pit to have expansions of the final pit brought about by the discovery of additional ore with development drilling, or a reduction in the cutoff grade and increase in the maximum stripping ratio brought about by changing economic conditions. Under these circumstances, an artificially supported slope would have to be mined out with the resulting loss of the investment in the support system. In cases where the boundaries of the ore body are defined by sharp geologic contacts rather than by a cutoff grade, the depth of the pit is determined by the bottom of the ore body rather than the maximum stripping ratio, and the development drilling has been extensive enough so that there is a low probability of additional ore being discovered, artificial support could be advantageous.

Where expensive installations such as mills, smelters, and railroads are located on the perimeter of the pit, artificial support could be used advantageously to permit the recovery of additional ore without endangering the facilities. Noneconomic considerations may also make artificial support advisable in situations where the pit perimeter is at a property boundary.

Tension Tendons and Rock Bolts. Rock bolting has proved to be a very successful means of ground support in underground mining. The

merit in this system is that it is an active support system where the rock bolts increase the capability of the rock to carry the load rather than a passive support system such as timber or steel sets where part of the rock load is transferred to the support system.

In jointed hard rock the excavation of an open pit reduces the confining stress of the rock in the pit slope allowing expansion and the reduction of the integrity of the rock mass by the opening of joints and other structural features. This reduction in strength of the rock mass can result in major slope failure or raveling. Long rock bolts or cable tendons under tension can reduce such disaggregation of the rock mass by applying a compressive stress to the rock mass. In the case of potential plane shear failure, this compressive stress properly directed can increase the normal stress along the potential failure plane, thereby increasing the shearing resistance. By installing wire mesh across the pit face tied into stringers between the rock anchors, loose surface material can be constrained minimizing raveling. Such a system of rock anchors and wire mesh has been reviewed in detail by Barron, Coates and Gyenge (1970) in a study which included a trial installation of such a system. This study demonstrated that installation of a support system utilizing tensioned wire rope tendons in 3.89 inch diameter holes as deep as 190 feet was technically feasible. Their cost analysis indicated that for a 500 feet deep pit with a 50° slope, the support system would cost \$433 per lineal foot if no wire mesh was used and \$748 per lineal foot with wire mesh covering the pit face.

Grouting. Although grouting has been successfully utilized to improve rock mass strength in underground workings where the rock is under compression, it usually is not a suitable system for open pit slopes. Injection of grout under pressure into a pit slope where the confining stresses are low would result in the opening of joints with the reduction of any effective cohesion which might be present. The strength of the bonding between the grout and the wall rock could be less than the reduction in effective cohesion. Furthermore, Coulson (1970) has shown that the residual shear strength of grouted joints is considerably less than that of ungrouted joints. Thus, grouting could actually reduce the stability of a pit slope.

Retaining Walls. Passive support systems, (such as retaining walls) where the support system is designed to carry the excess load of the moving ground, are not feasible in open pit operations because of the large size of open pits. The cost of the retaining wall to support a pit slope several hundred feet deep would be far in excess of the cost of stripping the slope back to a stable angle.

Drainage. Although drainage of groundwater is not actually an artificial support system, it is included here as it is a method of improving the stability of the slope by artificially changing the conditions within the pit slope. The effectiveness of drainage in preventing and containing slides in soil has been well established (Terzaghi 1950, p. 120). Application to rock slopes is more difficult because of the generally low permeability and the anisotropism and non-homogeneity of the fluid flow in a fractured rock mass. The problem of

analyzing drainage patterns in fractured rock has been treated in detail by Sharp (1970) and Louis (1967).

Stability Analysis

For purposes of analyzing the stability of a slope, a design model is necessary. The model consists of the geometry of the slope, the mechanical properties of the rock mass, and the mode of failure. These aspects of a design model are interrelated as the mode of failure is a function of the geometry and the mechanical properties of the rock mass. The development of a design model can be based on a semi-empirical classification of slides, an assumed theoretical model, or a combination of the two.

Classification of Slides

The classification of slides can be approached from a number of different aspects: the type of material, the geometry, the rate of movement, the type of movement, and the causes of movement. Combination and permutations of all the aspects give an almost unlimited number of categories.

Classification serves three purposes. It can (1) provide descriptive terminology, (2) organize the variables involved, and (3) determine models for design purposes. Systems of classification will vary depending on the primary purpose of the classification. Although pit slide classifications are used for all the above mentioned purposes, the main purpose is for design models.

Geologically, slides fall in the general category of mass wasting as distinguished from stream erosion and other processes of denudation. Over the years a number of classifications have been proposed of which those of Heim (1882), MacDonald (1913), Terzaghi (1925), Ladd (1935) and Sharpe (1938) are the most notable. Reviews of their classifications are given by Sharpe (1938) and Patton (1966). One of the more recent is that of the Highway Research Board (Varnes 1958), Figure 5) which is a modification of Sharpe's classification.

Coates and Brown (1961) proposed a classification system specifically for mine slope failures which follows the "bedrock" section of the Highway Research Board classification. They argue for a simplified system containing only three or four categories on the basis that it is more useful than a complex system. This system is given in Figure 6.

A system used by Lacy (1963) is similar to that of Coates and Brown except that he does not include block flow.

Rotational Slump. There is general agreement among classification systems on the rotational slump category. This is a characteristic failure for soils and analytical design methods have been developed in considerable detail. There is some question of the applicability of rotary slump to rock slopes as it would only occur in an isotropic or simple horizontal planar anisotropic material. A poorly indurated shale and a highly altered or weathered intrusive are two situations where rotary slump could occur.

Plane Shear. The plane shear category of Coates, called translational by Lacy, includes the rockslide and block glide categories of the Highway Research Board. In the author's opinion, this is by far

TYPE OF MOVEMENT	TYPE OF MATERIAL			
	BEDROCK		SOILS	
<u>FALLS</u>	<u>ROCKFALL</u>		<u>SOILFALL</u>	
<u>FEW UNITS SLIDES</u>	ROTATIONAL <u>SLUMP</u>	PLANAR <u>BLOCK GLIDE</u>	PLANAR <u>BLOCK GLIDE</u>	ROTATIONAL <u>BLOCK SLUMP</u>
		<u>ROCKSLIDE</u>	<u>DEBRIS SLIDE</u>	<u>FAILURE BY LATERAL SPREADING</u>
<u>MANY UNITS</u>				
<u>DRY FLOWS</u>	ALL UNCONSOLIDATED			
	ROCK FRAGMENTS	SAND OR SILT	MIXED	MOSTLY PLASTIC
	<u>ROCK FRAGMENT FLOW</u>	<u>SAND RUN</u>	<u>LOESS FLOW</u>	
			<u>RAPID EARTHFLOW</u>	<u>DEBRIS AVALANCHE</u> <u>SLOW EARTHFLOW</u>
<u>WET</u>		<u>SAND OR SILT FLOW</u>	<u>DEBRIS FLOW</u> <u>MUDFLOW</u>	
<u>COMPLEX</u>	COMBINATIONS OF MATERIALS OR TYPE OF MOVEMENT			

Figure 5. Highway Research Board Classification of Landslides. (Varnes, 1958)

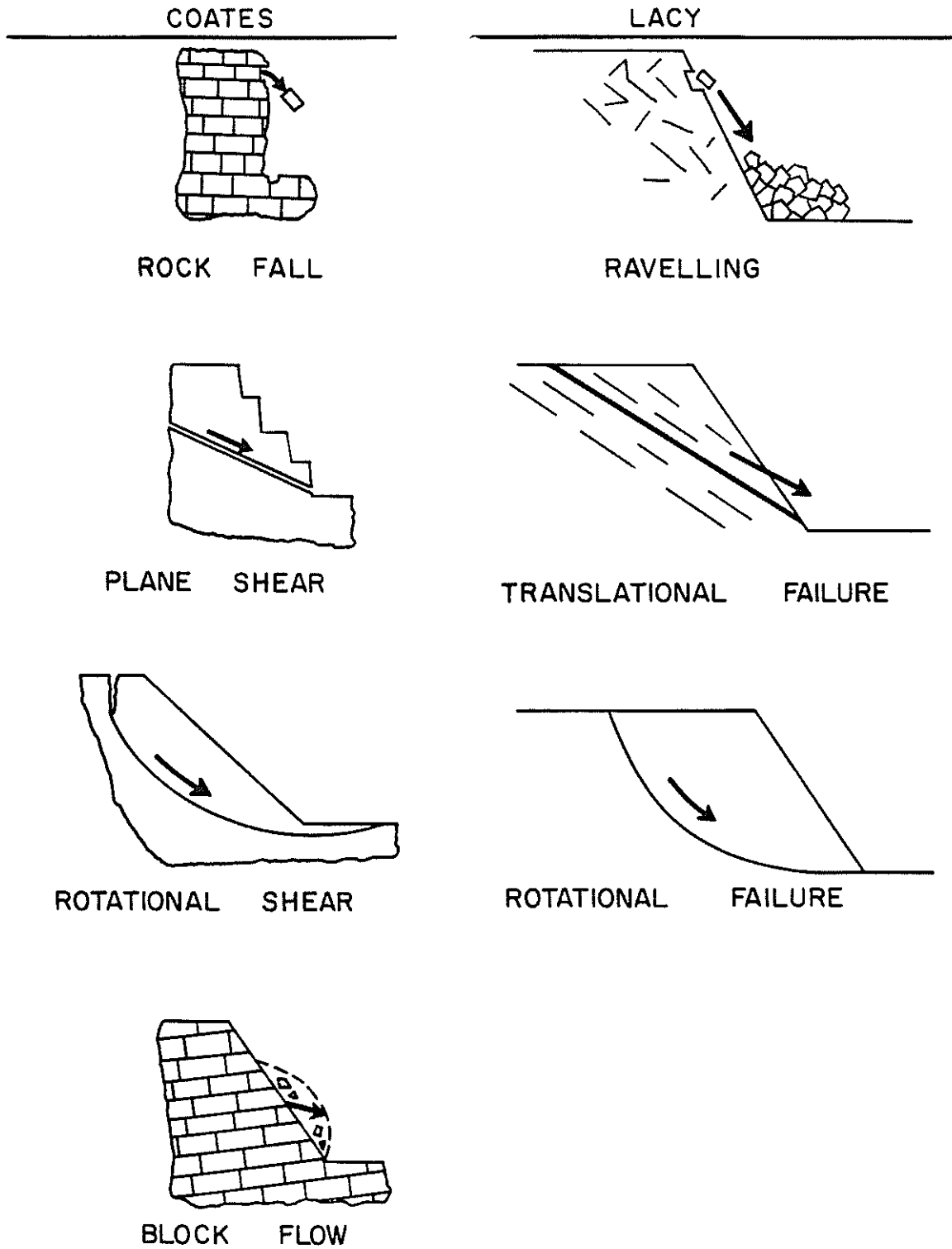


Figure 6. Classification of Pit Slope Failures.
 (After Coates, 1970; Lacy, 1963)

the most common form of open pit slide. The rock substance or intact rock of a pit slope is almost always strong enough to support a high steep slope, whereas planes of weakness with lowered shear strength are almost always present.

Rockfall. The term rockfall as used by Coates and Brown (1961) is synonymous with the term ravelling as used by Lacy (1963). This is the situation in which a large number of individual blocks fall or roll down a pit slope that is steeper than the angle of repose for loose material.

Individual rockfalls are a common occurrence but are usually considered more of an annoyance than a serious failure. When the number of individual rockfalls is extensive enough to form talus slopes at the angle of repose of loose material, rockfalls or ravelling limits the slope to the angle of repose unless corrective measures are taken.

Block Flow. Coates' block flow category follows the systems of Sharp and Varnes in that it differentiates movement with internal deformation as flow rather than slide where there is little internal deformation. The Frank slide in Alberta, Canada that Coates (1970, p. 6-21) cites as an example of block flow is classified as a rockfall avalanche variety of rock fragment flow by Varnes (1958, p. 35).

One of the difficulties in classification of slides is that there is not a clear-cut dividing line between categories. A predominately plane shear failure may exhibit a number of features characteristic of rotational slump, such as the formation of headwall graben, backward tilting of headwall blocks, and upthrust of the toe. If failure occurs along a number of planes of weakness, the failure surface

can approach a circular arc. It can be argued that the rotational shear is simply a limiting case of plane shear where there are an infinite number of plane surfaces.

Often in the rockfall or ravelling situation the initial movement is of a plane shear nature and only after the rock has slid from its original position does true falling and rolling occur. Thus, rockfalls or ravelling can be considered a special case of many small plane shear failures.

As displacement occurs, the moving material in a slide undergoes large changes in the stress distribution which can cause the sliding mass to lose its original structural integrity. Thus, a plane shear failure can be transformed into a rotary slump or a block flow as the sliding material becomes a disaggregated mass.

Methods of Analysis

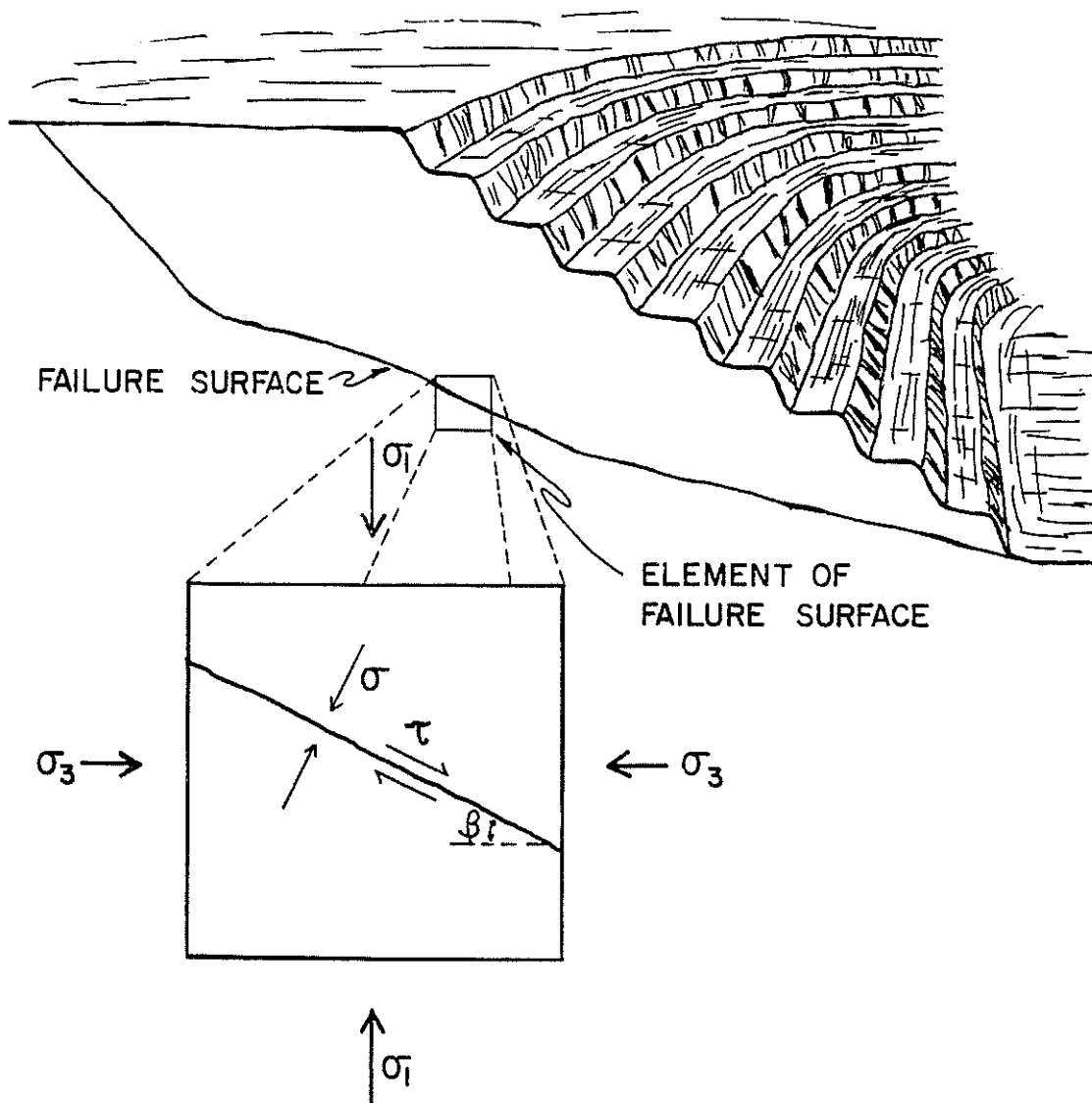
Ravelling. Analysis of the ravelling mode of failure is based on the integrity of the rock mass, the size and shape of the individual blocks, and the angle of repose of the loose material. Since the integrity of a rock exposed in a pit face is time-dependent and is also a function of the blasting techniques, empirical evidence from existing slopes is important.

Plane Shear. For many slopes plane shear is the most probable failure mode. For these slopes the following assumptions can be made:

1. The rock mass is heterogeneous. Chemical composition and physical properties will vary with position in the rock mass.

2. The rock mass is discontinuous. Geologic structural features (faults, joints, bedding) transect the rock mass so that the physical properties vary abruptly.
3. The rock mass is anisotropic. Physical properties are a function of orientation as well as position, i.e., there are preferred orientations of jointing, faulting, bedding and other structural features.
4. The strength of the structural features is so much less than that of the intact rock that the failure surface will be primarily along the structural features.
5. The strength, or resistance to shear, of a structural feature is a function of the normal stress on the surface.

On the basis of these assumptions the stability of a proposed slope can be determined, in principle, if one can (1) measure the attitude and position of the structural features, (2) determine the shear strength of the structural features, and (3) compute the stresses acting on the structural features. As an illustration, consider the simple situation of a planar structural feature such as a fault dipping into a pit (Figure 7). A unit area of the fault would be acted on by a stress which would be a combination of the weight of the overlying material, a stress induced by the configuration of the pit, seepage stresses if water were present, and possibly regional tectonic stresses. The stress distribution can be resolved into a normal stress and a shear stress along the fault. If a value for the shearing resistance can be assigned to the fault, the stability of the slope can be computed. Obtaining the necessary data for a rigorous solution is virtually



LIMITING EQUILIBRIUM

Shear Stress = Shear Strength

$$\tau = (c_e, \sigma \tan \phi)$$

c_e and $\tan \phi$ are strength parameters of the failure surface

Figure 7. Theoretical Stability Conditions.

impossible at present because of the complexity of any real rock mass; thus, approximate values for rock properties must be used and simplifying assumptions must be made.

For the plane shear mode of failure, a limiting equilibrium analysis can be made where the weight of the sliding block is the driving force and the strength of the failure plane is composed of an effective cohesion and a friction angle as in the Mohr-Coulomb relationship. A two-dimensional analysis can be used when the failure plane is parallel to the pit face (Jennings 1970). If the failure surface is composed of the intersection of two fractures, it can be analyzed with a three-dimensional graphic method (John 1968).

Rotational Shear. Failure on a circular arc is usually analyzed as a two-dimensional vertical section. A failure circle is assumed and the stability is computed by summing the moments of vertical slices around the center of the circle. The circle with the lowest stability is found by trial and error iteration. This type of analysis has been described in detail by Fellenius (1936), Janbu (1954), and Bishop and Morgenstern (1960). Although the circular arc method has proven to be successful in the design of soil slopes, it has limited application to rock slopes as a circular failure surface is the exception rather than the rule in rock slopes.

A variation of the circular arc analysis which has potential application to rock slopes has been developed by Morgenstern and Price (1965). In their method the shape of the potential failure surface is arbitrary and need not be circular. Thus, a noncircular failure surface

defined by geologic structural features could be analyzed for rotational failure.

Finite Element. The stresses in a pit slope are affected by variations in the physical properties of the rock, the geometry of the pit, and regional tectonic stresses. When the rock in a pit slope is anisotropic and non-homogeneous, the orientation and magnitude of the stresses would depart significantly from the simple vertical gravitational load model.

The finite element method is a mathematical modeling technique which is capable of computing the stress distribution in a pit wall (Yu and Coates 1970). Accurate determination of the physical properties of the rock mass and the initial stress conditions is necessary, however.

Although basically an elastic analysis, the finite element method can approximate nonelastic deformation of faults or other geologic structural features by the introduction of elements with a very low modulus of deformation (Hammel 1970).

Organization of a Pit Slope Design Study

The stability of final slope angles can be assessed on the basis of mathematical stability analysis, empirical case history data from existing slopes, or a combination of the two. The choice of the slope angles is also influenced by the mining method and safety considerations. For example, haul roads, access roads, or conveyor belts may reduce the overall slope angle.

The pit geometry is in turn determined by mineral distribution, slope angles, economic parameters, mining methods and safety

considerations. Figure 8 is a flow chart showing the relationship between these factors.

The geologic structure and rock strength, which are input for stability analysis, may be obtained from a variety of methods. The specific investigations most suitable for a pit must be determined on the basis of the local circumstances.

Since the pit geometry is also an input to stability analysis, slope design is an iterative procedure.

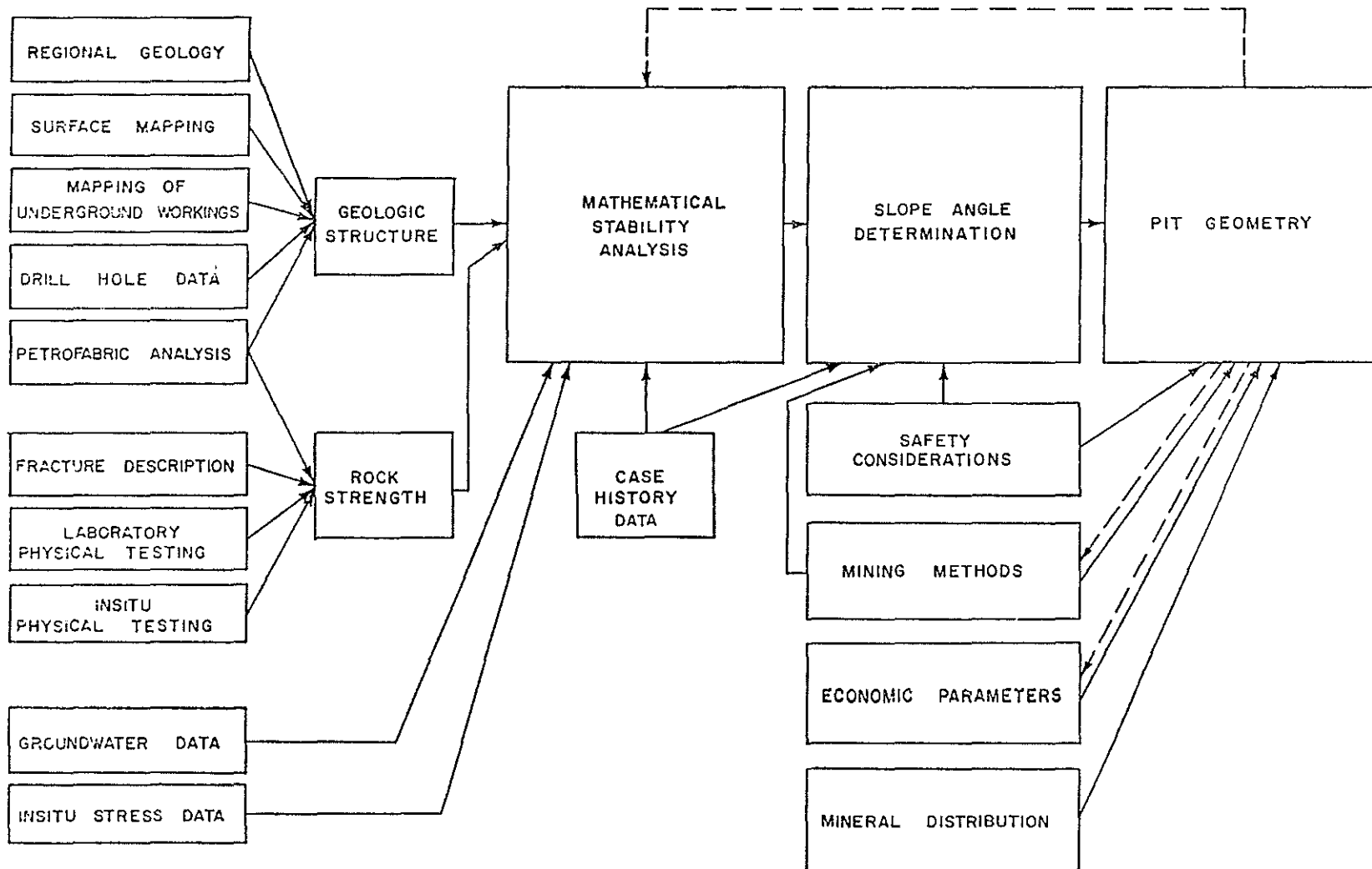


Figure 8. Generalized Flow Chart for Pit Slope Design

CHAPTER 3

MECHANICAL PROPERTIES OF FRACTURES

Obtaining meaningful values for the mechanical properties of a rock mass is difficult. Laboratory testing, where a small specimen of intact rock is tested under stress conditions which may not resemble those in the field, cannot give direct values of the strength or deformation properties for the rock mass particularly as the effect of fractures is not included.

Large scale direct shear tests of natural fractures are an improvement in that potential failure planes are tested but are expensive and can still only test specimens with a maximum size on the order of one foot, whereas a fracture in the field often has an extent of tens to hundreds of feet. Collection of undisturbed representative samples is difficult and the actual stress distribution within the sample during testing is questionable.

In situ tests which can test even larger volumes of rock in an undisturbed state are difficult to perform, usually requiring elaborate excavation in special underground openings. The cost is therefore so high that only limited tests can be conducted for critical constructions such as dam abutments.

By systematic description of geologic structural features it should be possible to make predictions of rock behavior by correlation with similar rock conditions where behavior is known or by extrapolation

of test data. As pointed out by McMahon (1967), the parameters used in describing rock for engineering purposes will be similar to index properties used in soil mechanics in that they may not have precise mathematical meaning but will derive their usefulness from empirical correlation. Satisfactory indices of rock mass properties must be simple and easily measured and give reproduceable results when measurements are made by different observers.

Geologic Structural Features

At the present time there is no agreed upon single term to describe the geologic structural features that affect the mechanical behavior of rock. Those features would include faults, joints, bedding planes, cleavage, schistosity, foliation, contacts and unconformities. The wide variety of features and the interdisciplinary nature of the subject almost preclude the existence of an accepted terminology.

W. R. Crane (1931) used the term "planes of weakness" for geologic structures controlling ground movement in mining operations. The Soviet engineering geologists also use the term "zones and planes of weakness" in literature on slope stability (Komarnitskii, 1968) as well as "system of weakening elements". Terzaghi (1962) referred to geologic structural features as "mechanical defects of rock".

The term "discontinuity" is applied to geologic structural features such as joints, bedding planes and cleavage planes by Deere (1964), Patton (1966), Londe (1965) and Mueller and John (1963). Although accepted by the engineering field, the use of "discontinuity" in this sense conflicts with the common application of the term in the

geologic literature to changes in physical properties in the interior of the earth, such as the Mohorovicic Discontinuity.

The American Geological Institute (AGI) Glossary (1960) differentiates between structure, "the sum total of the structural features of an area" and structural feature, "features produced in the rock by movements after deposition, and commonly after consolidation, of the rock." However, the term "structure" is often used in the sense of structural feature, e.g., Ramsey (1967, p. 4). Structural feature or structure is too inclusive to apply to planes or zones of weakness in rock as it also applies to features such as folds. When applied to engineering there is a conflict with the engineering definition of structure as "something built or constructed as a building, a dam, a bridge", (Webster's New World Dictionary, 1970).

The author has used the term "fracture" in a general sense including faults, joints, fissures and other related reasonably planar natural breaks in a rock mass (Weaver and Call, 1965). This usage parallels the definition suggested by Mitcham (1963) who, after a review of the literature, advocated the following definitions:

A fracture is a surface of rupture of physical or physio-chemical bonds on which relative displacement can range in magnitude from infinitesimal to large.

A joint is a fracture without significant relative displacement of the walls, which is a member of a group of fractures spatially extensive in three dimensions generally, or within the bounds of a given rock body.

A fault is a fracture on which the walls have been relatively displaced to a significant degree parallel to the fracture.

A fissure is a fracture whose walls have been opened significantly by separation in a direction normal to the plane of the fracture (p. 1157).

There is some objection to this use of the term "fracture" as it is also applied to the characteristic breakage of a mineral, i.e., conchoidal fracture (AGI Glossary, 1960). Another connotation of fracture is that of an artificially induced break, such as fracturing produced by blasting or "hydrofracing."

Properties of Individual Fractures

The attitude and position of fractures are basic parameters that determine failure geometry.

The strength of a fracture is a function of the geometry of the fracture and the composition of the wall rock and filling.

Geometric Parameters

Extent. The distance which a fracture can be traced is the extent. This usage is different from that given by John (1962). That which he terms extent is referred to here as continuity.

Continuity. The percent of discontinuous rock in the plane of a fracture can be defined as continuity. Considering a potential failure plane along a fracture, the amount of intact rock would be a measure of the cohesion. Terzaghi (1962) has expressed this relationship as:

$$c_i = \frac{cA_F}{A}$$

where:

c_i = effective cohesion

c = cohesion of intact rock

A = total area of the section through the rock

A_g = total area of gaps within the section

Continuity as defined above would be:

$$C = \frac{A_g - A}{A}$$

so, effective cohesion could be expressed as:

$$c_i = \frac{c}{C}$$

This expression corresponds to the two dimensional extent described by John (1962). Stacey (1968) refers to a joint property classification system proposed by Jennings which includes continuity divided into five categories (Table 2). The classifications shown in Table 2 were used in the DeBeers slope study (Piteau, 1970).

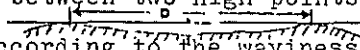
The relationship for effective cohesion given above was considered by Terzaghi (1962, p. 253) to be of theoretical interest only "...because, first, it is impractical to determine the value A_g for a given section through the rock, and second, for any given rock formation the value of c_i for sections approximately parallel to any given plane may have any value greater than zero." This dismissal of a relationship as "merely theoretical" because of measurement difficulties reflects an attitude which, if applied to soil mechanics, would negate much of Terzaghi's own work. Indirect approximations can, by empirical correlation, produce usable design data as has been demonstrated by the successful use of index properties in soil mechanics.

Table 2. Classification of Joint Properties (After Jennings, in Stacey 1968).

JOINT PROPERTY	Roughness of joint faces*	Waviness of the joint for a 24in. base length +	Continuity of the joints	Gouge thickness	Hardness of joint material**		
					Soil	Rock	
C A T E G O R Y	1	Slickensided	> 2.0inches	8% cuts through joints, balance solid material	No gouge at all	Very soft	Very soft
	2	Smooth	1.0-2.0inches	16% cuts through joints, balance solid material	0-0.5 inches	Soft	Soft
	3	Defined ridges	0.5-1.0inches	33% cuts through joints, balance solid material	0.5-1.0 inches	Firm	Hard
	4	Small Steps	0.25-0.5inches	67% cuts through joints, balance solid material	1.0-2.0 inches	Stiff	Very hard
	5	Very rough	0-0.25inches	100% cuts through joints	> 2.0 inches	Very stiff	Very, very hard

Several joint properties are not included on this table: the strike and dip of a joint can be determined exactly; further descriptive properties are not divided into categories, e.g. joint type is recorded as B (Bedding plane), F (fault) etc., rock type as S (shale), SS (sandstone), Q (quartzite) etc. Gouge material is recorded similarly.

* Depending on rock type, each category is assigned a value for the friction angle e.g. for quartzite, categories 1 to 5 may have values 25°, 30°, 35°, 40°, 45°.

+ The waviness factor is defined as the offset d between two high points a distance D apart, a being adjusted proportionately for $D=24$ inches

 The value of the friction angle is increased according to the waviness e.g. for categories 1 to 5 in the table, 4°, 3°, 2°, 1° and zero respectively would be added.

** Recorded as S1, S2..S5 and R1..R5 respectively. Hardness is defined in everyday descriptions e.g. S1 (very soft soil) is "easily moulded in fingers; shows distinct heclmarks", R4 is "hand-held specimen breaks with hammer end of geological pick under more than one blow".

It is possible to obtain an estimate of two-dimensional continuity by measuring the continuity of the trace of a fracture on an outcrop or in an underground opening. Either a direct percentage measurement, the five-category classification of Jennings, or a simple three-category classification of continuous, broken, and discontinuous fracture can be used depending on the precision warranted.

Planarity. The degree to which a fracture approaches a true plane is the planarity. The effect of irregularities on the shear strength of a fracture has been studied in detail by Patton (1966). He showed by field and laboratory studies that for low normal stress the shear strength of a fracture could be represented by introducing the angular deviation (i) of irregularities into the Coulomb equation:

$$\tau = C + \sigma \tan (\phi + i)$$

Evidence from Patton's field studies indicated that first order irregularities (those with a length one foot or greater) were more important than smaller scale, second order, irregularities.

The measurement of irregularities by Patton's method of photographing the fracture and measuring the irregularity on a projection of the photograph is time consuming and difficult. A simple descriptive classification was proposed for the Kimbley pit study (Weaver and Call, 1965) consisting of three categories: planar, wavy and irregular. Deere (1964) had advocated a similar classification using the terms Plane, Curved and Irregular.

A five-category classification based on the maximum offset of a fracture between two high points, 24 inches apart, has been proposed by Jennings (1968). He defines the attribute as Waviness.

For small scale irregularities, less than one inch, or more descriptively, the roughness of a fracture surface, Deere (1964) has proposed the terms Slick, Smooth and Rough. Jennings has extended this to a five-category classification with the descriptive terms slickensided, smooth, deformed ridges, small steps, and very rough.

Termination. The manner in which a fracture ends is designated as the termination. The type of termination of fractures affects the geometry of a compound failure surface and the amount of intact rock in the failure surface. McMahon (1967) proposed the following classification:

- (1). Termination in rock
- (2). Termination against minor joints
- (3). Termination against minor and major joints
- (4). Termination against major joints
- (5). Anastomose
- (6). Feathering

This classification scheme requires differentiation between major and minor joints, a distinction which in many cases is not clear cut and cannot be made until after the mapping is completed and the data on the joints compiled.

A simpler classification used in the Tazadit slope study is as follows:

- (1). Termination in rock
- (2). High angle termination against another fracture
- (3). Low angle termination against another fracture
- (4). En echelon termination

Even with this simplification it was found to be difficult to apply in the field as individual fractures or fracture sets exhibited more than one type of termination.

Thickness. The distance between the walls of a filled fracture is the thickness. This is a rather self-evident parameter of a fracture. Intuitively it would seem logical that a fracture with a thick gouge zone would have a lower strength than one with a thin filling, although beyond a minimum thickness, the difference in thickness may have little effect on the strength on the basis that failure can occur along a plane which is independent of the total thickness.

Tightness. The measure of the amount of open space in a fracture is the tightness. This attribute has been proposed by Deere (1964) for describing rock drill cores. He advocated a simple classification of tight or open. If two pieces of core could be fit together with no gaps and there was no alteration or indications of water passage, the break would be classed as tight. Conversely, if the fracture walls could not be fit together and were stained or altered, it would be classed as open.

Compositional Parameters

A fundamental contribution to the shear strength of a fracture is the frictional resistance of the material on the sliding surfaces. The fundamental coefficient of friction for pure minerals is difficult to obtain as it is strongly dependent upon the smoothness and the cleanliness of the surfaces being tested, and upon the presence or absence of water (Horn and Deere, 1962; Coulson, 1970). This variation is

greatly reduced when natural joints or rough-sawn surfaces of rocks are tested. In general, the friction angle of rock surfaces falls in the range of 22° to 35° (Coulson, 1970).

Layered silicate minerals, the micas and clay minerals, show an appreciably lower friction angle than rock surfaces. Thus, the presence of alteration or clay gouge in fractures will have an important effect upon the shear strength.

The coefficient of friction of unpolished surfaces of massive silicates or rocks shows a slight increase in sliding friction with the presence of water. Shear tests on micas and clays show a reduction in shear strength between dry samples and saturated samples. Thus, for design purposes, the presence of water can be considered to have negligible effect on the shear strength of fresh unaltered fractures unless the rock is composed predominately of micas or clay minerals. For fractures filled with clay gouge or rocks composed of micas or clay minerals a lower shear strength must be used for saturated conditions.

Properties of Fracture Sets

Two or more reasonably parallel fractures constitute a fracture set. All of the attributes of single fractures can be applied to fracture sets as mean values or the predominant values.

Extent

Extent is a two-dimensional parameter for an individual fracture which can be extended to three dimensions for fracture sets. Thus, there can be an extent normal to the fracture set as well as parallel to the fracture set.

Continuity

The continuity parameter can also be generalized to three dimensions. As pointed out by John (1962), the continuity (which he calls extent) would be the number of square yards of fracture per cubic yard of rock.

Mean Attitude

The most rigorous method of estimating the mean attitude is by use of directional cosines (Whitten, 1966), thus:

$$\bar{u} = \frac{u_i}{N}$$

$$\bar{v} = \frac{v_i}{N}$$

$$\bar{w} = \frac{w_i}{N}$$

where:

N = number of fractures

u, v, w = directional cosines

This use of directional cosines requires that the attitudes be true vectors, i.e., lines with a sense. The normal to a fracture, which is the conventional method of describing the attitude of a planar feature, is an undirected line and is thus not a true vector. By assigning a direction (projection to lower hemisphere of the reference sphere, for example), directional cosines can be computed for fractures. Where the range of attitudes is less than 104° , Agterberg (1961) has shown that the mean attitude can be satisfactorily approximated by the arithmetic mean strike and arithmetic mean dip.

Dispersion

For N unit vectors, the length R of the resultant vector will approach N the more closely clustered the orientation of the vectors. Thus, the difference $N - R$ is a measure of dispersion (Watson, 1966).

A spherical normal distribution has been developed by Fisher (1953). On the basis of this distribution, statistical methods have been developed for analyzing vector orientation data (Watson, 1966, p. 736). Application to fracture set data is limited, however, as a symmetric, unimodal attitude distribution is required—a rare situation in jointed rock.

There is a theoretical objection to using the Fisher distribution for fracture set data. Fracture normals are axial and have no direction, thus they intersect the reference sphere twice. To limit the fractures to a single projection pole, a hemisphere is commonly used.

For limited ranges of strike and dip, the conventional variance and standard deviation can be computed for strike or dip. Mueller (1964) appears to have used this approach.

A joint dispersion index has been proposed by McMahon (1967) based on equal area fabric diagrams. The more dispersed the fracture sets, the larger the area a given concentration contour will cover. By measuring the per cent of the total area covered by a specific contour, a relative dispersion can be computed.

Spacing

Spacing is the distance between fractures measured along the normal to the fracture set. Commonly, the arithmetic average spacing is used to describe the spacing of fracture sets (John, 1962). As the distribution is strongly skewed toward smaller spacings, the mode is probably a better statistic for spacing.

The inverse of spacing, which is the number of fractures per unit distance along the normal, is sometimes used instead of spacing. The terms frequency (Price, 1966), intensity (Weaver and Call, 1965), and degree of jointing (John, 1962) have been applied to the inverse of spacing.

Properties of Rock Mass

The following parameters apply to the entire rock mass.

Fabric

The term fabric (Gefuge) was applied to rock by Sander (1930). Turner (1948, p. 149) interprets Sander's use of fabric as "...all the structural and textural features of a rock as manifest in every recognizable rock element from the configuration of the crystal lattices of the individual grains up to and including large scale features which require field investigation." In this study, the concern is primarily with the large scale features as they are more significant with respect to rock mass strength.

Fabric is usually portrayed by plotting the poles of fractures and other structural features on a Schmidt Equal Area Net, although other projections have been used (Pincus, 1951, 1953; Piteau, 1970).

An initial step in the interpretation of fabric diagrams is to establish if the fracture pattern is anisotropic (has preferred orientation) or is random. Often the clustering of points is so pronounced that preferred orientations can be determined upon inspection. When there is doubt, statistical tests can be applied.

Winchell (1937) used a Chi square comparison between the sample pattern and a random pattern based on a Poisson exponential random model. Chayes (1946) applied a correlation coefficient test comparing unit area counts with adjacent unit areas. Pincus (1951), Spencer (1959), and Friedman (1964) have also used derivations from the Poisson exponential distribution as a test for nonrandomness. Discussions of these methods are given by Pincus (1953) and Chayes (1946).

As pointed out by Friedman, these tests do not take into account the specific orientations represented by points on a Schmidt diagram. Thus, girdle distributions, which are geologically significant, could appear random by these tests. Nonrandomness of a point diagram is not proof of nonrandomness of the true fabric. Sampling bias can give an apparent anisotropism. Proper sampling techniques can reduce this effect or, alternately, appropriate weighting of the sample data can remove much of the bias. Once an anisotropic fabric pattern has been established, the objective of a conventional petrofabric study is to interpret the preferred orientations in light of the geologic history of the area, or, conversely, to make inferences on the stress and displacement history from the fabric pattern.

According to Friedman, there are two approaches to the interpreting of rock fabric, the kinematic and the dynamic. The kinematic

approach utilizes chiefly symmetry to infer the orientation of displacements. The dynamic approach considers the stress-strain relationships of rock to establish the stress history.

Because of the complex history of many areas, and in particular mining districts, the interpreting of fabric diagrams is often unsuccessful or uncertain. From the engineering standpoint, the past history of a rock mass is useful only as a prediction of future behavior. In general, fractures represent planes of weakness so that the fracture pattern or fabric determines the most likely failure geometry. Emery (1966) has challenged this claiming that faults and other fractures are zones where stress has been relieved and failure is more apt to occur in unbroken areas where unrelieved residual stresses are greatest. This may have some validity in underground openings where the stresses approach the rock substance strengths, but in the author's experience in open pits where the stresses and confinement are much lower than the strength of the rock substance, failures are almost always associated with major faults and fracture systems.

Terzaghi (1962) questions fabric studies for slope design. He argues that fabric studies are of limited use as failure may occur on a random, undetected fracture. Mueller (1964) counters this on the basis that application of probability statistics will give information on fracture attitude distributions from which satisfactory engineering conclusions can be drawn.

Unit Rock Block

An attribute of the rock mass advocated by John (1962) is the unit rock block which is the smallest intact rock unit produced by fracture systems. He defines it for a rock mass with three fracture systems as:

$$V = (d_a) (d_b) (d_c)$$

where:

d = distance between fractures

John does not say how it would be calculated where there are less than or more than three fracture systems.

Rock Quality Designation

Core recovery is a function of intact rock strength, fracture spacing, orientation and strength as well as drilling methods. It is, therefore, an indirect measure of overall rock mass strength. A modified core recovery, the percentage of core in pieces greater than four inches, is used by Deere (1968) as an index of rock strength. He refers to this as Rock Quality Designation, or RQD.

Since core recovery is also a function of core size and drilling methods, Deere recommends that 1 1/2" or larger double wall core barrels be specified and the drilling be closely supervised.

The angle at which the drill hole intersects a fracture set will affect the RQD. A drill hole intersecting a fracture set obliquely will have a greater apparent fracture spacing than a drill hole normal to the same fracture set. Thus, the intersection angle should be noted along with the RQD.

Joint Breakage

The joint breakage index proposed by McMahon (1967) is the percentage of joint faces exposed to the total area of an excavated surface or outcrop. During excavation, rock will tend to break along joint faces. If the joint strength is high, there will be a greater percentage of breakage through intact rock, thus the joint breakage index is a measure of joint strength.

Joint breakage can be measured by a point counting system similar to that used in petrography. A surface exposure can be measured using a transit. The cross hairs are moved at intervals across the exposure, and at each point it is noted whether a joint face or broken rock face is observed. For underground openings, measurements can be made along a tape stretched along the rib. McMahon (1967) states that 200 points are sufficient to give a $\pm 5\%$ reproducibility.

Either regular or random distances between measurement points can be used. McMahon used random distance for outcrops and regular distances for underground. Random distances would be preferable as a regular distance could correspond to a joint spacing which could bias the results.

The joint breakage index is also a function of the orientation. Where jointing is parallel to the face, a higher joint breakage index is obtained. Thus, the angle between the exposed surface and the nearest joint set should be specified along with the joint breakage index.

PART II

TAZADIT PIT SLOPE STUDY

CHAPTER 4

TAZADIT PIT

The Tazadit pit is located in the Kedia d'Idjil, Mauritania, West Africa near F'Derik, formerly Fort Gouraud (Figure 9). The Kedia is a triangular shaped inselberg composed of folded and brecciated Precambrian quartzites and phyllites surrounded by a plain of Precambrian granites, gneisses and quartzites. The highest point of the Kedia is 500 meters above the plain.

The Kedia is about 25 kilometers long and 10 kilometers wide. The center is composed of a large mass of brecciated quartzite bounded by a steeply dipping banded hematite quartzite (BHQ) formation on the north. Within the BHQ, which contains from 35% to 45% iron, are lenses of high grade hematite ore with a grade of 60% to 68% iron.

The presence of high grade iron ore was known since the early part of the century but, because of the remote location, was not seriously investigated until 1952. Exploration and development was conducted by MIFERMA and ore shipment started in 1963. Currently three pits are in production of which Tazadit is the largest, and several more are under development.

The Tazadit deposit consists of lenses of hematite in the north west corner of the Kedia (Figure 10). The ore body, which dips 60° to 70° to the southwest, is 1,000 meters long, from 100 to 200 meters wide, and extends to at least 500 meters in depth. The ore outcropped at the

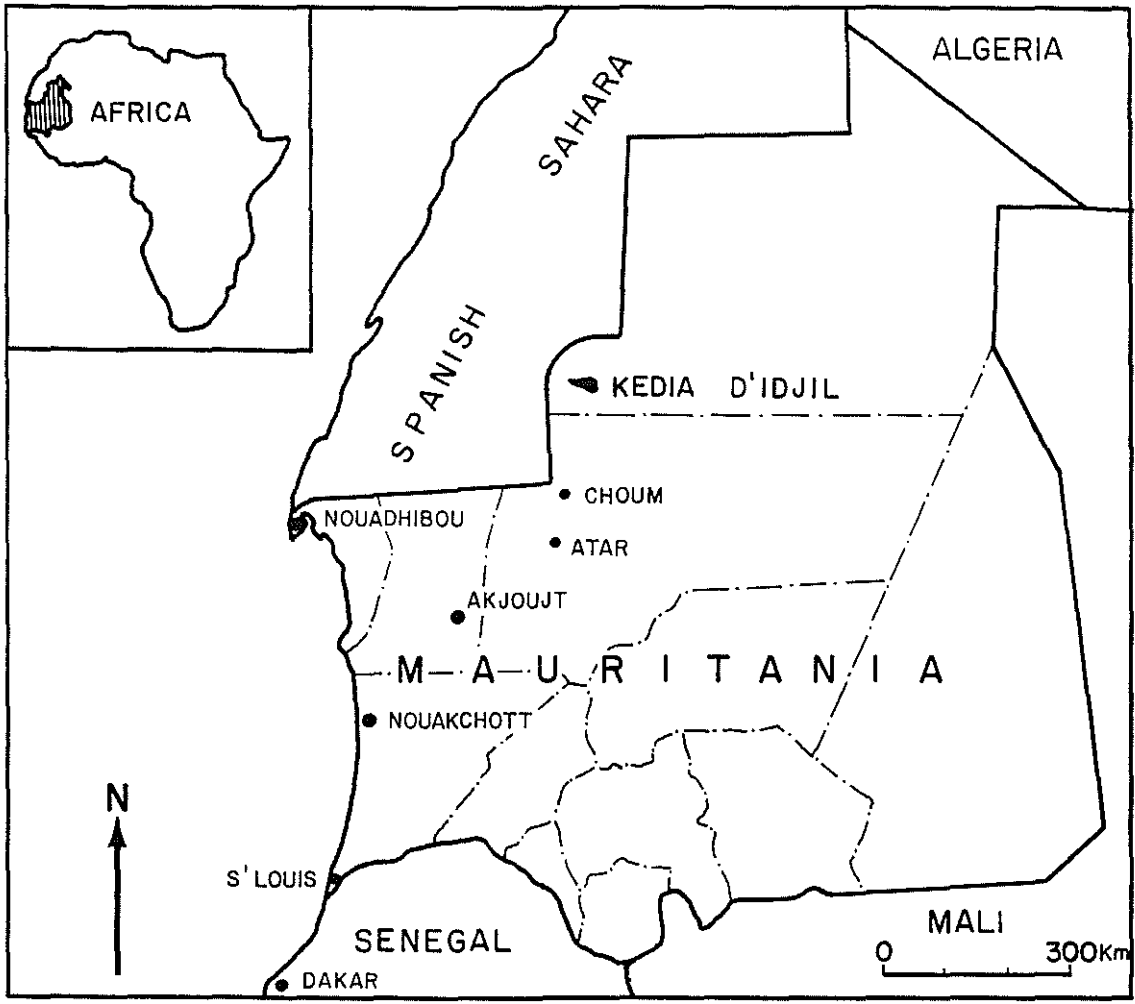


Figure 9. Location of the Kedia D'Idjil.

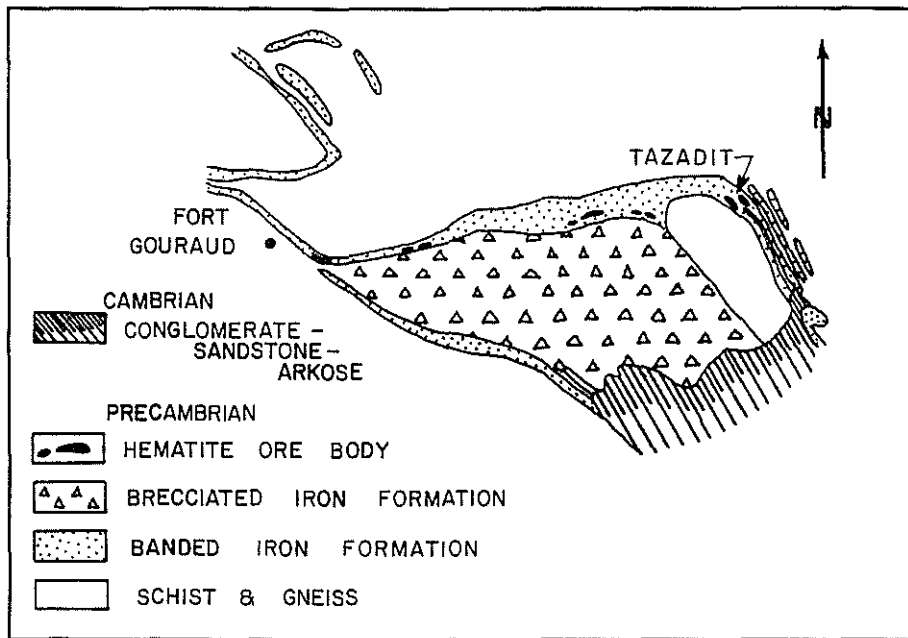


Figure 10. Generalized Geology of the Kedia D'Idjil.

surface forming a ridge with a maximum elevation of 726 meters. In January 1970 the pit had been mined to an elevation of 562 meters (Figure 11). Current production is about 4.5 million metric tons per year.

A pit optimization analysis by Reibell (1969) indicated that the final pit depth would be about 350 meters. Because of the steeply dipping, tabular shape of the ore body, the final pit depth and the profitability of the mine are strongly dependent on the angle of the final pit slopes. For this reason, the Tazadit Pit Slope Study was conducted to determine the optimum slope angles for the Tazadit Pit. The study consisted of detailed geologic mapping, core drilling, physical testing of core samples, large scale direct shear testing, plane shear stability analysis, and finite element analysis.



Figure 11. View of the Tazadit Pit Looking Northwest.

CHAPTER 5

GEOLOGIC INVESTIGATIONS

The basic objectives of the geologic investigations were as follows:

1. To determine if there are major zones of weakness such as faults or lithologic units unfavorably oriented for slope stability.
2. To determine the rock fabric. Fabric consists of the attitude, relative position and geometric characteristics of the structural features. The important structural features considered in this study are bedding planes, joints, faults and lineation.
3. To determine the subsurface lithology and structure for the finite element analysis.

Surface Mapping Methods

The exposed bench faces on the footwall (northeast) side of the Tazadit pit were mapped using a modification of the pit mapping technique used at the Bingham Canyon open pit in Utah, U.S.A.

A 1:1,000 scale pit map was used as a base map. Rock types, contacts, faults and other structural features observed on the bench face were plotted to scale on field sheets which were later transferred to a compilation map. The mapping was done by a team of two geologists;

one made the observations and measurements at the bench face, the other recorded the information on the field sheet. A total of 2.6 kilometers of bench face was mapped.

The attitudes (strike and dip) of the structural features were measured with a magnetic compass and clinometer (Tropochex or Brunton). This technique has been found to have an accuracy of $\pm 6^{\circ}$ for strike and $\pm 2^{\circ}$ for dip under field conditions.

Magnetic Declination

Magnetite in the pit area caused variations of up to 10° in magnetic declination from point to point in the pit. It was therefore necessary to map the variations in declination to correct compass readings. Declination values were obtained for 63 points in the pit by comparing compass readings with known geographic directions obtained with a theodolite from survey reference stations. From these observations an isogonic map was constructed (Figure 12).

The declination increases fairly regularly from the footwall to the hanging wall. Along the top edge of the pit on the hanging wall side, the declination is more variable and a consistent pattern was not established.

Magnetic compass readings taken during pit mapping were corrected for declination by referring to the isogonic map.

Fracture Set Sampling

Fracture sets were determined on the basis that three or more approximately planar parallel fractures constituted a fracture set.

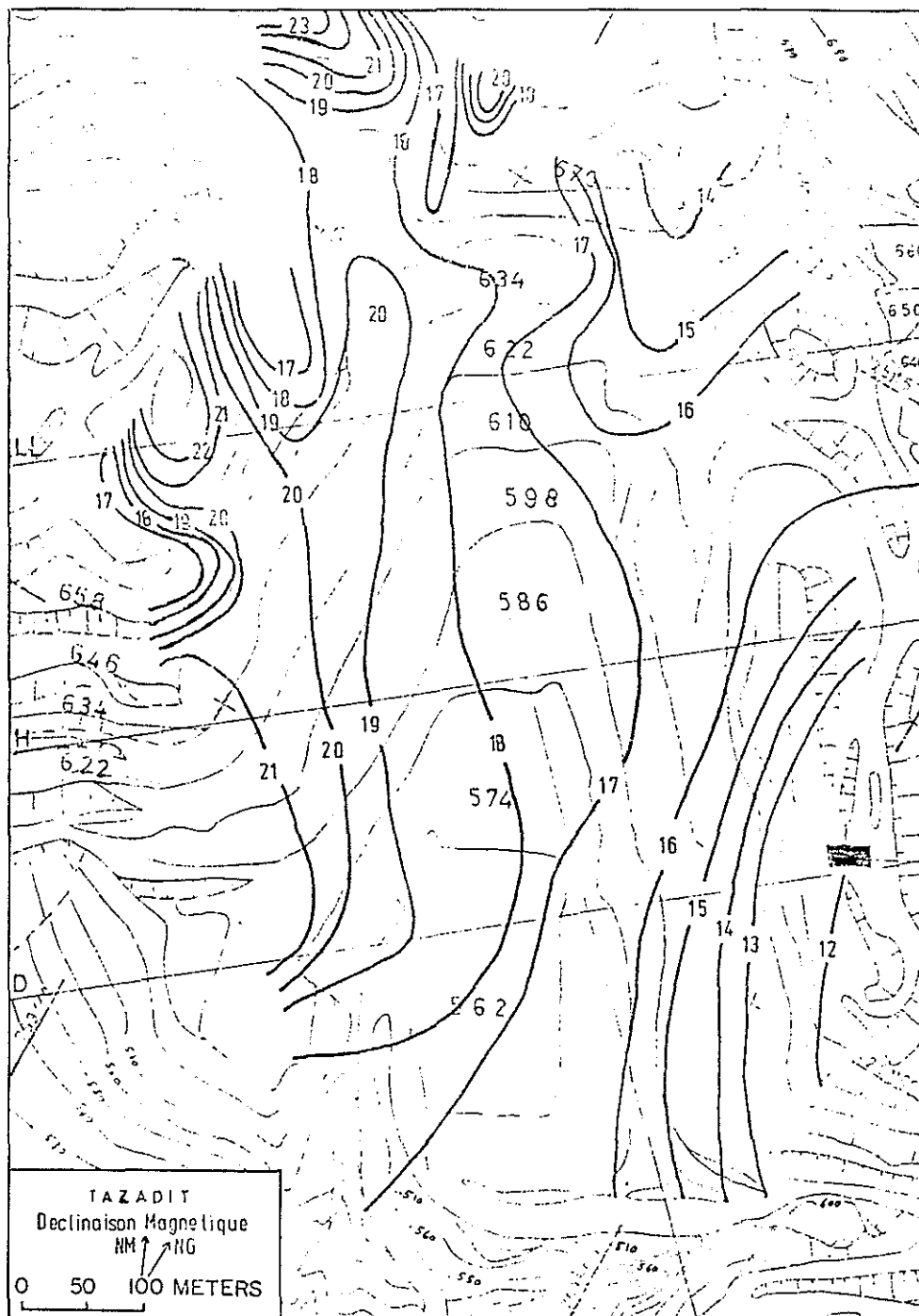


Figure 12. Isogonic Map of the Tazadit Pit.

If a fracture set consisted of bedding planes, it was recorded as bedding, otherwise it was considered to be jointing. Figure 13 illustrates the appearance of fractures in the pit face.

The mean attitude of each fracture set was measured and recorded on the field sheet with a standard geologic symbol.

The attitude and position alone is not sufficient to evaluate the relative importance and strength characteristics of planar structural features, therefore a tabular data sheet (Figure 14) was used in conjunction with the field mapping sheets to record additional information. This sheet allowed for systematic classification of properties and organization of data for computer processing. It also served as a check list to insure that all the information had been recorded for each structural feature. The following information was recorded on the sheets:

Location. The pit area was divided into 50 meter X 50 meter squares along the regional coordinate system. All the observations within a square were given the coordinates of the southeast corner of the square. This is sufficiently precise for statistical analysis and saves considerable time in measuring and recording locations.

Attitude of the Bench Face. The dip and the strike of the bench face at the point of observation were also recorded.

Rock Type. A numerical code for rock type was established and the number corresponding to the type of rock at the point of observation was recorded. When the structural feature was a contact between rock types, the two types were recorded.

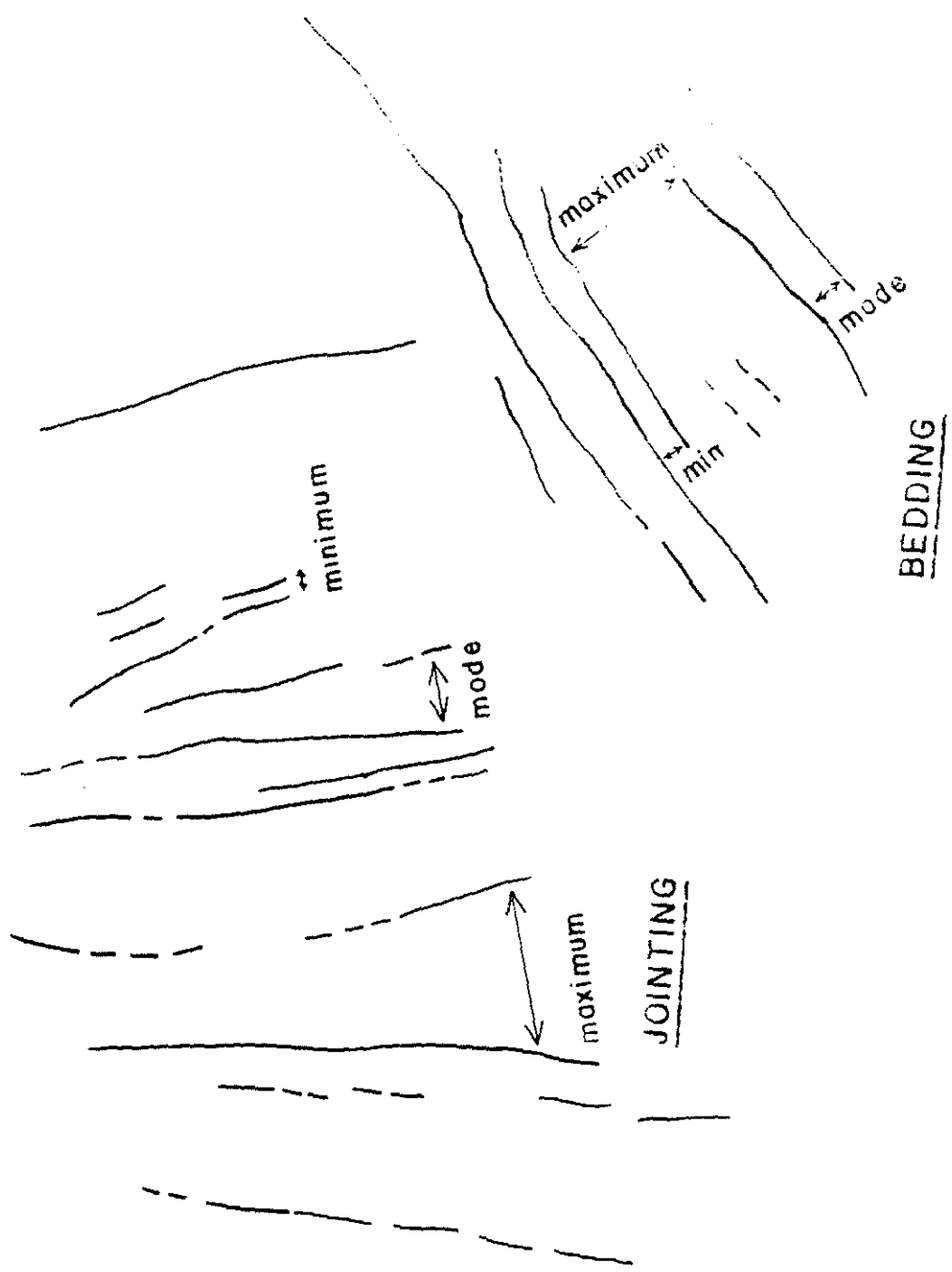


Figure 13 overlay



Figure 13. Appearance of Fractures in the Pit Face.

Type of Structural Feature. Bedding, jointing, faulting, breccia zones, shear zones, fold axes and lineation were the structure types recorded.

Geometry. The continuity, planarity, surface roughness and type of termination were recorded with a numerical code for the categories shown in Figure 15.

Spacing. The spacing (distance between fractures) was estimated by eye. Three values were recorded: the mode, the minimum and the maximum. An example of this type of measurement is shown in Figure 13.

Thickness. When a fracture such as a fault or breccia zone was observed to have an appreciable thickness, an average value was recorded.

Fracture Filling. Provision was made to record the type of fracture filling as it can be an important characteristic affecting fracture strength. It was found, however, that with the exception of fault gouge and some secondary oxide in near surface fractures, there was no significant fracture filling.

Detail Line Mapping

In contrast to the footwall where important stratigraphic differences occur, the hanging wall consists entirely of banded hematite quartzite (BHQ); therefore, a spot sampling technique was used to determine the fabric.

At each sampling point a measuring tape was stretched horizontally along the bench face. For every fracture with an extent

PIT TAZADIT

LEVEL 598

BY RC/PJ
DATE 10/3/70

PAGE 11

LOCATION		FACE		ROCK		STRUCTURE		DEC.	GEOMETRY				SPACING			THICKNESS	FILLING						OBSERVATIONS	N				
E	N	STK	DIP	T	T ₂	T	STK	DIP		C	P	R	T	MODE	MIN.	MAX		R	Q	O	X	A	D	O	G			
759.300	2511.150	151	75	24		1	168	71	17	2	2	2	2	20	5	80		V									10-3-70	1
759.350	2511.150			30		7	254	76	17									V										2
				30		1	131	72	17	3	3	1	3					V										3
759.350	2511.100			30		2	336	15	17	2	1	2	3	100	30	200		V										4
				24		1	112	72		1	2	2	3		1	30												5
		154	70																									
				30		1	172	72	16	2	2	1	3					V										6
				30		2	28	24	16																			7
				30		7	210	57	16																			8
759.400	2511.100			23		1	135	66	16	2	2	2	3	20				V										9
				23		8	201	62	16																			10
				23		8	278	59	16																			11
				23		2	300	20	16	3	1	2	4	15	5	20												12

TYPE OF ROCK					STRUCTURE			GEOMETRY													
10	BHQ	20	QTZITE	30	SCHT.	40	ORE	50	MIX	1	BDNG	5	SHEAR	CONTINUITY		PLANARITY		ROUGHNESS		TERMINATION	
										1	CONTINUOUS	1	PLANAR	1	SMOOTH	1	IN ROCK				
										2	JNTG	6		2	MICONTINUOUS	2	WAVY	2	ROUGH	2	> 20°
										3	FAULT	7	FD AX.	3	DISCONTINUOUS	3	IRREGULAR			3	< 20°
										4	BREC.	8	LIN.							4	

Figure 14. Fracture Mapping Data Sheet.

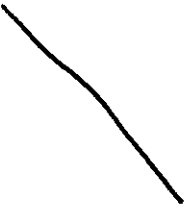
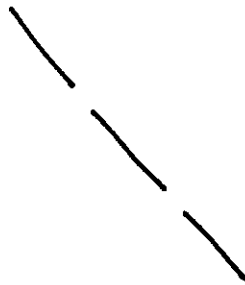
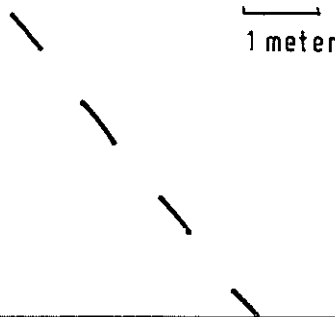
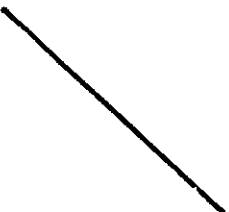
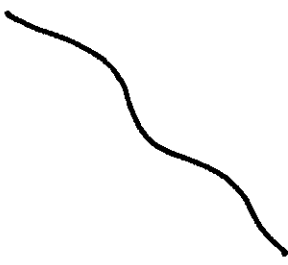
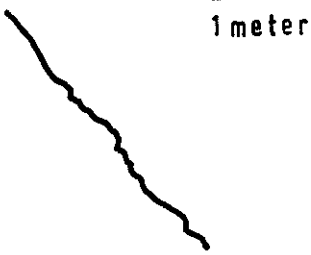
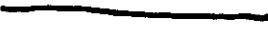
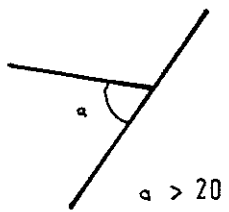
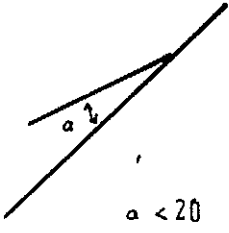
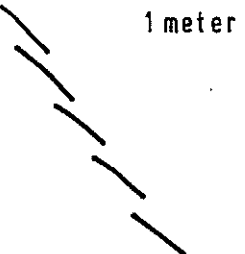
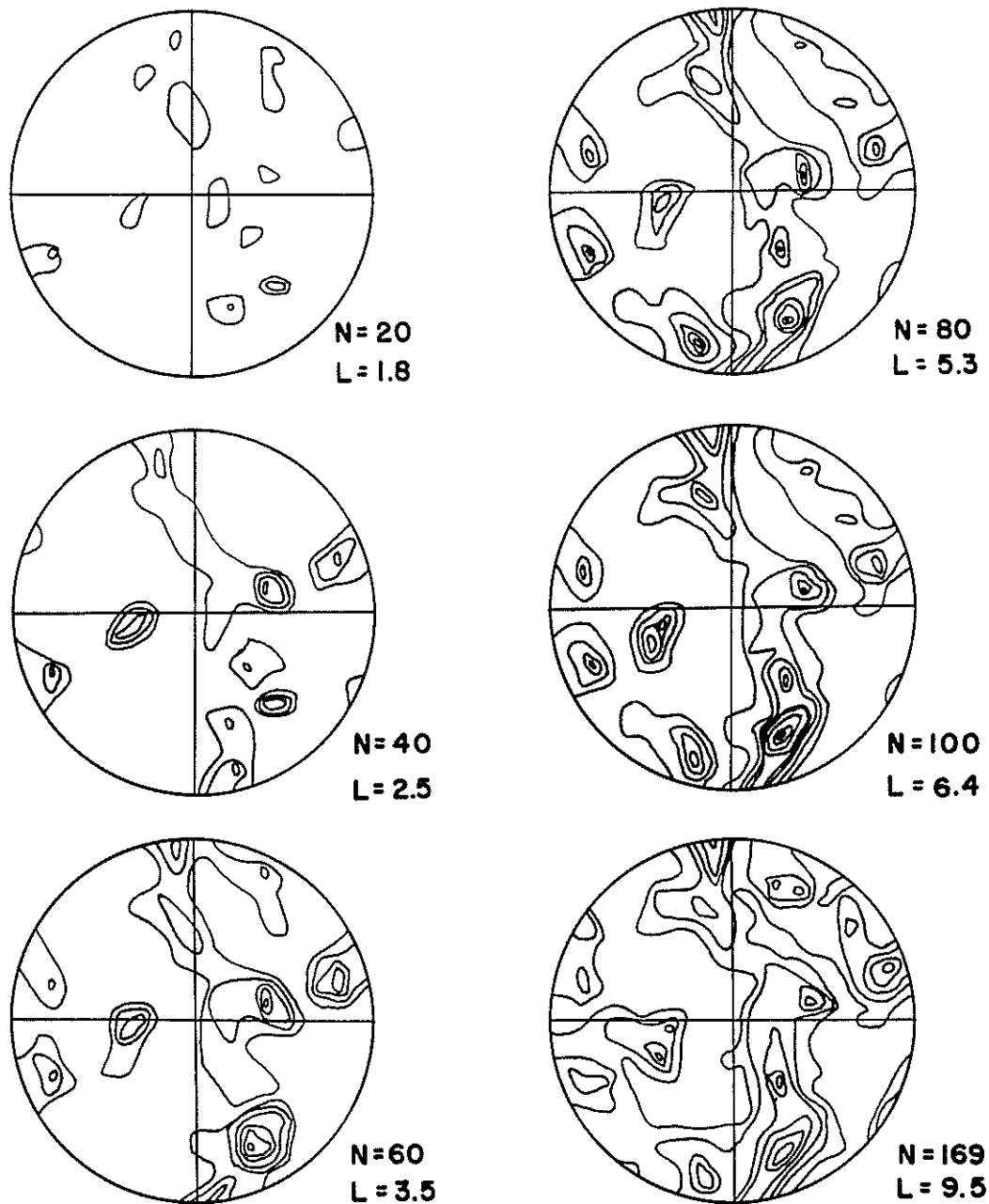
CONTINUITY			
CONTINUOUS	MICONTINUOUS	DISCONTINUOUS	
			
PLANARITY			
PLANAR	WAVEY	IRREGULAR	
			
ROUGHNESS			
SMOOTH	ROUGH		
			
TERMINATION			
IN ROCK	AGAINST CROSS FRACTURE		EN ECHELON
	HIGH ANGLE	LOW ANGLE	
			

Figure 15. Geometry of Planar Structural Features.

greater than 30 cm, lying in a zone 1 meter above and 1 meter below the tape, the following information was recorded:

- (1) The distance along the tape where the projection of the fracture intersected the tape. When the fracture was parallel to the tape, the point along the tape where the observation was made was recorded.
- (2) Rock type.
- (3) Type of structure.
- (4) Attitude of the fracture.
- (5) Geometry of the fracture. The classification of continuity, planarity, roughness and termination was the same as that used for fracture set mapping.
- (6) Thickness (when applicable).

Observations were begun at the end of the tape and continued along the tape until a minimum of 100 fractures was recorded. This resulted in a sample length between 10 and 15 meters. The choice of 100 fractures was based on the results of previous fracture studies which indicate that after about 80 observations the fabric is established and additional observations are beyond the point of diminishing returns. For example, Figure 16 shows the results of a sequential sampling of a detail line type sample from the Kimbley Pit Slope Stability Study. It can be seen that the increase from 80 observations to 160 observations, which doubled the work, produced only minor changes in fabric. A similar study by Pincus (1951) gave essentially the same conclusion.



N= number of fractures
L= length of line (meters)

Lower Hemisphere Equal Area Projection
1% Contour Interval

Figure 16. Detail Line Sample Size Test, Adit Data, Kimbley Pit, Nevada.

The detail line is an approximation of a point sample, therefore the smallest possible sampling area is desirable as increasing the area introduces the effect of changes in attitude in relation to position.

In addition to fracture observations, a minimum of 6 lineation measurements were made for each line.

A total of 10 detail line samples were taken. Although an attempt was made to choose the locations systematically, blasting in the pit limited the amount of exposed face and locations were therefore determined primarily by accessibility. Since the exploitation program is independent of the rock structure, the exposed faces at any one time approach a random sample of rock structure. Thus, the detail lines are reasonably representative of the structure of the hanging wall. The locations of the lines are shown in Figure 17.

To relate the fabric diagrams (Schmidt plots) with the appearance of the fractures in the bench face, photographs were taken and fracture sets represented by the major pole concentrations on the fabric diagram were identified on the photographs (Figure 18-24). Between the time the data was collected and the photographs were taken, the benches at the locations of Lines 4, 7, and 9 had been blasted; therefore, photographs of these lines are not included.

Compilation of Previous Work

For the area outside the pit, the geologic maps of Spindler (Plan No. 731, 1959) were used. After a review of the maps with the mine geologists and some spot checking, it was judged that the maps were accurate and that it was unnecessary to duplicate this work.

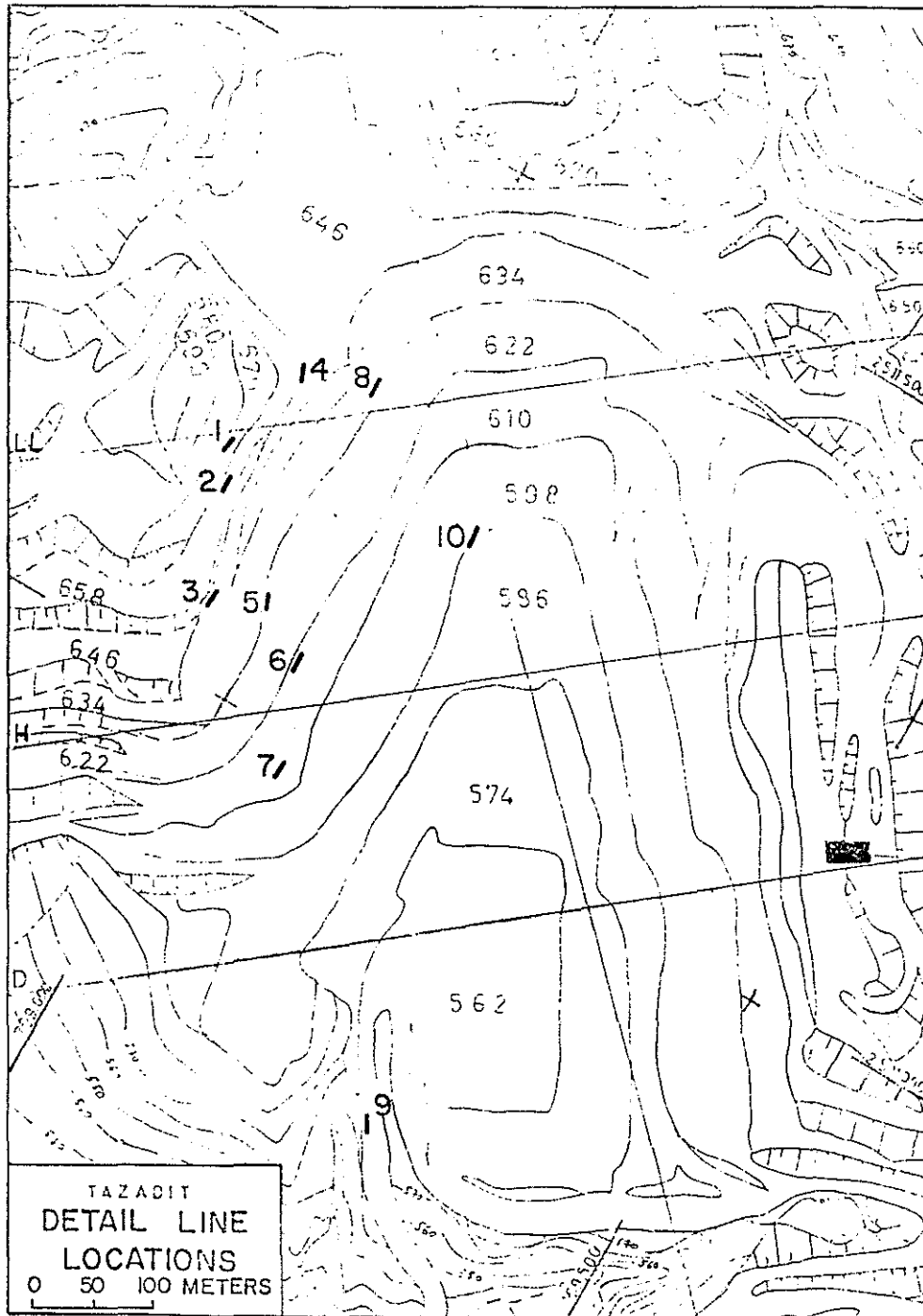


Figure 17. Location of Detail Line Samples.

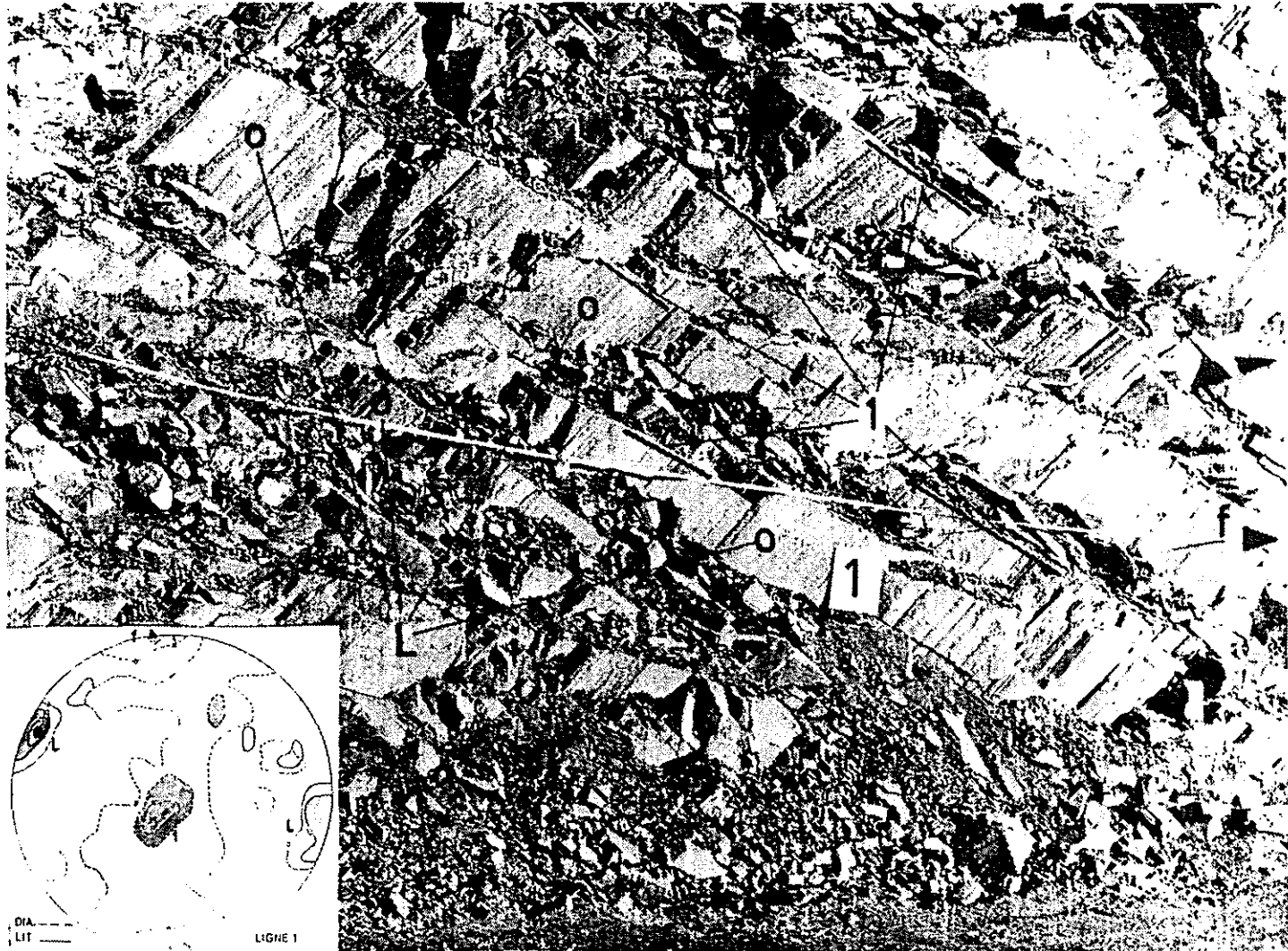


Figure 18. Detail Line 1.

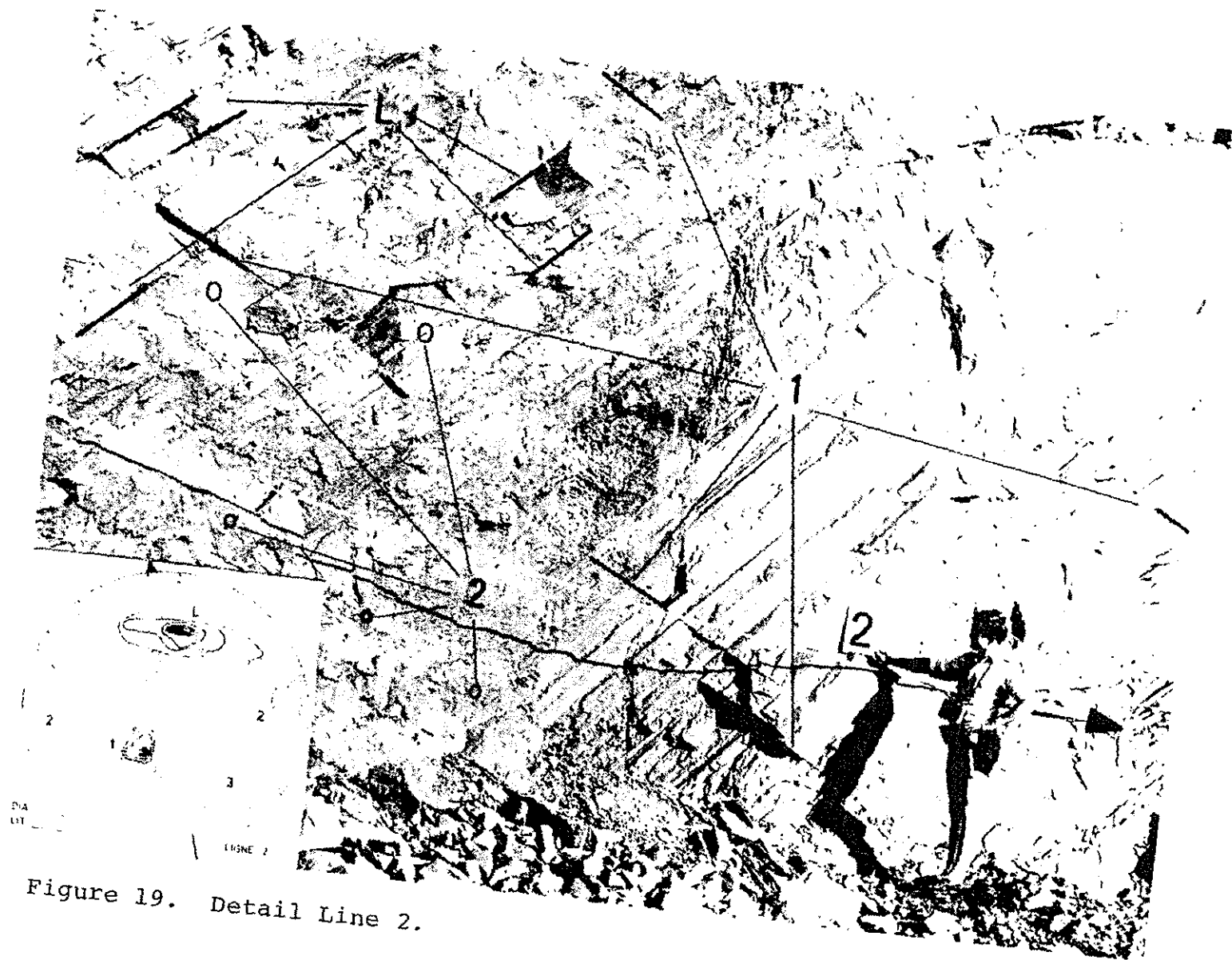


Figure 19. Detail Line 2.

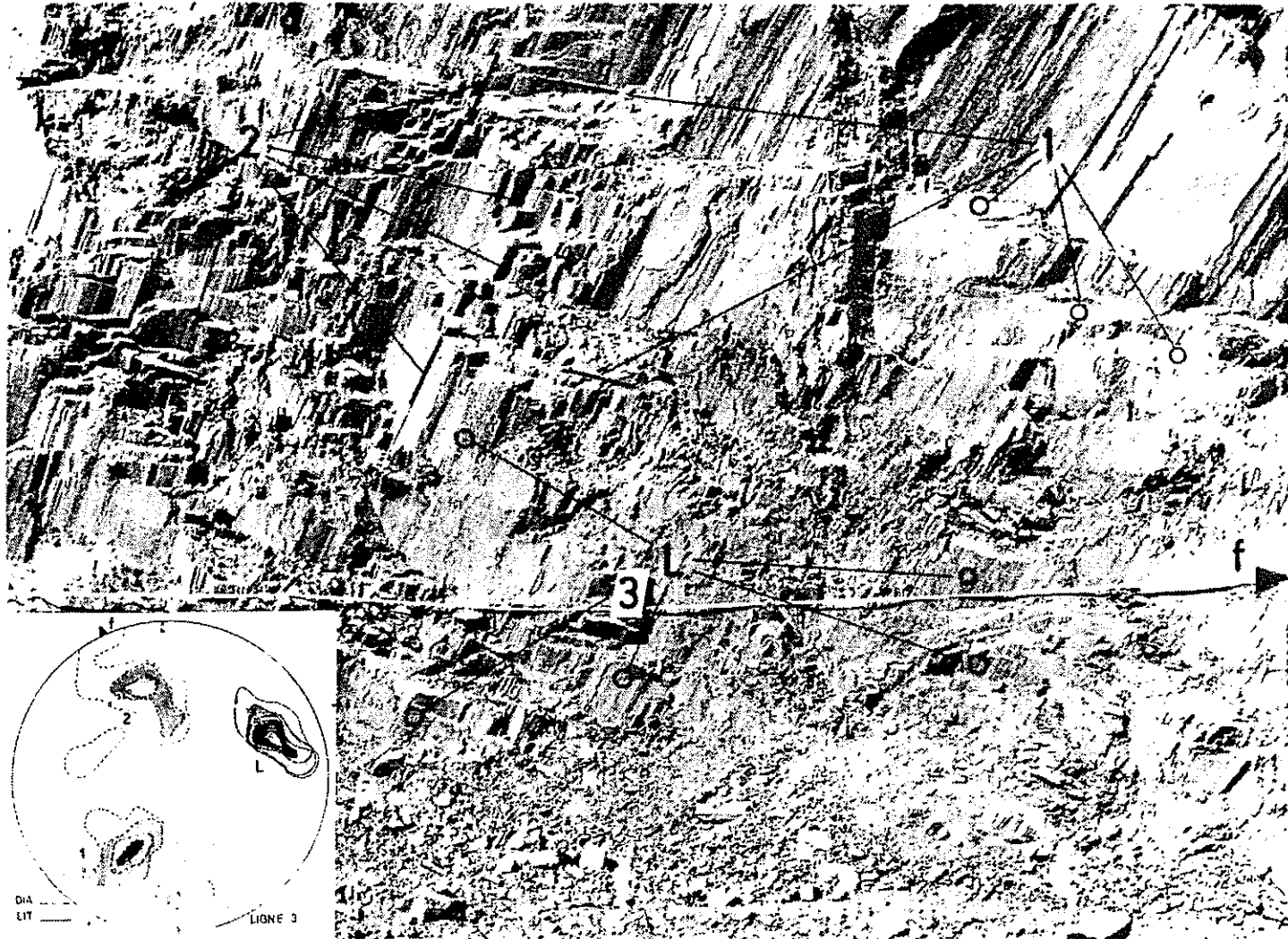


Figure 20. Detail Line 3.

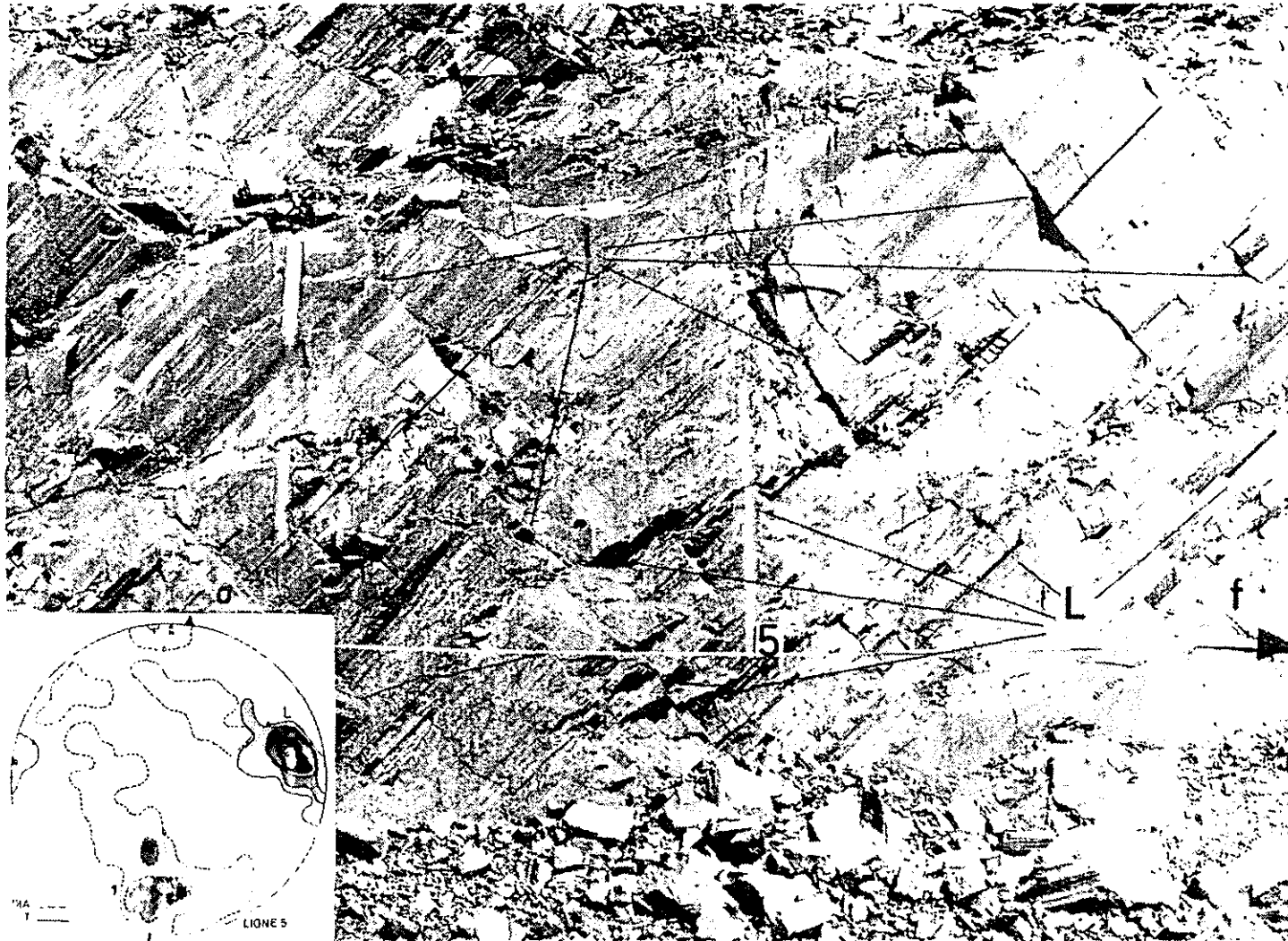


Figure 21. Detail Line 5.



Figure 22. Detail Line 6.

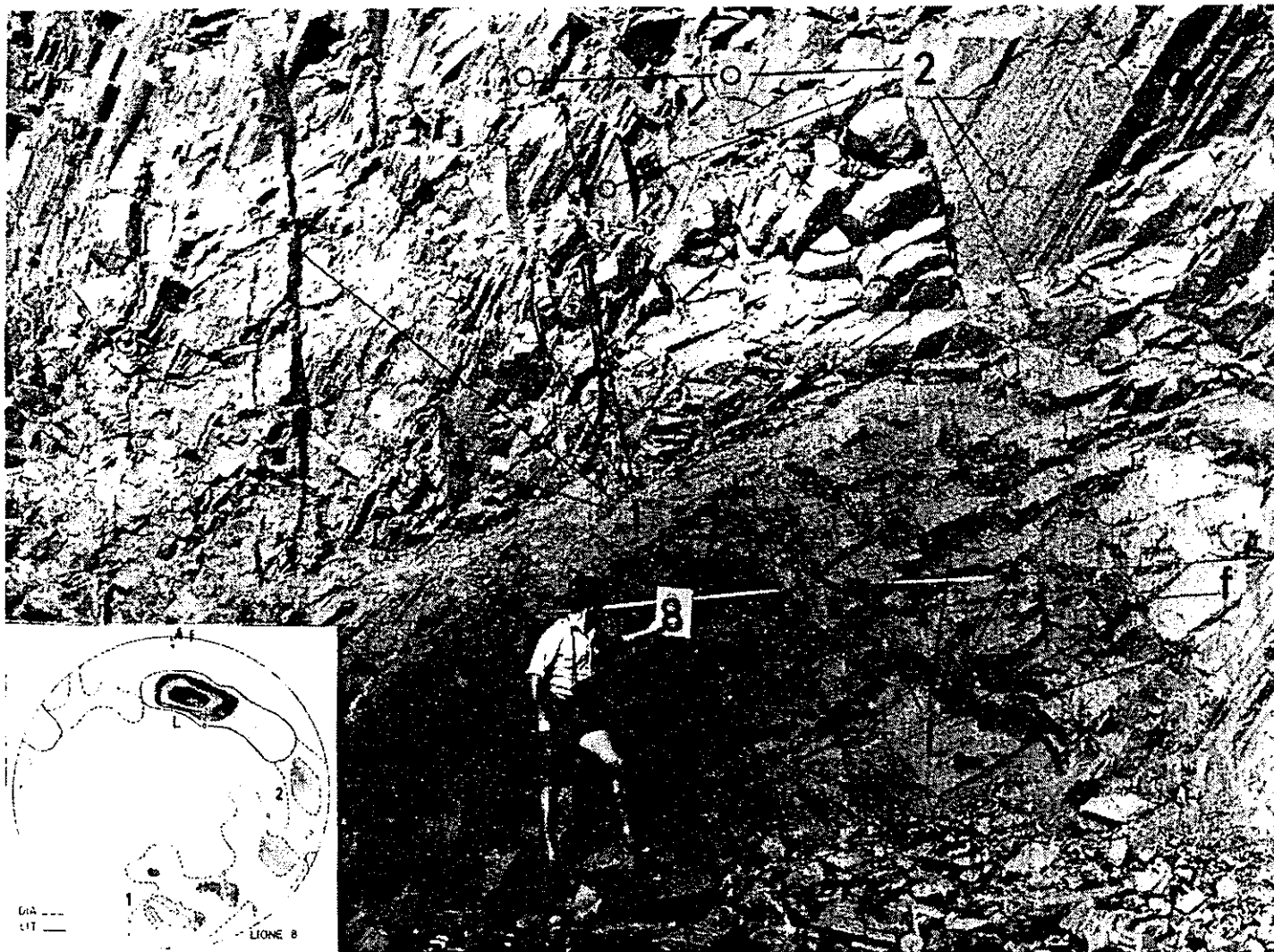


Figure 23. Detail Line 8.

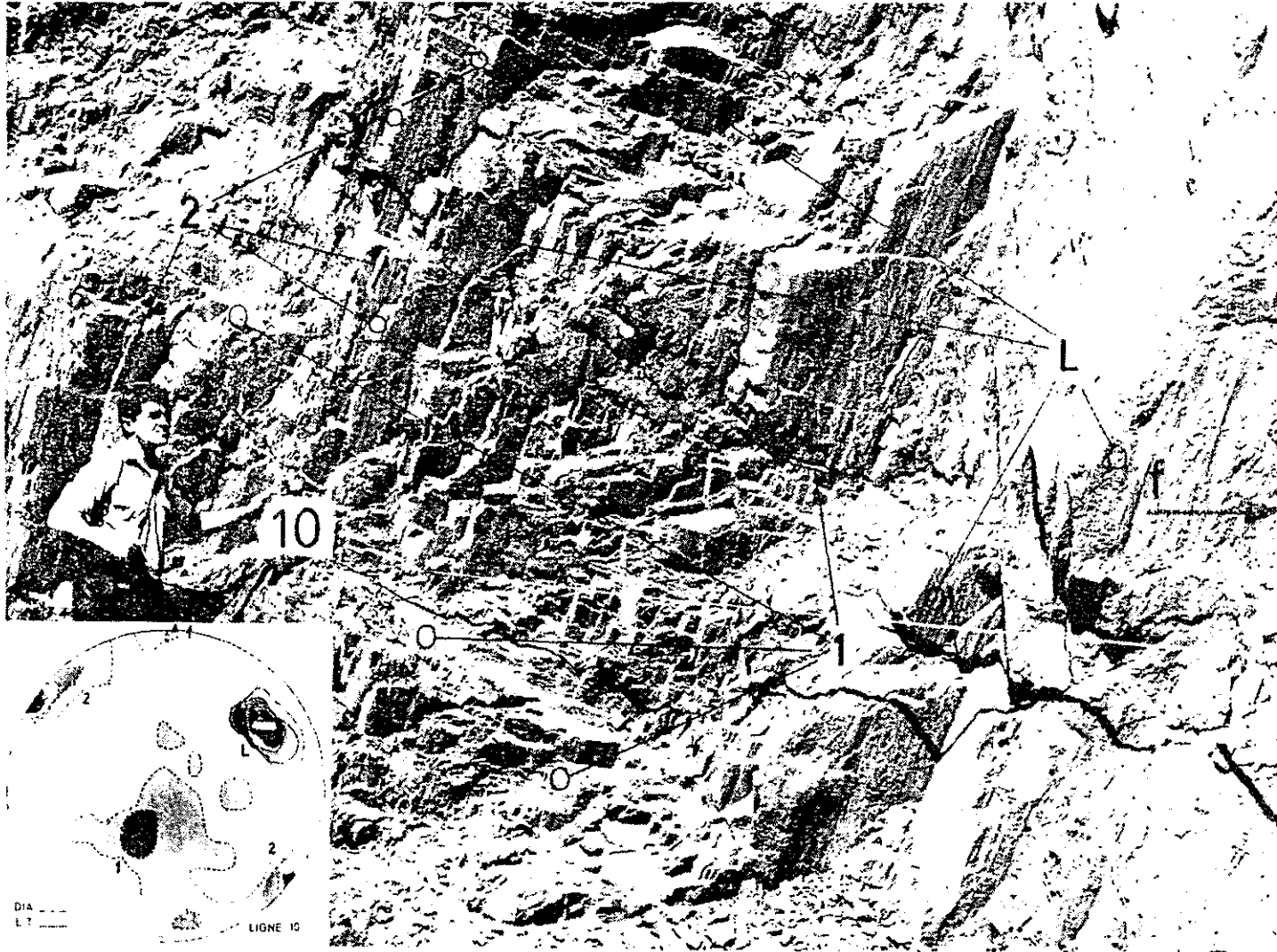


Figure 24. Detail Line 10.

Furthermore, much of the area is now covered with waste dumps and is therefore inaccessible. The observations of the attitude of bedding recorded on Spindler's map were compiled and put on cards for computer data processing.

The Geology Department assay maps and provisional geology sections were used to outline the ore body.

Subsurface Investigations

One of the most important aspects of the program was the determination of the rock type and the structure of the footwall. The objective of previous diamond drilling was to determine the extent of the orebody and the holes were extended only a few meters into the footwall. Thus, the footwall geology was known only by projection from limited surface exposures.

Five diamond drill holes were drilled in the footwall. The lengths ranged from 140 meters to 296 meters. In addition, a hole was drilled in the footwall to fill a gap in the previous diamond drilling pattern. A total of 1419 meters was drilled, of which 748 meters was HQ (64 mm diameter) and 671 meters was NQ (47 mm diameter). The location of the holes is shown on Figure 25.

The holes were logged for (1) rock type, (2) angle of intersection between bedding and the core axis, (3) percent recovery, (4) rock quality designation (RQD) which is a modified core recovery measure consisting of the percentage of the core greater than 10 cm, (5) drill pressure and speed, and (6) water loss. An attempt was made

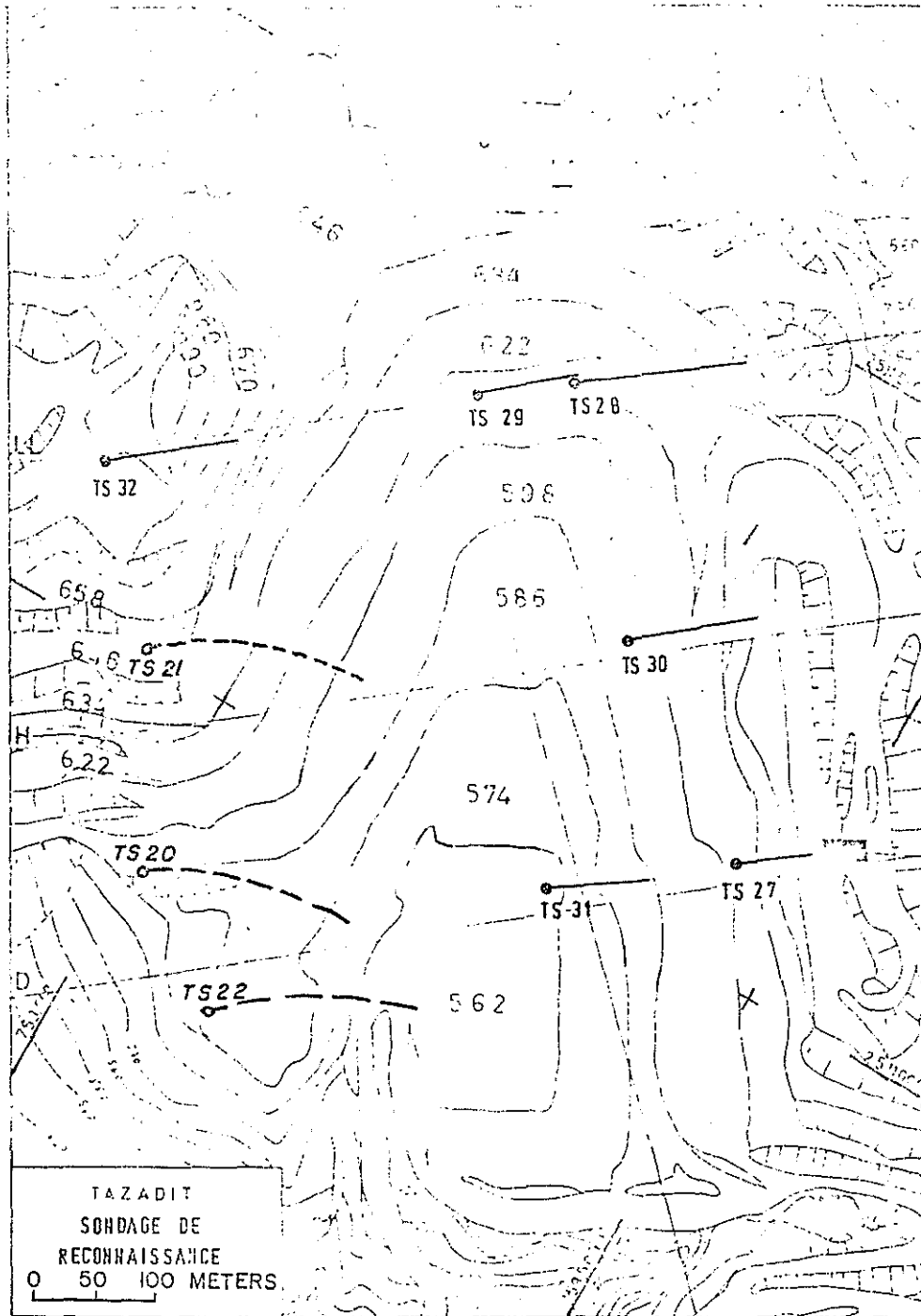


Figure 25. Location of Diamond Drill Holes

to record the hardness of the rock using an arbitrary scale of 1 to 4, but it was too subjective to be of much use.

Oriented Core

There are two basic techniques for obtaining fracture orientation from a drill hole; one is with a borehole camera, the other is with oriented core. Experience with a borehole camera during the Kimbley Pit Study revealed that the camera technique was time-consuming, expensive, and produced very poor information. During the preliminary planning of the Tazadit Pit Slope Study, it was decided to try the Christensen-Hugel Orienting Barrel system (Kempe 1967). Attempts to obtain the equipment from the Christensen Company were unsuccessful, however.

During the beginning of the study a simple technique for obtaining oriented core was developed utilizing available equipment and materials. A section of the Longyear wireline inner core barrel was filled with modeling clay and attached to an Eastman survey instrument. The device was lowered into a drill hole inside the drill rods and an imprint of the stub of core projecting into the drill rods was made in the modeling clay. After the section of core was drilled and pulled from the hole, the end of the core was fitted to the imprint and a reference line was drawn on the core parallel to an index mark on the Eastman photograph. The angle between the index mark and the vertical plane of the pendulum on the Eastman photograph, plus the direction and inclination of the hole obtained from a later Eastman survey of the drill hole provided sufficient information to orient the core.

The attitudes of fractures in the core were measured relative to the core axis and reference line. These attitudes were then converted to true dip and strike by rotation of the poles of the fractures on a stereographic projection. The fracture type and attitude were tabulated for computer data processing.

The technique was not developed until after hole TS 27 was completed. In the remaining 5 holes, 18 successful imprints were made giving a total of 127 meters of oriented core. From this oriented core, 362 attitude observations of bedding, joints and lineation were obtained.

Drill Hole Survey

All of the drill holes were surveyed using an Eastman survey instrument. This is a rapid and accurate system; however, the horizontal reference for the Eastman is a compass which is affected by changes in magnetic declination. Therefore, the holes were also surveyed with a Craelius instrument which uses oriented rods for a reference. There were only a few degrees difference between the Eastman and Craelius surveys of TS 27 and TS 28 after correction was made for declination. For TS 29, the difference was greater but it was probably caused by water in the hole affecting the Craelius. Malfunctioning of the Craelius prevented surveying of TS 30 and TS 31. The magnetic declination in the footwall is fairly regular however, and the Eastman survey was considered sufficiently accurate. TS 32 was surveyed with both instruments and there were differences up to 30° between the Craelius and Eastman directions. Because of the variable magnetic declination of

the hanging wall, the Crealius directions were considered to be more accurate at this location.

Core Samples

Samples of the core were collected to determine the density and mechanical properties of the rock, and for petrographic studies. The details of the sampling and the results of the tests are discussed in Chapter 6.

Previous Drilling

Several of the previous exploration diamond drill holes (TS 20, TS 21, and TS 22) penetrated the hanging wall. The logs were reviewed and the available core was examined. Samples of TS 22 were taken for density and mechanical properties tests. The location of the holes is shown on Figure 25.

Lithology

The rocks of the Tazadit pit consist of a metamorphic series of banded hematite quartzites (BHQ), phyllites, quartzites, quartzophyllites and micaceous quartzites of Precambrian age. The ore is a relatively pure hematite produced probably by desilicification of the banded hematite quartzites.

Field Classification

During his mapping of the surface geology of the Kedia d'Idjil, Spindler developed a detailed classification of the rocks. The BHQ, which is well exposed and of primary interest for mineralization, was

subdivided into a large number of facies. Quartzites and schists, because of their lesser importance and because they are relatively poorly exposed on the surface, were lumped into several simple categories. From the point of view of rock mechanics this classification is not satisfactory as there is little or no difference in the mechanical properties of the different facies of BHQ, whereas the schists and quartzites have definite major differences in mechanical properties. Thus, a simplified classification of rock types for use in field mapping was developed. The criteria used was ready identification in the field, division into units which had definite differences in mechanical properties, and when possible characteristics which would serve as specific stratigraphic markers. The following are the rock types utilized for field mapping and core logging.

Banded Hematite Quartzite. The BHQ consists of alternating beds of pure, white quartzite and beds of hematite or quartzite with a high percentage of hematite. The thickness of the individual beds ranges from several millimeters to one or two centimeters. Where the bedding is well developed, the white quartzite beds and dark hematite beds present a striped appearance. Such rock has been referred to as "zebrite" by the Miferma geologists.

The other extreme facies of the BHQ, which has been called the "jasperoid", has no developed bedding. The hematite is uniformly distributed in a fine-grained quartzite.

Between these two extremes there are varying degrees of bedding development. Complex micro-folding of the beds is common; both flexure

slip and slip folding are present (Figure 30). The hematite beds are less competent than the quartzite beds and under extreme cases of deformation, the quartzite has broken into fragments with rotation and displacement. Some quartzite beds are stretched into elongate stringers or augen. The iron content of the BHQ ranges from 35% to 45%.

Schistose Banded Hematite Quartzite. The schistose BHQ is similar to the regular BHQ except for the presence of intercalated beds of schist. In the extreme cases, the schistose BHQ consists of alternation of schist beds and quartzite beds rich in hematite. The schist is a fine-grained rock with a dark red color and occasionally contains phenocrysts of hematite and sometimes garnets. The schist beds tend to be somewhat thicker than the quartzite or hematite quartzite beds, now and then reaching a thickness of 10 cm to 15 cm (Figure 29).

Quartzite. The quartzite is dense, white, with a fine-grained granoblastic texture. The quartz content is 80% or greater. Bedding is obscure. (See Figure 27.)

Micaceous Quartzite. The micaceous quartzite is a quartzite containing 15% to 20% mica.

Schist. The fine-grained schist is composed of biotite and muscovite. The petrographic study by Bronner (1970) established that the schist is more properly classified as a phyllite. The term schist was retained in this report, however, to agree with common usage in the district.

Quartzose Schist. The quartzose schist is a quartzo-phyllite containing about 50% quartz.

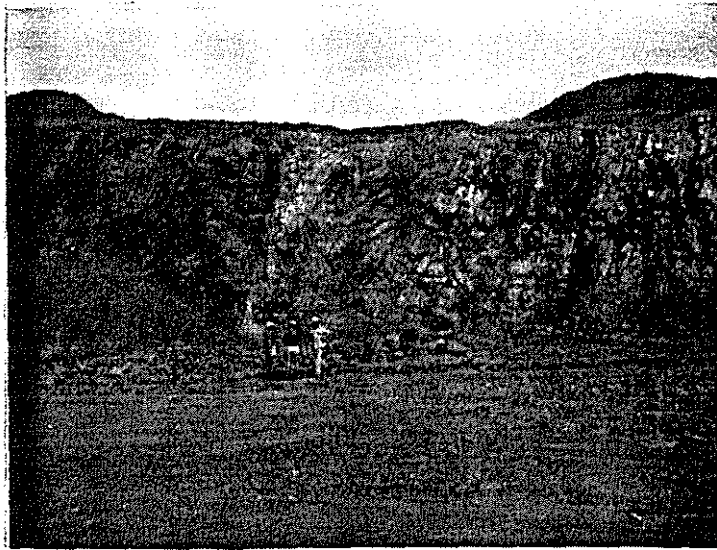


Figure 26. Footwall Contact Between Ore and Schist.

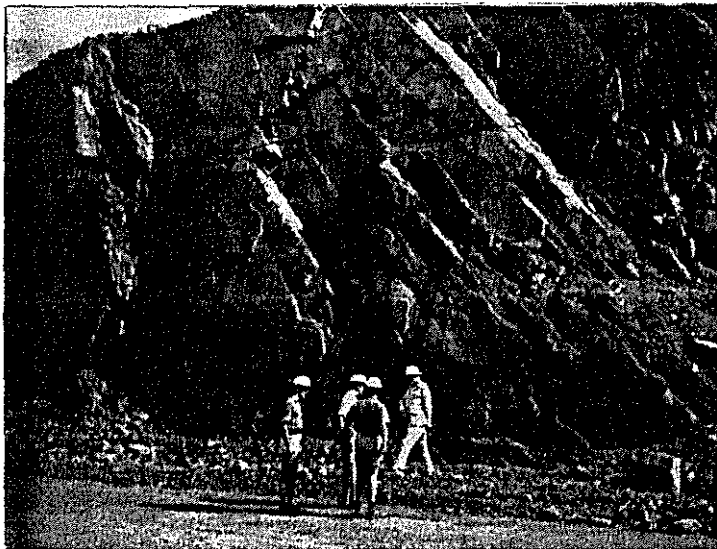


Figure 27. Quartzite, 586 Level, Footwall.

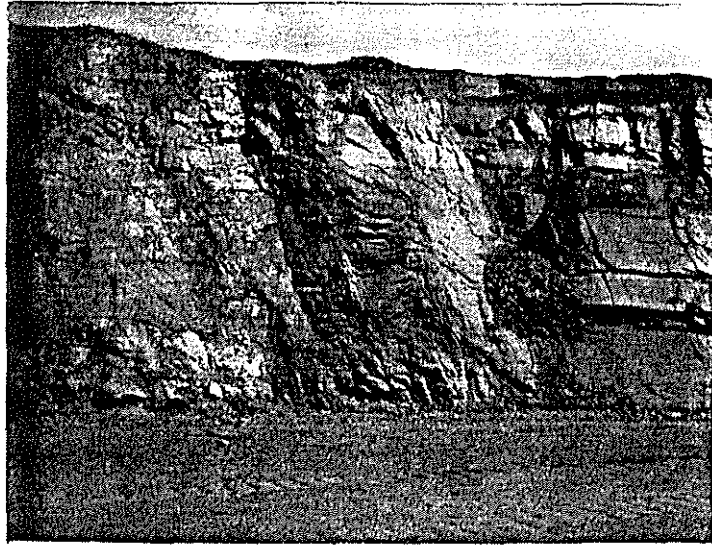


Figure 28. Folding of Schist and Quartzite, 586 Level, Footwall.

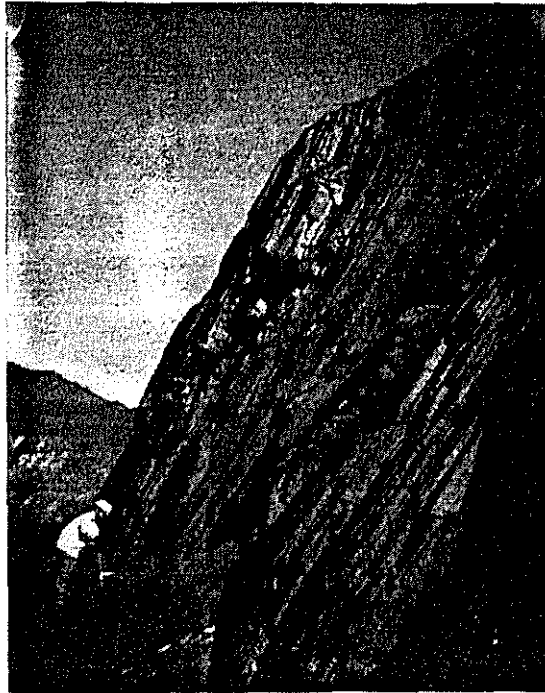


Figure 29. Schistose BHQ of the Footwall.



Figure 30. Microfolding of BHQ.

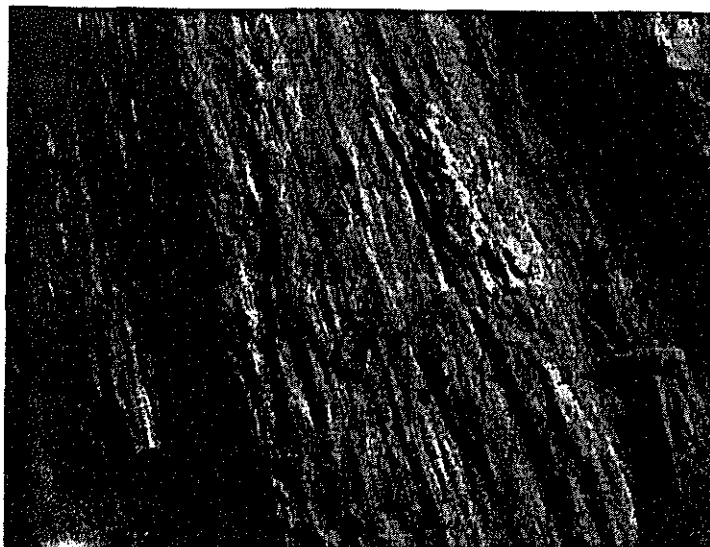


Figure 31. Lamination in the Footwall Quartzite.

Garnet Schist. The garnet schist is a phyllite containing altered crystals of the garnet almandine.

Schistose Quartzite. The schistose quartzite is a quartzite containing distinct beds of schist several centimeters thick.

A detailed petrographic description of representative samples of rock types from drill core was made by Bronner (1970). He recognized an additional rock type, bedded quartzophyllite, consisting of alternating beds of quartzite and phyllite. Because of the strong resemblance to BHQ, it was classified as such during field mapping and core logging.

Stratigraphy of the Footwall

With the information from surface mapping and diamond drilling it was possible to work out a rough stratigraphy of the footwall. Because of folding, the thickness of the units is quite variable and in several locations the same bed was observed repeated a number of times in the bench face. The lower contact of the schistose ore of the footwall appears to be the most consistent and recognizable stratigraphic horizon. Below the ore footwall contact the sequence is as follows:

- (1) schist containing a BHQ unit (2 to 10 meters)
- (2) schistose quartzite (often micaceous) (6 to 20 meters)
- (3) garnet schist with a thin irregular BHQ bed (6 to 16 meters)
(probably the bedded quartzophyllite of Bronner)
- (4) a second quartzite, often brecciated (5 to 16 meters)
- (5) a garnet schist (2 to 8 meters)
- (6) a third quartzite unit (3 to 7 meters)
- (7) a thin BHQ unit, probably bedded quartzophyllite (0 to 3 meters)
- (8) schist (2 to 9 meters)
- (9) a fourth quartzite (3 to 4 meters)
- (10) a thick schistose BHQ unit containing a thin bed of hematite
("the serpent"). (37 to 93 meters)

Below the BHQ is more quartzite and schist which may be a repeat of the first series but there is insufficient information to determine this. On the surface, to the northeast of the second series of quartzites and schists, there is a thick BHQ unit similar to the hanging wall BHQ.

General Geologic Structure

The Tazadit ore body is situated in a flexure of the BHQ formation which forms the north edge of the Kedia d'Idjil. The BHQ formation is isoclinally folded and dips steeply to the southwest. West of the Tazadit area the trend of the formation is east-west; to the east of the Tazadit area the trend is northwest-southeast. The flexure is just to the west of the Tazadit ore body, so the trend of the formation in the pit is predominantly northwest-southeast.

Folding

The folding is predominantly of the flexure slip type with much thickening, thinning, and doubling of the stratigraphic units. No definite stratigraphic marker horizons or age relationships have been established, so the interpretation of the folds as anticlines or synclines is speculative. As can be seen on the geologic map and sections (Figures 32, 33, 34 and 35 in pocket), the hanging wall BHQ is repeated to the northeast of the pit separated by the footwall quartzites and schists which Spindler interpreted as a faulted anticlinal fold. This interpretation would require a fold axis plunging to the northwest. The lineation and axis of the microfolding, mapped during the pit slope design study, plunge to the southwest, however. An

interpretation of the repetition of the BHQ as a synclinal fold with an axis plunging 50° to 60° to the southwest parallel with the fold axis mapped in the pit would be more logical. For slope design purposes it makes little difference whether the folding is synclinal or anticlinal; it could have some bearing on the relationship of the ore to the regional structure, however.

The definitions of structural features and the fold terminology used here are taken from Whitten (1966) to which the reader is referred for a full discussion.

Tectonism

In the study of the microstructure in the thin sections from core samples of the drill holes, Bronner (1970) recognized two phases of tectonism. The first phase consists of isoclinal folds of the bedding (S_0) with a fold axis (B_1), and an axial plane foliation (S_1). Because of the isoclinal nature of the folding, the angle between S_0 and S_1 is very small. The second phase of deformation was considerably less intense and resulted in open folding or kinking of S_0 and S_1 . These same tectonic features and relationships are observable on the macroscopic scale which support the interpretation of the microstructure.

Fabric

The significant structural features -- bedding, lineation and jointing -- are shown in Figure 36. Because of differences in technique and in location of the observations, separate plots were made for the original surface data of Spindler, the fracture set data of the footwall,

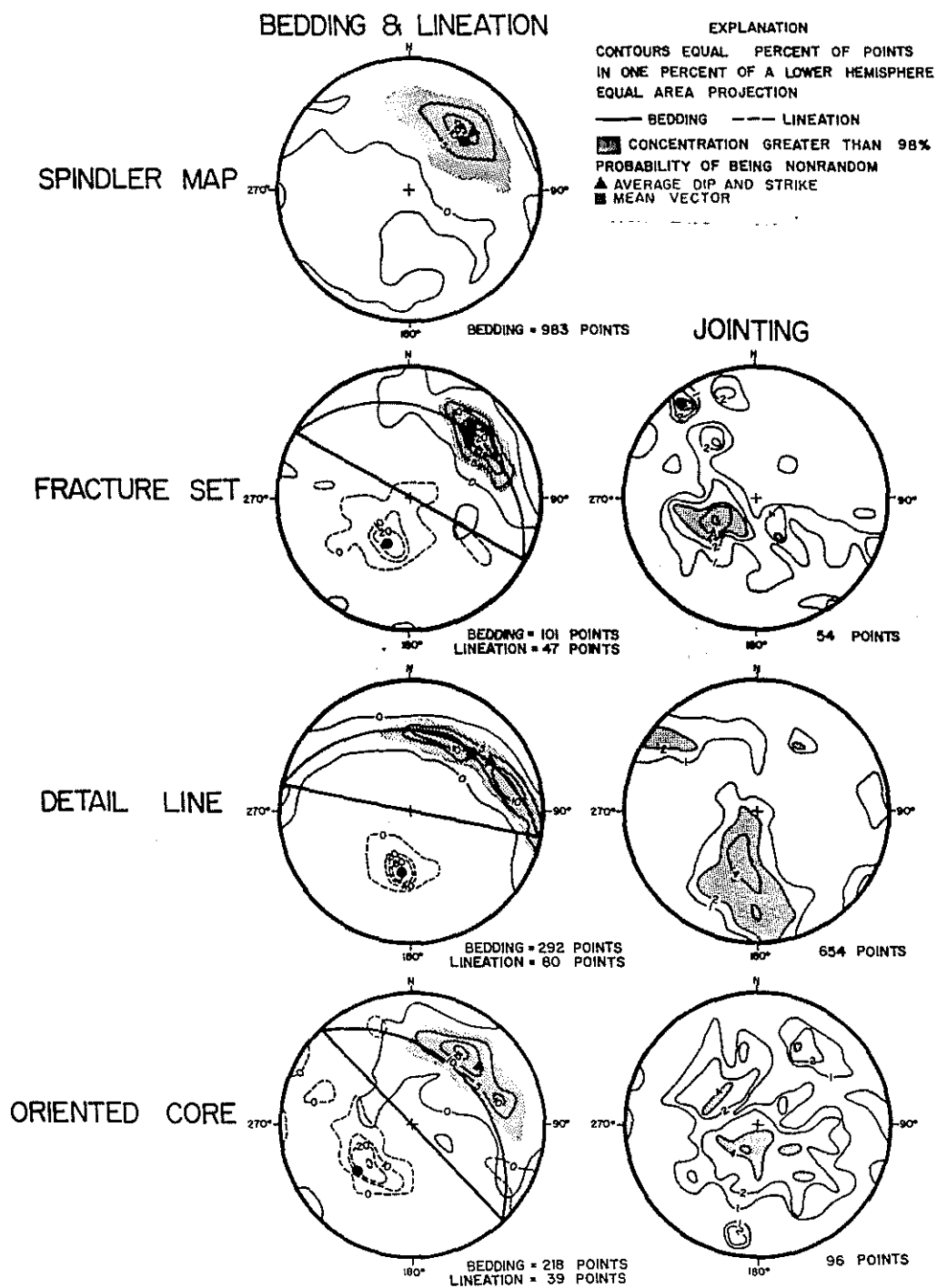


Figure 36. Fabric Diagrams of the Structural Features in the Tazadit Area.

the detail line data of the hanging wall, and the oriented core data from the drill holes.

The basic fabric shown in these plots is that of cylindroidal folding. The poles of the bedding lie on the great circle of the plane normal to the lineation. The lineation plotted on these diagrams represents the linear feature visible on exposed rock faces produced by the crenulation of the bedding, and also by the intersection of the bedding and the axial plane foliation. The lineation is parallel to the axis of small scale folding. Because of this parallelism, fold axes are included with the lineation although they were recorded separately during field mapping. This relationship between the lineation and the bedding is the π diagram (Sander 1942). The bedding would be the S surfaces and the lineation the B axis. The plane normal to the lineation is the ac plane of symmetry.

The bedding includes both the S_0 and S_1 planes described by Bronner (1970). The S_0 surfaces are referred to as bedding since they are thought to be primary sedimentary features, although it is possible they are pseudobedding resulting from tectonic deformation of the original sedimentary sequence. The intensity of phase one tectonism resulted in tight isoclinal folding and transposition deformation, therefore the primary axial plane foliation (S_1) is parallel with the bedding except at the crest of folds. S_0 and S_1 were not differentiated during pit mapping and the term bedding applies to both unless specified otherwise. In the BHQ, the S_0 is commonly contorted in multiple folds

from 1 to 10 centimeters and the S_1 foliation is the dominant through-going fracture system. In these cases the S_1 was mapped as "bedding".

Lineation

The lineation has a consistent southwest direction and a plunge between 50° and 65° . The folding can be considered to be primarily homoaxial, although there are statistically significant differences in the lineation observations. A summary of the mean attitude of lineation is shown in Table 3. An analysis of variance (Watson 1966), which assumes a Fisher spherical normal distribution, was applied to these data. The results of this test indicate that there is a significant difference in attitude between the fracture set total, the detail line total, and the drill hole total, although these differences are not large as can be seen in Figure 37. There are also significant differences between areas of the fracture set data, between individual drill holes, and between some of the detail lines. These differences can be the result of three factors: (1) a regional trend, (2) phase two tectonic deformation, and (3) sampling bias.

There is a suggestion of regional trend in attitude from east to west with the direction of the B axis becoming more southerly to the west and the plunge decreasing (Figure 38) as indicated by the difference between the B axis attitude of 212° direction and a 62° plunge for the footwall fracture set data and the B axis direction of 191° and a 53° plunge for the hanging wall detail line data. This trend also appears in the detail line data of the hanging wall. Detail line 10 has an orientation of 212° direction and 62° plunge, which is the same

Table 3. Mean Attitude of Lineation

Type of data	Number of Observations	Mean Vector			Mean Strike		Mean Dip	
		Strike	Dip	.05 cone of confidence	Strike	s	Dip	s
Fracture Set: area 1	10	207.7°	64.4°	7.0°	209.2°	17.7°	63.4°	8.0°
2	18	220.6	62.6	7.4	216.2	28.7	62.6	10.1
3	11	205.8	55.0	4.7	206.4	12.2	54.4	4.0
Fracture Set Total	39	212.2	62.5	4.2	211.6	22.9	60.5	9.1
Detail Line 1	8	188.7	52.4	5.0	188.6	10.6	51.9	2.3
2	7	189.0	52.2	5.0	188.7	8.7	51.9	3.1
3	7	192.8	47.9	2.7	192.9	3.6	47.9	2.2
4	10	185.3	52.3	1.9	185.3	3.6	52.2	2.0
5	9	184.3	52.4	1.6	184.3	2.3	52.3	1.8
6	9	188.1	51.5	2.0	188.0	4.0	51.4	1.7
7	9	190.4	53.6	1.4	190.4	2.8	53.6	1.3
8	9	192.9	52.1	2.4	192.9	5.3	52.0	1.3
9	3	201.9	50.1	4.7	202.0	3.7	50.0	0.8
10	9	212.7	62.1	3.5	212.6	9.1	61.8	2.8
Detail Line Total	80	191.4	53.2	1.4	191.9	10.2	52.8	4.0
Drill Hole TS 28	8	238.8	49.7	25.6	234.2	42.1	41.1	11.9
29	7	227.6	64.5	29.6	226.3	53.9	50.0	11.0
30	3	208.8	59.0	16.2	208.0	16.5	58.0	1.4
31	4	213.6	49.2	14.2	211.7	11.4	48.8	8.4
32	18	222.2	55.7	5.2	222.8	19.6	54.1	2.6
Drill Hole Total	40	224.3	55.9	6.7	223.5	33.5	50.5	9.6

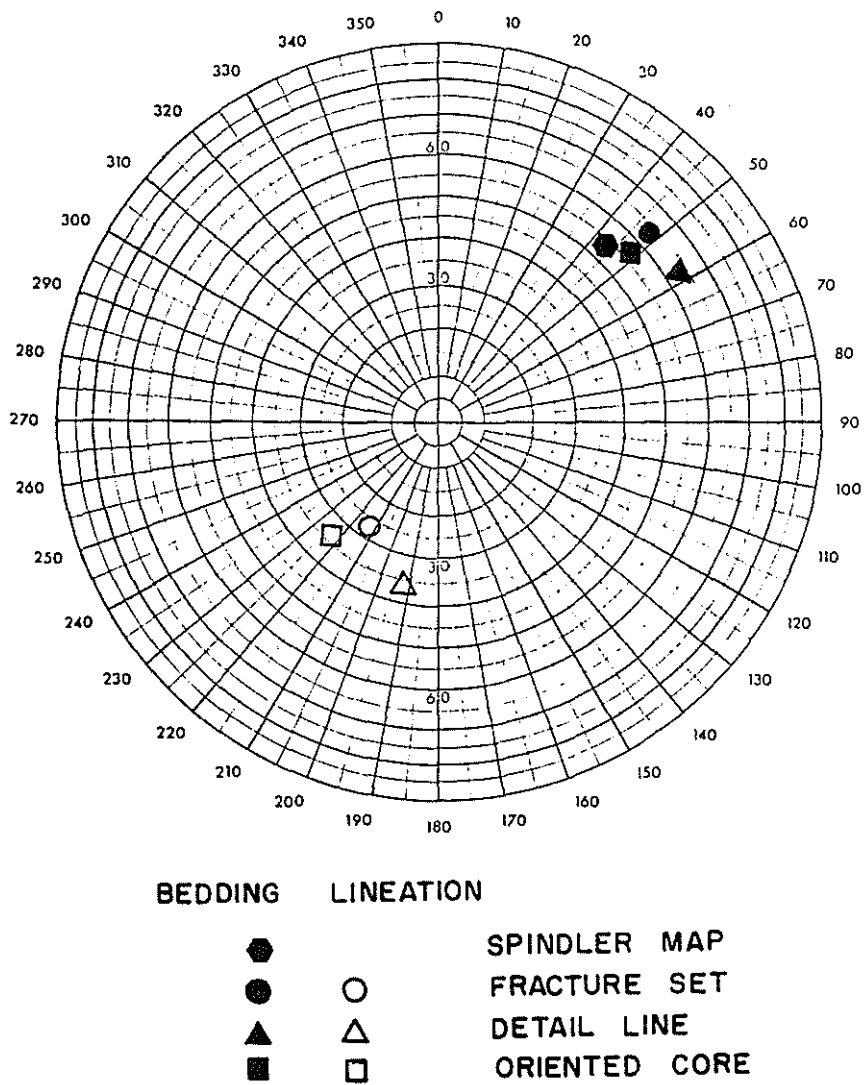


Figure 37. Mean Attitude of Lineation and Bedding.

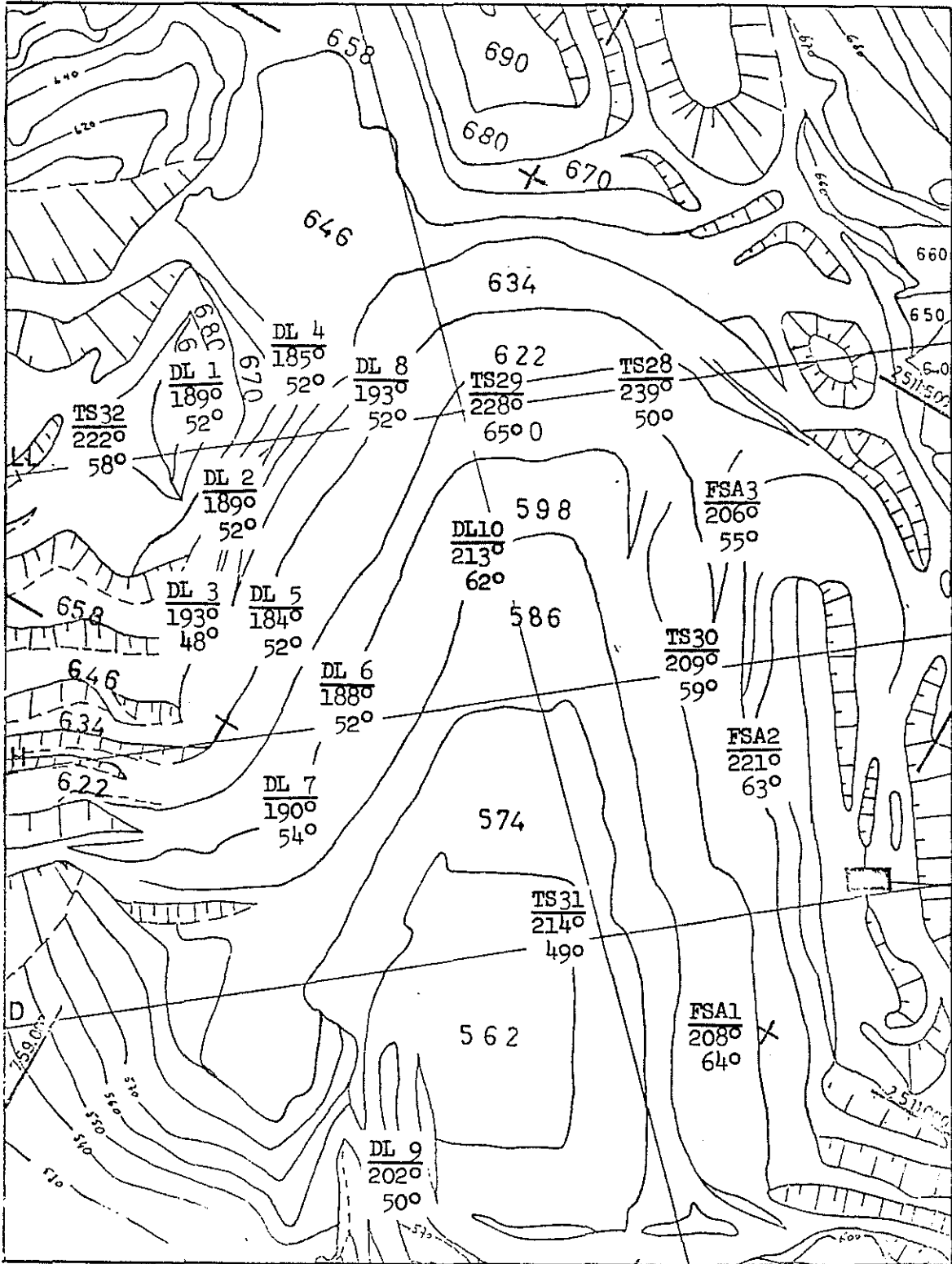


Figure 38. Orientation of Lination.

as the fracture set data, whereas Detail Lines 1 and 2 to the west have a direction of 189° and a plunge of 52° . This trend is consistent with the results of the trend surface analysis of the bedding orientation discussed below.

The superposition of the phase two deformation would produce local variations in the attitude of the primary lineation and would account for some of the variations in the observed attitudes of the primary lineation.

The major sampling error affecting the attitude measurements for the fracture set and the detail line data is the variation in magnetic declination. Although corrections for declination were made during the mapping, some of the variations in the strike of the lineation could be the result of local variations in magnetic declination, particularly in the hanging wall where the magnetic declination pattern is much more erratic. The plunge observations would not be affected, however, as they were measured with a clinometer. The drill hole data, obtained from oriented core, was more subject to measurement error as the technique is indirect. The attitude of the lineation which was measured relative to the core axis was rotated to the true attitude on the basis of measurements of core orientation. The lower precision of this method is reflected in the much larger cone of confidence for the mean vector (Table 3). Because of the small volume of rock sampled by a section of drill core, it was not possible in many instances to determine whether the lineation measured was primary (B_1) or secondary (B_2) lineation. The scatter of the data did not permit segregation of

B_1 and B_2 lineation in the fabric diagram. The inclusion of the B_2 lineation observations could account for the difference between the oriented core data and the detail line data as inclusions of the B_2 lineation would rotate the mean direction to the west and would decrease the plunge.

Bedding

Although the poles of the bedding lie on the great circle normal to the B axis, they are not evenly distributed along this great circle and there is a definite preferred attitude. This preferred orientation is evident in the four types of data as can be seen in Figures 36 37 and Table 4. The average strike and dip of the bedding is plotted rather than the mean vector computed with directional cosines, as the mean vector results in a flatter dip which lies off the great circle. When the range of dip and strike is small, the difference between the mean vector and the mean dip and mean strike is very small.

The attitude of the bedding is uniform in the southeast portion of the pit as shown in the fabric diagrams of Detail Line 9, drill hole TS 31, and Fracture Set Area 1. (See Figure 32.) To the northwest of Section H, the folding is more intense and the bedding attitudes are more variable although still conforming to the π diagram great circle.

To test for systematic variations in the attitude of bedding, a trend analysis was made of the surface mapping observations of Spindler using the vector trend program of Fox (1967). The area between North 2510900 and North 2511700 and East 759000 and East 759700 was divided into 100 meter by 100 meter squares called "cells" giving an array of

Table 4. Mean Attitude of Bedding

Type of data	Number of Observations	Mean Vector			Mean Strike		Mean Dip	
		Strike	Dip	.05 cone of confidence	Strike	s	Dip	s
Spindler Map	932	132.7°	49.1°	1.7°	135.5°	36.5°	53.9°	11.7°
Fracture Set: area 1	26	136.0	63.2	5.5	135.8	14.5	64.0	7.8
2	34	128.8	64.7	9.0	130.2	29.9	67.4	9.6
3	41	146.0	56.6	7.1	143.9	29.5	59.6	8.9
Fracture Set Total	101				139.1	24.8	63.3	9.5
Detail Line 1	11	117.4	47.9	72.9	112.2	75.3	76.9	10.1
2	29	101.1	49.5	6.3	100.8	22.1	51.8	5.2
3	23	164.7	64.1	4.0	164.3	9.3	64.4	6.3
4	27	103.8	51.6	15.8	102.9	45.0	61.1	13.2
5	28	166.9	69.1	11.7	156.9	42.1	72.1	8.4
6	30	136.2	56.9	29.3	115.1	69.5	75.3	9.1
7	26	161.9	67.4	24.7	139.3	64.2	77.0	8.5
8	34	100.3	53.4	7.6	99.8	26.8	56.7	7.8
9	33	128.1	49.8	6.3	128.7	24.6	52.2	7.2
10	28	151.4	64.0	4.3	151.2	9.5	64.1	9.2
Detail Line Total	269	134.1	54.2	5.1	147.8	36.7	63.9	12.9
Drill Hole TS 28	40	125.1	48.2	5.8	127.3	20.3	49.6	14.2
29	56	135.5	54.4	7.4	129.1	38.3	58.8	11.1
30	49	159.6	67.9	8.6	158.0	33.7	70.9	9.7
31	40	126.1	51.3	4.1	126.0	15.1	52.2	8.4
32	33	137.6	53.4	8.7	135.9	31.5	57.5	5.6
Drill Hole Total	218	138.0	54.5	3.5	139.0	31.2	58.0	13.2

eight rows of cells and seven columns. The number of observations in each cell varied from 1 to 37. The vector mean for each cell was computed with the results as shown in Figures 39 and 40. The predominant direction is a northwest-southeast strike (the overall mean vector strikes 133° and dips 57.5°). Northwest of Section LL the strikes are more to the east-west and between Sections H and LL there are several cells with almost north-south strikes. These deviations from the mean are shown in Figure 41, which is a map of the residuals obtained by subtracting the mean strike of each cell from the overall mean strike.

To test for systematic changes in strike, a linear trend surface was fitted to the data as shown in Figures 42 and 43. The linear trend surface shows a systematic increase in strike from 115° in the northwest to 149° in the southeast. This trend is consistent with the regional change in strike of the bedding from east-west along the north flank of the Kedia to north-south on the east flank of the Kedia. Nineteen percent of the variability of the data is accounted for by this linear trend, but deviations of as much as 50° from this trend occur as can be seen on the plot of the residuals (Figure 44).

A second order polynomial (linear plus quadratic) trend surface was fitted to the data as shown in Figures 45 and 46. This surface accounts for 43.7% of the variability of the data and the maximum deviation is reduced to 38° as shown on the residual plot (Figure 47).

The band of high residuals which lie roughly along Section H and represent strikes which cannot be accounted for by regional trends are in agreement with other geologic information indicating anomalous

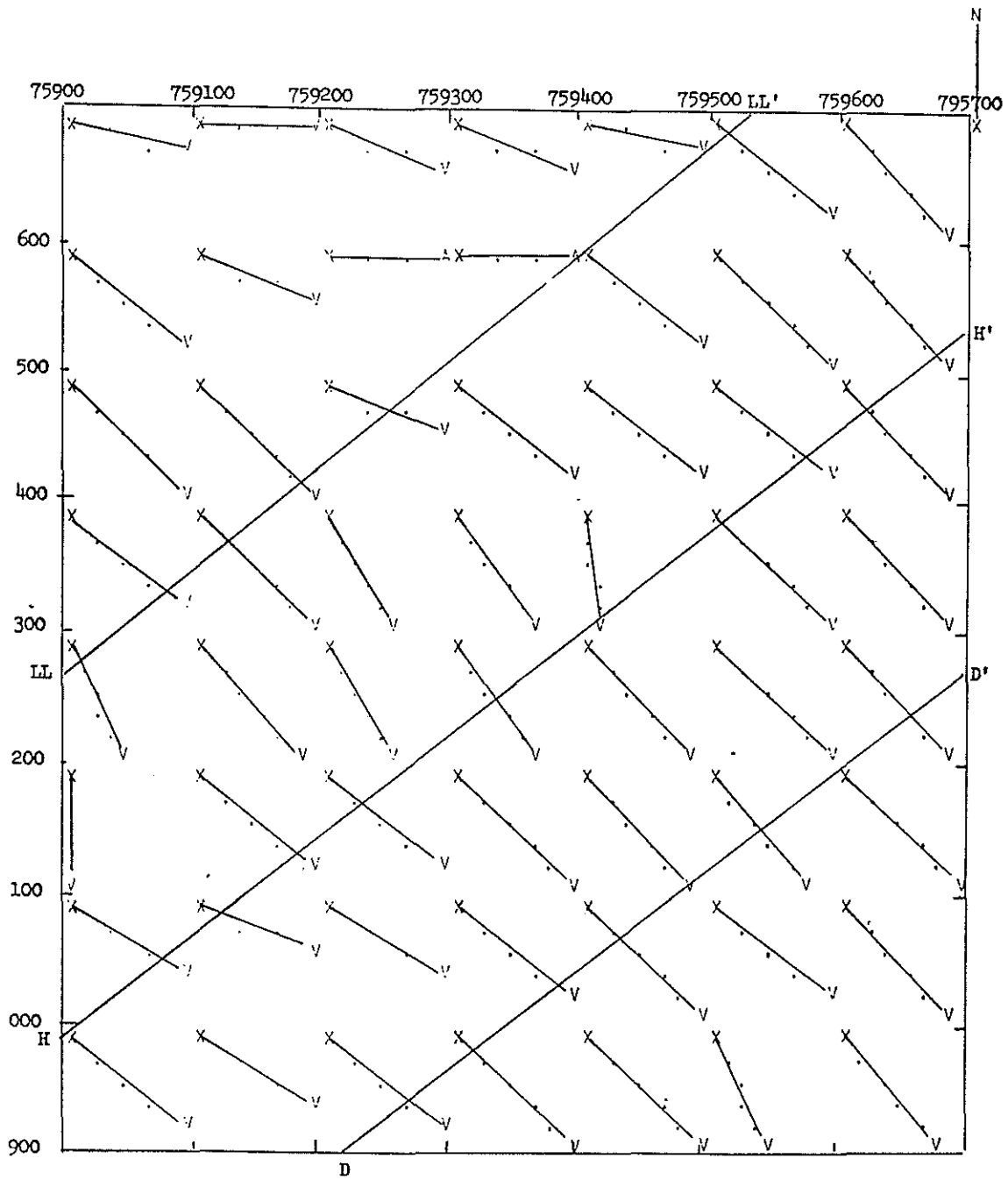


Figure 39. Vector Mean Strike of Bedding -- Graphic Plot.

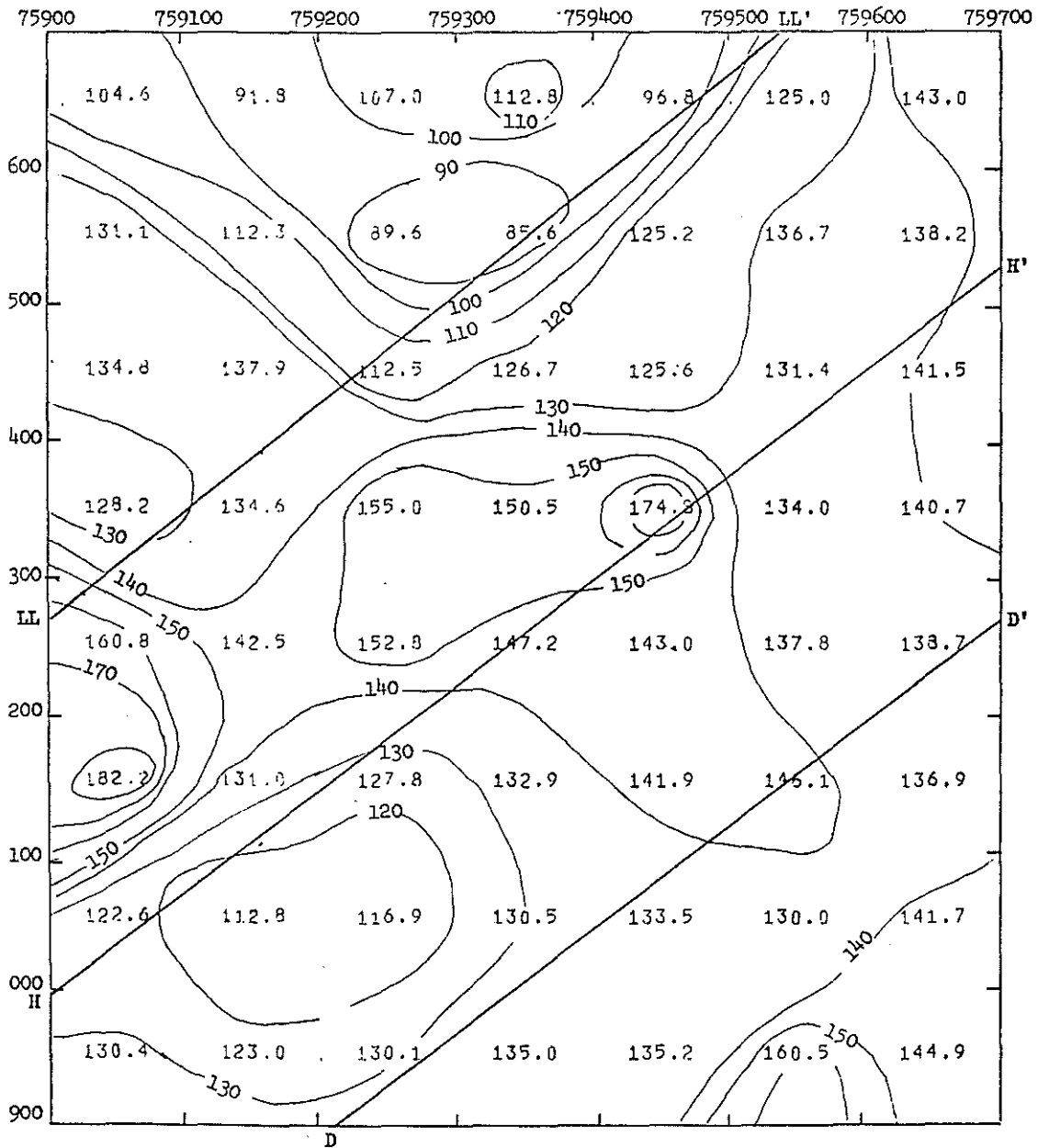


Figure 40. Vector Mean Strike of Bedding -- Numerical Plot.

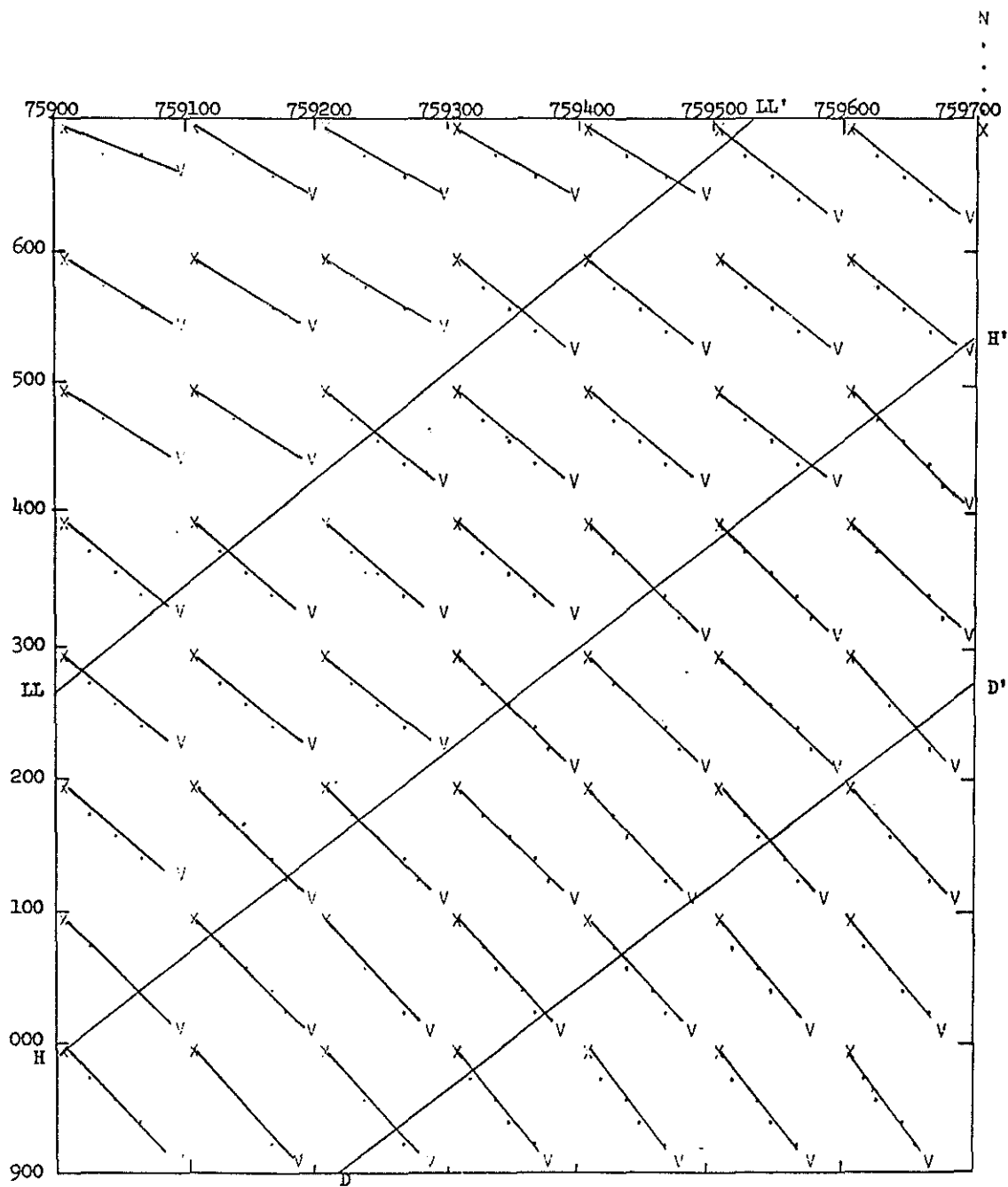


Figure 42. Linear Trend Surface of Vector Mean Strike of Bedding -- Graphic Plot.

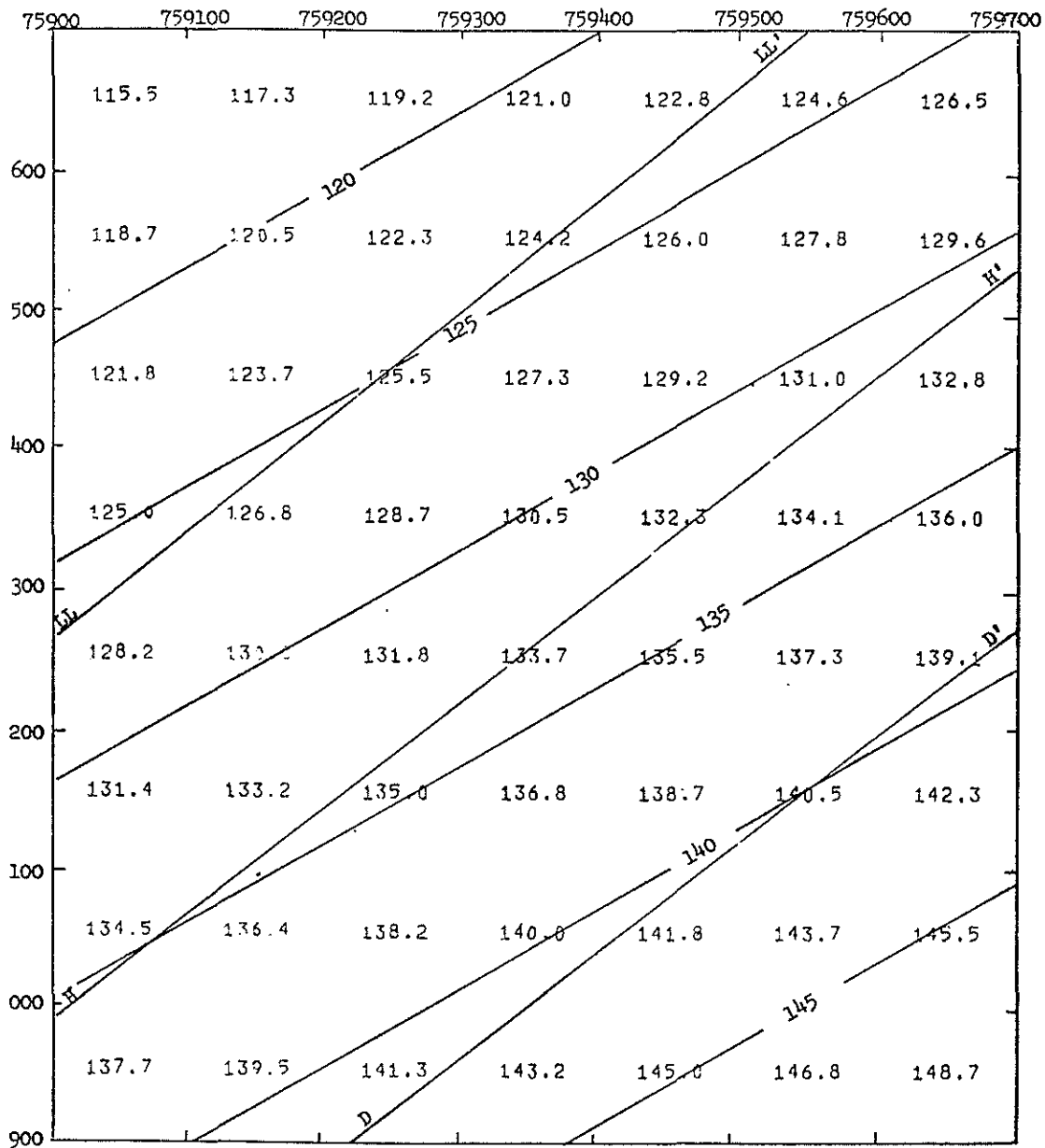
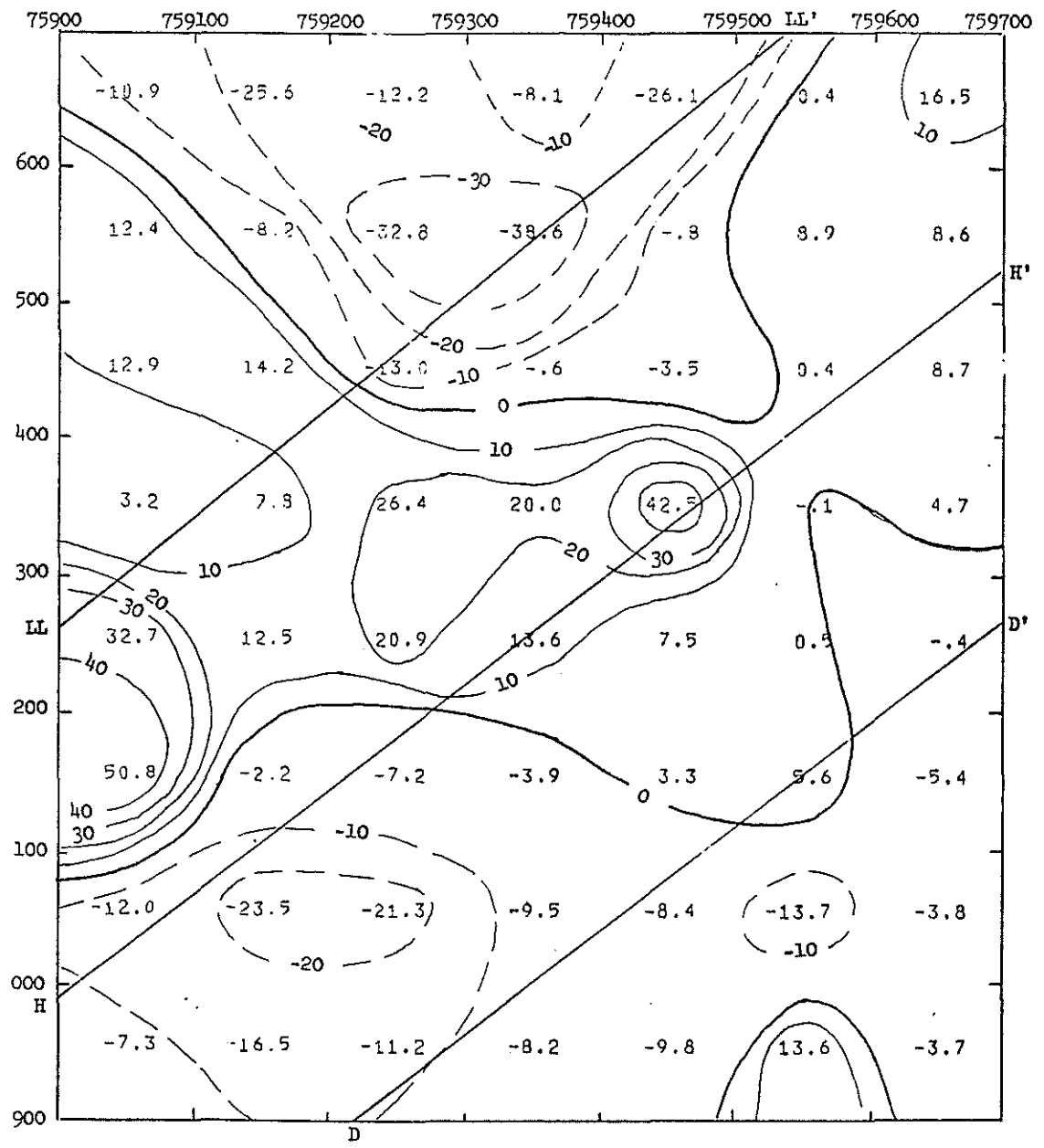


Figure 43. Linear Trend Surface of Vector Mean Strike of Bedding -- Numerical Plot.



Percentage Reduction in Total Sum of Squares = 19.330

Figure 44. Linear Residuals -- Observed Strike of Bedding Minus Linear Trend Surface.

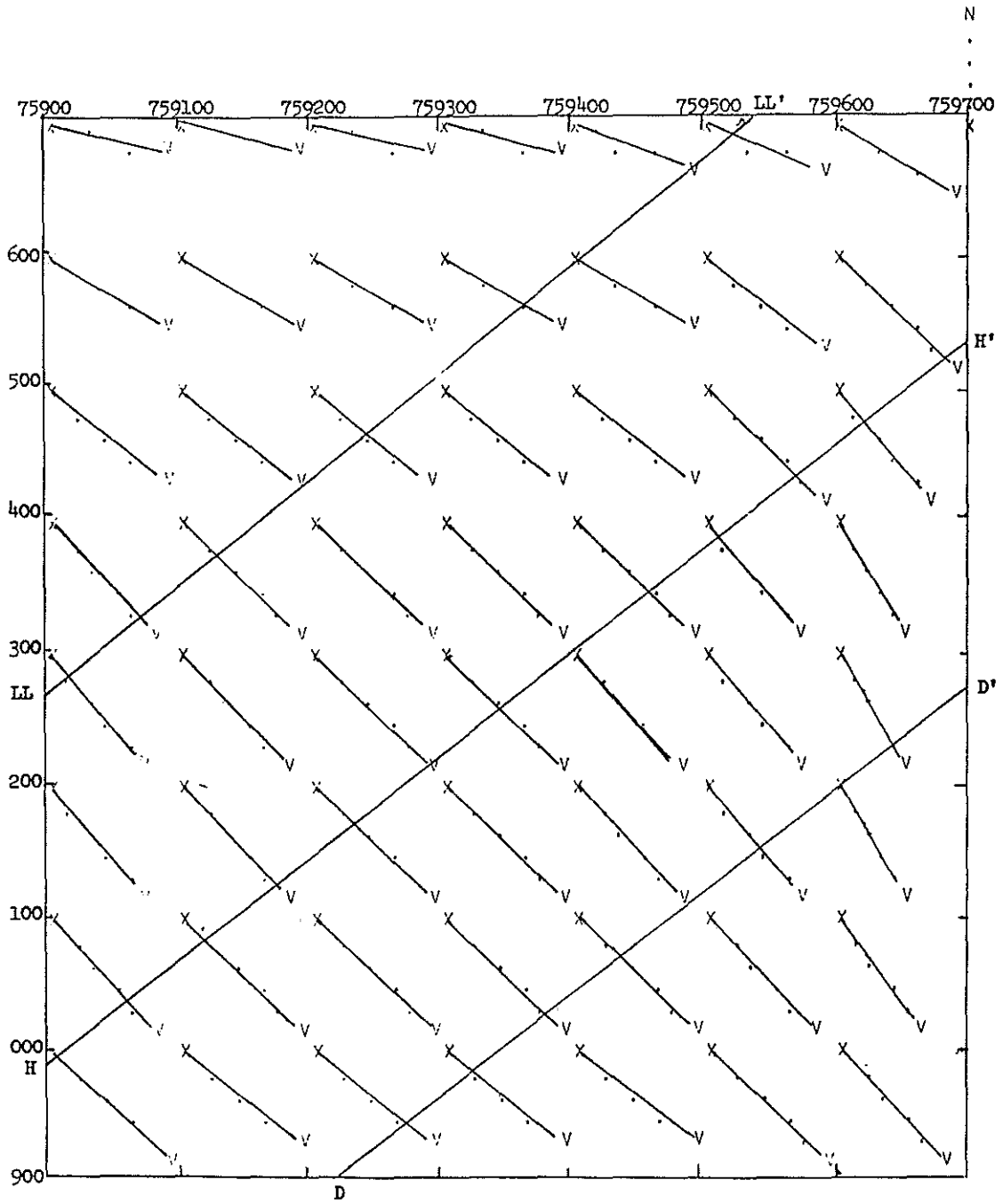


Figure 45. Linear Plus Quadratic Trend Surface of Vector Mean Strike of Bedding -- Graphic Plot.

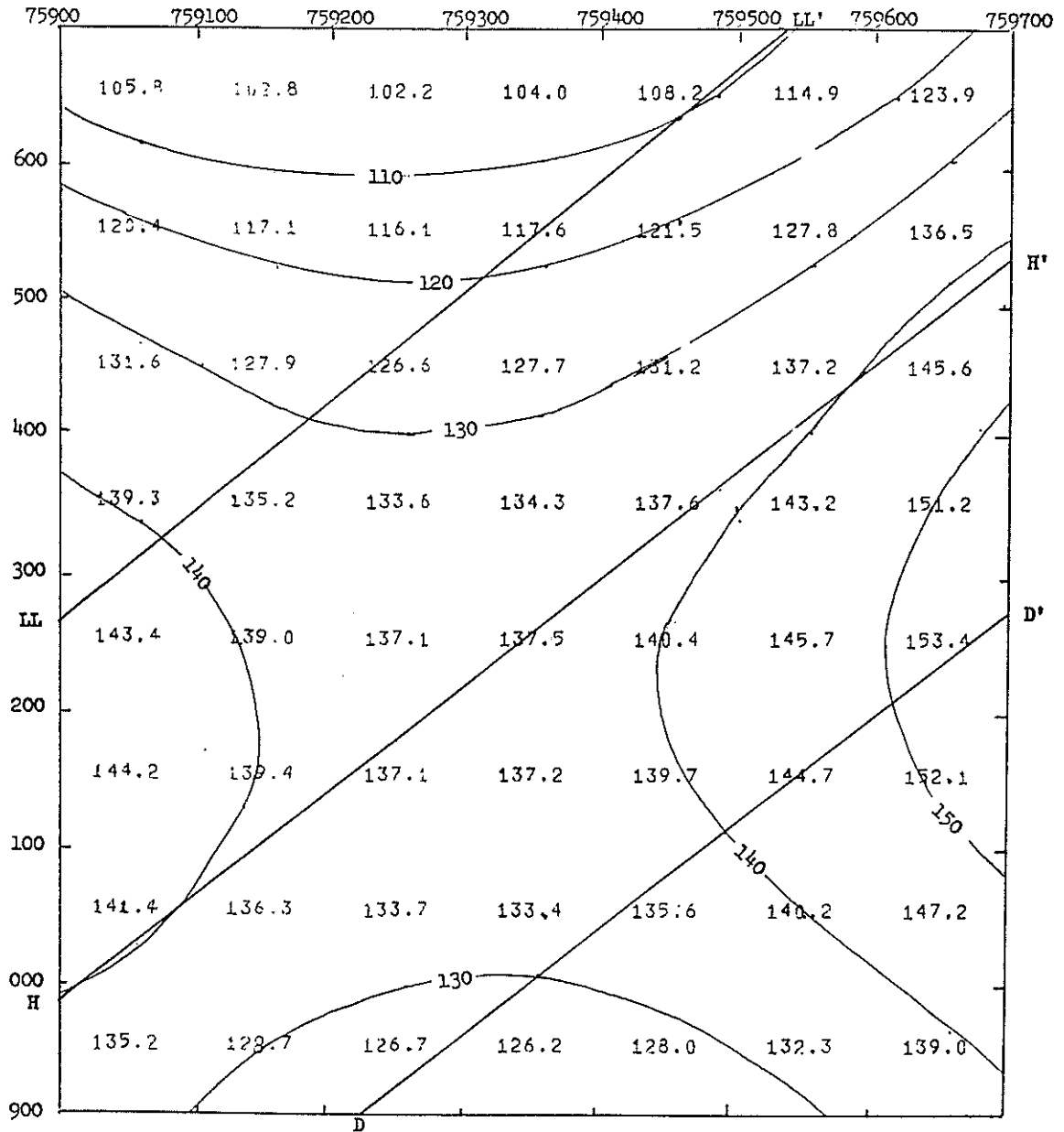
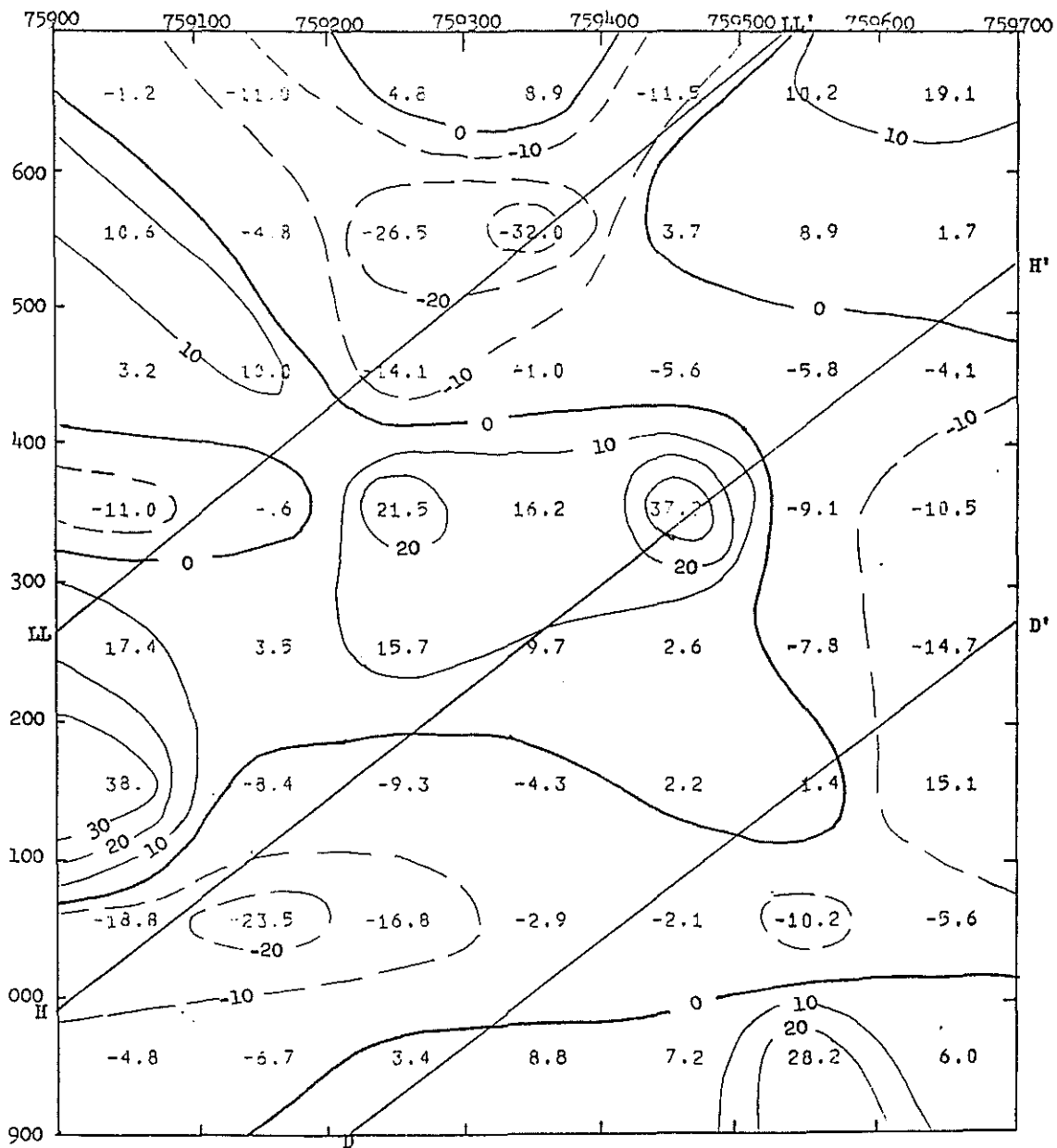


Figure 46. Linear Plus Quadratic Trend Surface of Vector Mean Strike of Bedding -- Numerical Plot.



Percentage Reduction in Total Sum of Squares = 43.754

Figure 47. Linear Plus Quadratic Residuals -- Observed Strike Minus Linear Plus Quadratic Trend Surfaces.

conditions exist in the vicinity of Section H. As can be seen on the geologic map, the ore body narrows abruptly at Section H and there is a noticeable change in direction of the footwall schist. Just to the northeast of Section H, on the 598 bench, the quartzites and schists are much more complexly folded and there are several areas of brecciation with rounded blocks of quartzite in a schist matrix. No major fault was found in the area however which would account for this deformation. This zone is a transition between the more regular bedding orientation in the southeast and the more complex folding that occurs in the northwest of the pit adjacent to the axis of the main flexure of the Kedia.

Jointing

The predominant joint orientations, as shown in Figure 36, are consistent with a general picture of a cylindroidally folded tectonite. One set is parallel to the ac plane of symmetry, as shown by the concentration of joint poles in approximately the same position on the fabric diagrams as the lineation (B). A second major concentration of joints is nearly vertical and strikes approximately at right angles to the bedding. Both of these joint sets are present on the fabric diagrams of the fracture set data, the detail line data, and the oriented core data with the exception of the absence of steeply dipping joints on the oriented core data. This absence of high angle joints is predominately a sampling bias.

A drill hole is a linear sample with a very small cross sectional area, thus a joint set which is parallel to the drill hole will not be intersected by the drill hole except in that very rare instance where

the drill hole happens to lie directly on a joint. The orientation parallel to the drill hole, which would not be included in a linear sample such as the drill hole, has been referred to as the "blind zone" by Terzaghi (1965). The fabric diagrams for the drill holes are shown in Figure 48. The blind zones are all orientations within 10° of being parallel to the drill hole plotted on the diagrams. For any given length of drill hole, the number of observations of a joint set in the blind zone orientation would be less than thirteen percent of the number of observations of a joint set with the same spacing oriented at right angles to the drill hole. As can be seen in Figure 48, almost no observations were recorded in the blind zones.

In view of the general correlation between oriented core, detail line, and fracture set data for the bedding and the lineation, it is reasonable to assume that the jointing at depth is essentially the same as that mapped on the surface by the detail line and fracture set methods, and that the difference in the joint pattern for the oriented core is the result of blind zone bias.

The detail line sampling method is biased as it is also a linear method. The bias is much less pronounced than in the oriented core method, however, as a much larger volume of rock is sampled with the detail line. In the Tazadit pit detail line sampling, all fractures in a zone one meter above and one meter below the line were included. The irregularity of the pit face in the horizontal plane is in the order of magnitude of one meter, thus the cross sectional area sampled would be approximately two square meters as compared to 17.4 square

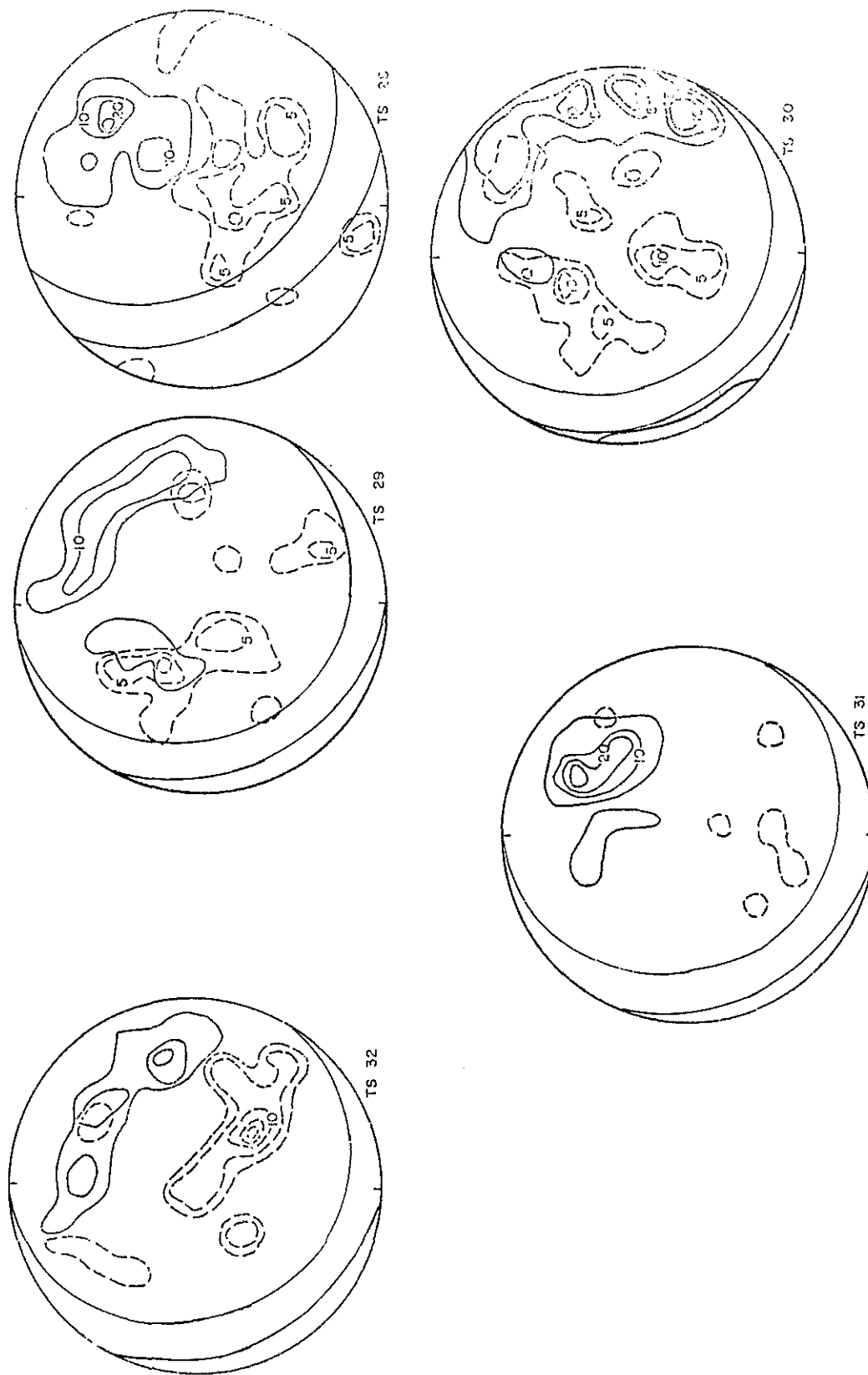


Figure 48. Oriented Core Blind Zones.

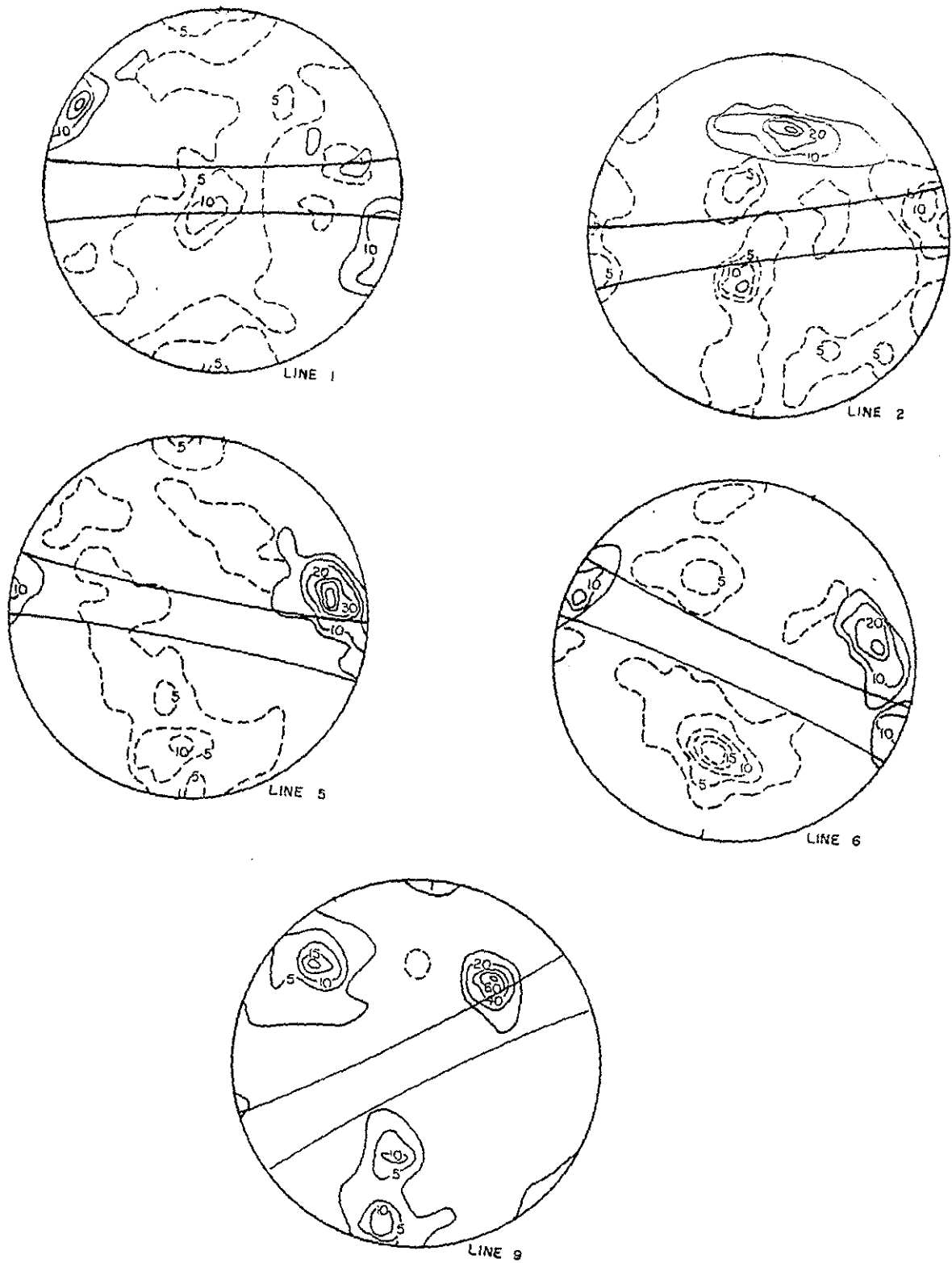
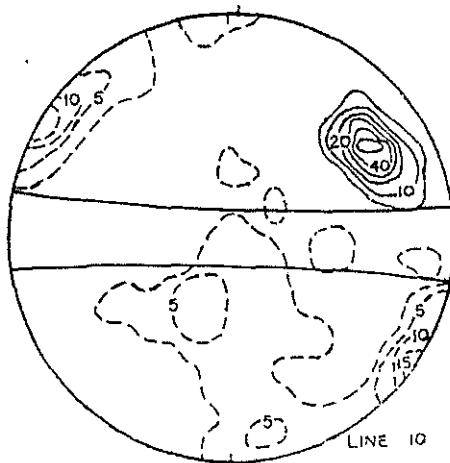
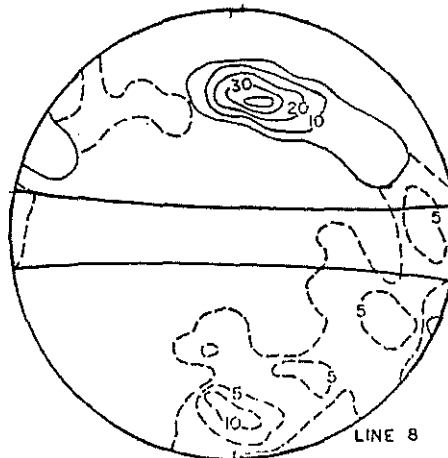
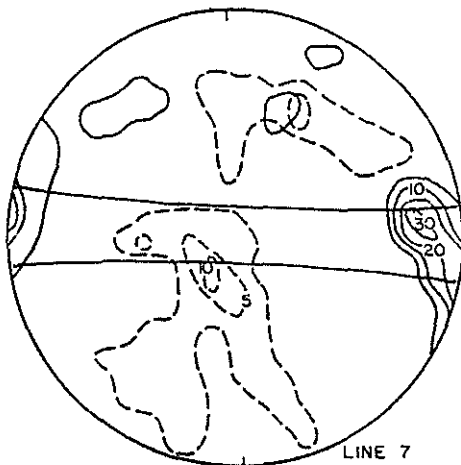
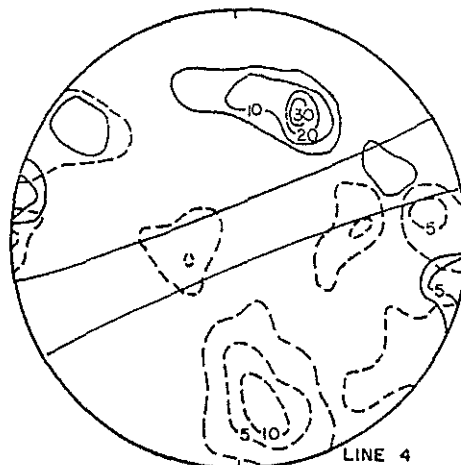
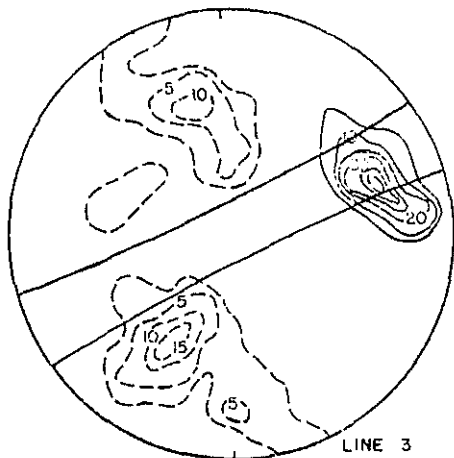


Figure 49. Detail Line Blind Zones



centimeters for NQ drill core. The blind zone for a detail line comprising those attitudes parallel to the line would appear on a fabric diagram as a belt at right angles to the direction of the line as shown in Figure 49. By comparing this blind zone diagram with the fabric diagrams of the detail lines shown in Figures 18 through 24, it can be seen that fractures lying in the blind zone were recorded. Also by comparing the photographs with the fabric diagrams, it can be seen that the major joint systems in the pit face are represented on the fabric diagram. Since most of the detail lines were oriented north-south, the detail line data would be biased in favor of vertical east-west striking structures, which would account for the differences between the fabric diagram of the detail line data and the fabric diagram of the fracture set data in Figure 36.

In addition to the two major joint sets mentioned above, a number of secondary joint sets were recorded. These may be related to the phase two tectonism.

Fracture Spacing

Fracture spacing is highly variable depending upon the type of fracturing (bedding or jointing), rock type, degree of weathering, and location. Thus no single number is adequate to describe fracture spacing. The microstructure study of the thin sections Bronner (1970) demonstrated that the fabric elements are present at the microscopic scale and thus are penetrative features and represent fundamental anisotropism of the rock. The fractures recorded in the fracture set mapping and detail line mapping, however, are definite discontinuities

along which the rock had broken. The spacing recorded is, therefore, more indicative of the ability of the rock to split along potential planes of weakness than the true spacing of the potential planes of weakness. Blasting has an affect upon the observed fracture spacing as the amount of separation of the rock in the pit face along the fundamental weakness planes is a function of the amount of energy input into the rock by the blasting. However, as almost all of the pit faces mapped were blasted with the same hole size, hole spacing, and charge, the variations in spacing induced by blasting would not be large.

Bedding

Banded Hematite Quartzite. The schistose BHQ of the footwall has a pronounced anisotropism parallel to the bedding as shown by the Brazilian tension tests (Table 7, p. 119) in which the tensile strength in the direction along the bedding was five times greater than the tensile strength normal to the bedding. Thus, the bedding planes of the schistose BHQ tend to separate quite easily and commonly the observed fracture spacing parallel to the bedding is 1 to 2 centimeters. This is also partially due to desilicification and weathering, the extreme case of which is the plaquette condition where the BHQ is reduced to plaquettes only a few millimeters thick. The spacing measurements taken during the fracture set mapping ranged from a maximum of 50 centimeters to a minimum of less than 1 centimeter. Excluding the plaquetted area, the fracture set observations gave a range of 5 to 25 centimeters for the most common spacing in the schistose BHQ. In

the plaquetted areas the fracture spacing parallel to the bedding is less than one centimeter. Since the plaquetting is primarily a near-surface phenomenon, the fracture spacing for bedding in the final pit wall would be an estimated 10 to 25 centimeters. This estimate is supported by the RQD measurements from the drill holes where the median RQD for the schistose BHQ is 65%, indicating that over half of the core was in pieces longer than 10 centimeters.

The anisotropism of the BHQ of the hanging wall is much less than that of the footwall schistose BHQ. The Brazilian tensile strength along the bedding was only 28% greater than the tensile strength measured normal to the bedding. Thus the fracture spacing of the hanging wall BHQ bedding is considerably greater than the schistose BHQ of the footwall, except where desilicification has reduced the BHQ to the plaquette condition. As a rough estimate, the fracture spacing for the bedding of the hanging wall BHQ would be in the range of 25 to 100 centimeters with some areas of appreciably larger spacing except near the surface where plaquetting has occurred. This larger fracture spacing for the hanging wall BHQ is confirmed by the RQD measurements of hole TS 32 where the median was 84%.

Quartzite. The quartzite rock substance is almost isotropic, and the fracture spacing is determined predominantly by the presence of thin shale partings. The spacing recorded in the fracture set observations was predominantly between 15 and 20 centimeters with a maximum value of 80 centimeters and a minimum of 1 centimeter. The

median RQD for the quartzite is 70%, which is slightly higher than the 64% for the schistose BHQ and less than the 84% for the hanging wall BHQ.

Schist. The schist has a strong degree of foliation and therefore has a very pronounced anisotropism. Only five observations were made of bedding fracture spacing for the schist, which is too small a sample to indicate more than an order of magnitude. The mode of these observations fell in the 5 to 25 centimeter range with maximum spacing of 50 centimeters and minimum spacing of 1 centimeter; thus the fracture spacing of the schist would appear to be similar to that of the schistose BHQ. The RQD recorded from the drill holes indicated a median value of 51%, which is appreciably lower than that of the schistose BHQ. This low RQD is related to the pronounced foliation of the schist.

Ore. The bedding fracture spacing observations of the ore ranged from 1 centimeter to 30 centimeters for the mode, a maximum observed value of 150 centimeters. This large range in spacing for the ore is the result of the different types of ore. There is a rocky hard ore that is a massive material with fracture spacing in the range of 50 to 100 centimeters, a normal hard ore with fracture spacing in the range of 5 to 10 centimeters, and plaquette ore with fracture spacing less than 1 centimeter. The variation in the ore type is reflected in the composite RQD which has a mode between 80% and 90%, a second mode between 50% and 60%, and a third mode at 20%.

Jointing

In general, the jointing has wider spacing than the bedding fractures, there is less variability between rock types, but there is

a greater range between the minimum spacing and the maximum spacing. An exception to this generalization is in areas of deformation in the footwall where the quartzite has failed brittlely resulting in intense fracturing, whereas the adjacent schists have deformed nonelastically with minimal fracturing. The mode of the joint spacing for the footwall fracture set data is between 40 centimeters and 50 centimeters, a minimum spacing of 10 centimeters to 15 centimeters, and a maximum spacing between 110 centimeters and 130 centimeters. The joint spacing observations in the ore were slightly higher with a mode of 63 centimeters, a minimum of 17 centimeters, and a maximum of 140 centimeters; the differences may not be significant because of the small number of observations.

To obtain an estimate of the fracture spacing for the BHQ in the hanging wall, eight joint sets were chosen from the detail line data and the spacing computed for each set. The mean vector orientation for each set was computed and the distance between the joints measured along the detail line was converted to the true distance normal to the joints. The results of these calculations are shown in Table 5. The average spacing of these joint sets varied from 14 centimeters to 143 centimeters. The maximum spacing ranged from 50 to 274 centimeters. Because of the difficulties in projecting irregular structures to the tape, the minimum values computed by this method are not significant as the computed spacing is less than 1 centimeter, which is within the accuracy with which the position of the fractures can be recorded.

Table 5. Detail Line Joint Spacing

Line	Set	Strike	Dip	Number	Line Length	Corrected Line Length	Average Spacing	Maximum Spacing
1	1	300°	17°	23	11.0 m	2.95 m	0.14 m	.50 m
2	1	302	23	3	15.3	5.1	0.25	
3	1	294	32	5	10.6	5.06	1.43	2.58
4	1	262	61	26	10.8	9.35	0.31	1.17
6	1	271	48	27	14.5	8.03	0.23	1.69
7	1	302	58	24	12.7	10.75	0.37	1.69
8	1	267	70	13	12.1	9.92	0.64	1.49
9	1	275	76	11	11.6	10.09	0.69	2.74
10	1	258	81	10	10.3	8.41	.59	1.47

CHAPTER 6

ROCK STRENGTH

The strength of the rock mass, defined as the rock including the structural features such as bedding, jointing and faulting, is a function of the strength of the intact rock or rock substance and the strength of the structural features.

Intact Rock Strength

Unconfined Compressive Strength

A common method of classifying the strength of intact rock is on the basis of the uniaxial compressive strength. Deere (1968) has proposed a classification system which also includes the elastic modulus. He divides the compressive strength into five categories:

1. very low strength (less than 4000 psi)
2. low strength (4000 to 8000 psi)
3. medium strength (8000 to 16,000 psi)
4. high strength (16,000 to 32,000 psi)
5. very high strength (above 32,000 psi)

The second element of his classification is on the basis of the ratio of the modulus of elasticity to the compressive strength. The modulus ratio is divided into three categories:

1. below 200:1 - low modulus ratio
2. 200:1 to 500:1 - average modulus ratio
3. above 500:1 - high modulus ratio

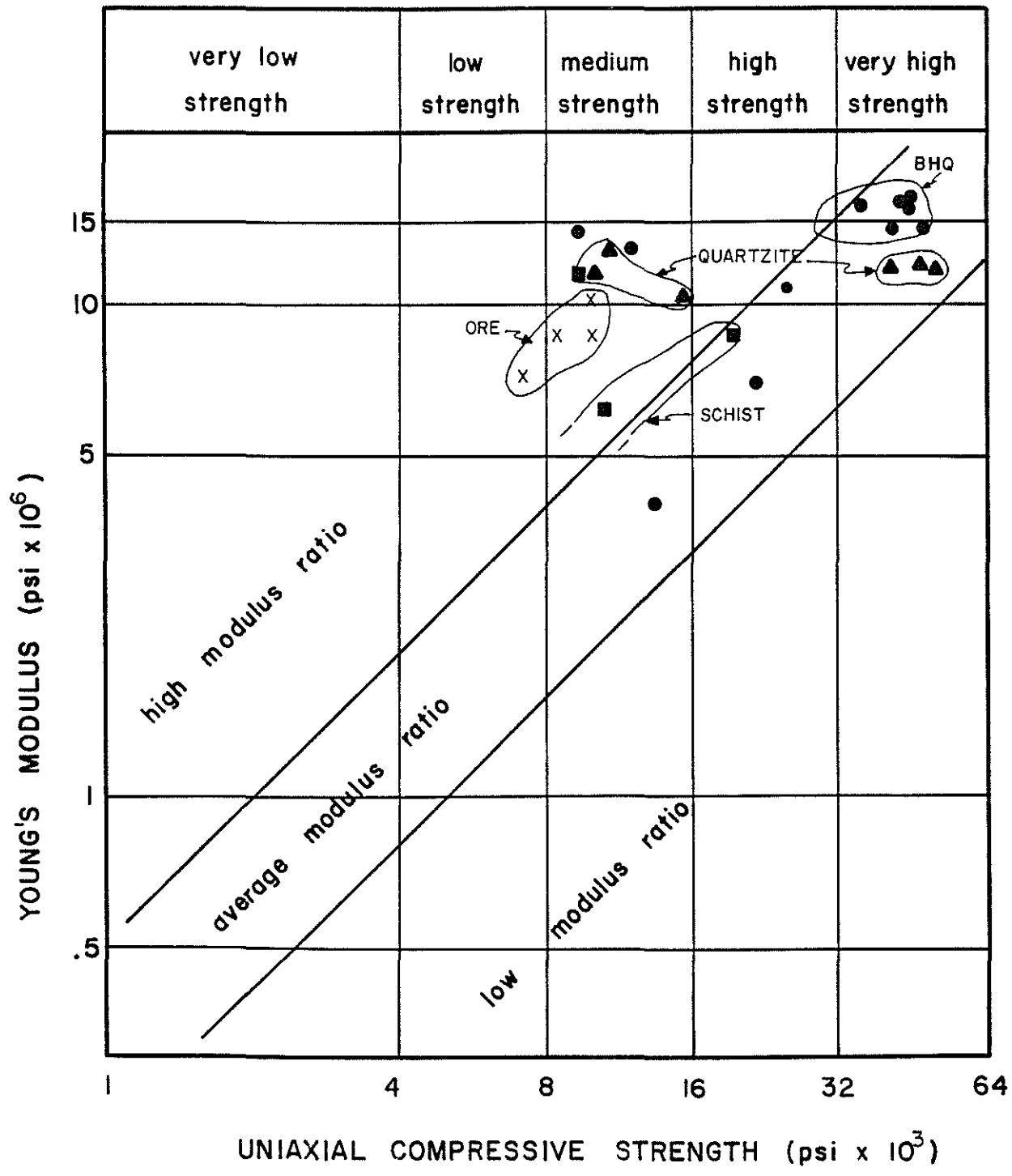


Figure 50. Engineering Classification of Intact Rock, Tazadit Pit.

This system is portrayed graphically in Figure 50. The results of the physical testing of Tazadit rocks are plotted here also.

Uniaxial compressive tests of core from the Tazadit pit were made at the Elliot Lake Research Laboratory of the Canadian Department of Energy, Mines and Resources (Table 6). On the basis of these tests, the rock types of the Tazadit pit may be classified as follows:

Banded Hematite Quartzite (BHQ). Of the twelve BHQ samples tested, seven fell in the very high strength, average modulus ratio category. The other five samples were medium to high strength. This second group probably represents premature failure along structural features. Therefore, the BHQ can be classified as very high strength, average modulus ratio.

Quartzite. The quartzite and micaceous quartzite fell into two groups: (1) a very high strength, average modulus ratio group, and (2) a medium strength, high modulus ratio group. Two samples of the latter group were noted to have failed along structural features. Two samples broke during preparation and could not be tested. Although the intact quartzite could be considered to have a very high strength, average modulus ratio, the intensive fracturing greatly reduces the effective rock mass strength.

Hematite Ore. The ore samples tested indicate a consistent medium strength, high modulus ratio.

Schist. Only two samples of schist were tested to failure. They indicate a medium strength, high modulus ratio. This represents the upper limit of the schist however, as the lower strength

Table 6. Results of Physical Testing of Tazadit Pit Rock Samples

Rock Type	Axial Stress (Kp/cm ²)	Confining Stress (Kp/cm ²)	Elastic Modulus (1000Kp/cm ²)	Poisson's Ratio
Hanging Wall	2,290 ± 1,050	0	89.9 ± 33.0	0.18 ± 0.10
	4,270 ± 1,300	140	105.5 ± 19.6	0.20 ± 0.04
	4,940 ± 1,000	280	---	---
Iron Ore	770 ± 160	0	61.2 ± 8.4	0.22 ± 0.07
	1,650 ± 90	140	68.2 ± 10.5	0.50
	2,420 ± 440	280	---	---
Schistose BHQ	1,690 ± 1,010	0	99.8 ± 16.2	0.24 ± 0.12
	2,700 ± 910	140	69.5 ± 0.7	0.32 ± 0.24
Quartzite	750 ± 30	0	87.2 ± 6.3	0.19 ± 0.11
	2,450 ± 1,040	140	101.2 ± 22.5	0.21 ± 0.07
	1,780 ± 1,100	280	---	---
Micaceous Quartzite	2,770 ± 1,050	0	83.7 ± 7.0	0.10 ± 0.03
	1,510 ± 360	140	76.6 ± 4.9	0.15 ± 0.03
	2,600 ± 220	280	---	---
Garnet Schist	1,050 ± 460	0	66.8 ± 14.8	0.16 ± 0.07
	2,100 ± 440	140	75.2 ± 7.0	0.14 ± 0.04
Green Schist	---	0	40.0	0.37
	1,000	140	39.4	0.40
Red Schist	830	140	---	---

schist was too broken to prepare samples. A more realistic classification would be low strength, average modulus ratio.

Tensile Strength

The tensile strength of the intact rock was determined by the Brazilian disc tension test. In this test a disc of the rock is compressed between plattens and a tensile failure is induced in the disc parallel to the principal stress direction. The tensile strength from a Brazilian test of rock is generally about 1.6 times the pure tensile strength as the failure plane is forced to occur parallel to the principal stress direction rather than being permitted to occur along the weakest plane. The Brazilian test was chosen as it is a simpler and less expensive test than the pure tension test.

The results of the tests are shown in Table 7. The micaceous quartzite showed the highest tensile strength, the BHQ slightly less. The schistose BHQ and the ore have a still lower value. The schistose BHQ, which has the most well developed anisotropism in the form of alternating beds of quartzite and schist, showed a large differentiation (6:1) between the tensile strength parallel to the bedding and the tensile strength across the bedding. The loading parallel to the bedding plane would correspond to the tensile strength of the bedding planes, the loading at right angles to the bedding would correspond to the tensile strength of the beds themselves. The BHQ, on the other hand, showed a slightly lower tensile strength for the bedding than for the bedding planes. Because of the small number of samples, this result could be due to the variations in individual specimens rather than

Table 7. Brazilian Disc Tensile Strength

Rock Type	Number of Specimens	Tensile Strength kg/cm ²	Standard Deviation
BHQ (a)	5	179	27
BHQ (b)	2	137	
Schistose BHQ (a)	12	15	1
Schistose BHQ (b)	11	90	13
Ore	8	90	15
Quartzite	6	210	15

a = loaded parallel to bedding

b = loaded perpendicular to bedding

actual properties of the rock substance. The samples of ore and micaceous quartzite were more isotropic and no difference in tensile strength was detected between loading parallel and at right angles to the bedding. With a large number of samples, a differentiation could possibly have been made between the tensile strength of the bedding planes and the tensile strength of the beds themselves.

Confined Compressive Strength

Specimens of the rocks from Tazadit pit were tested under confinement in a triaxial apparatus to determine the effect of confinement on the physical properties and particularly on the compressive strength.

The BHQ showed an increase in compressive strength with confinement with a Mohr envelope as shown in Figure 51. The linear envelope appears to have a slope of 56° and a cohesion intercept of 340 kg/cm^2 . The envelope is curved on the tensile side of the normal stress axis to intercept the tensile strength value obtained from the Brazilian test.

The ore showed a similar behavior with the Mohr envelope having a slope of 45° and a cohesion intercept of 160 kg/cm^2 (Figure 52).

The quartzite and the micaceous quartzite showed no consistent increase in strength within the confining pressures employed. As pointed out above, the quartzite rock substance had a very high strength but many of the samples failed on fracture surfaces at a much lower stress. This bimodal failure distribution accounts for the erratic results of the confined compressive test. As indicated by Hergot (1970) a much larger number of samples would be necessary to establish the Mohr

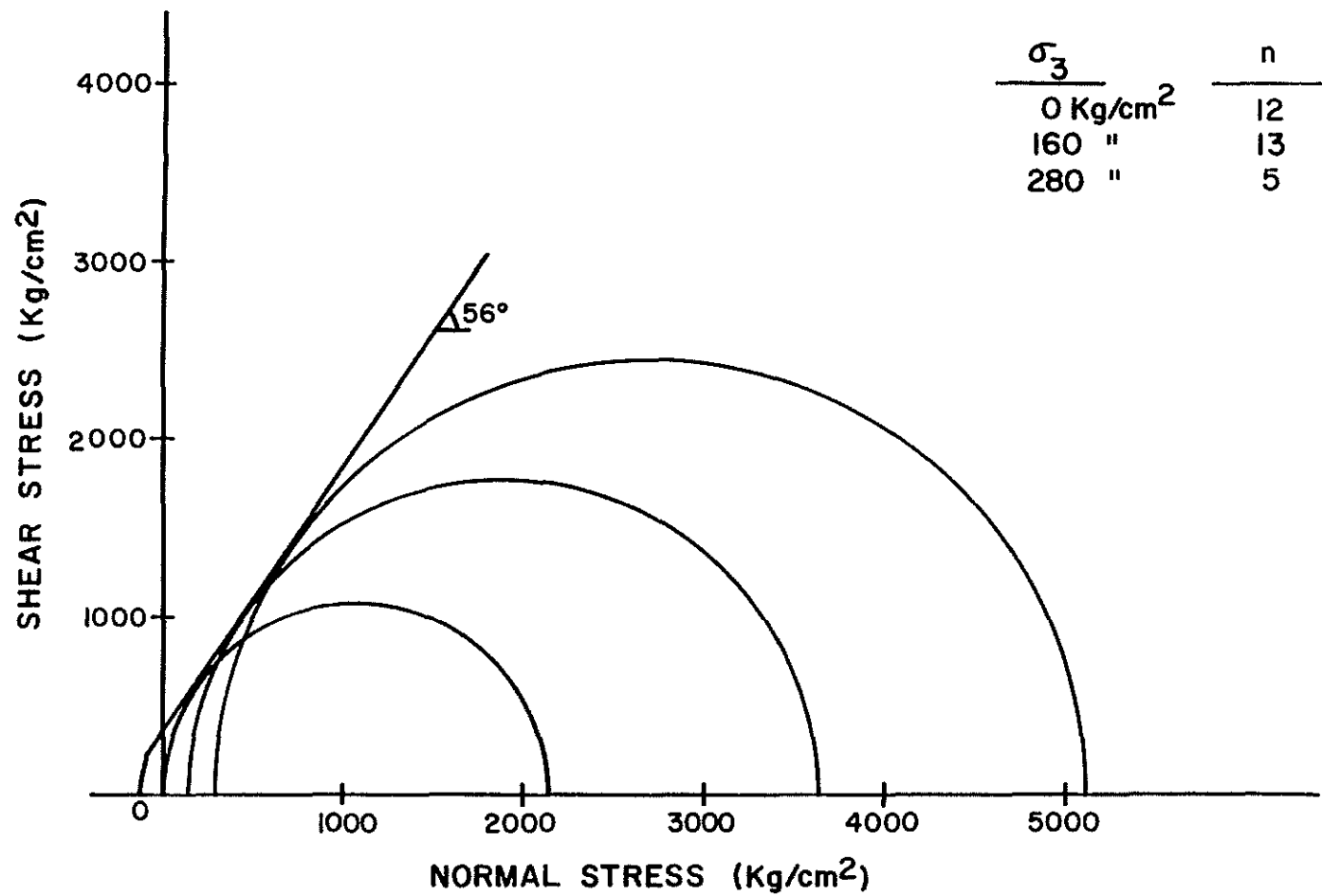


Figure 51. Hanging Wall BHQ Mohr Diagram.

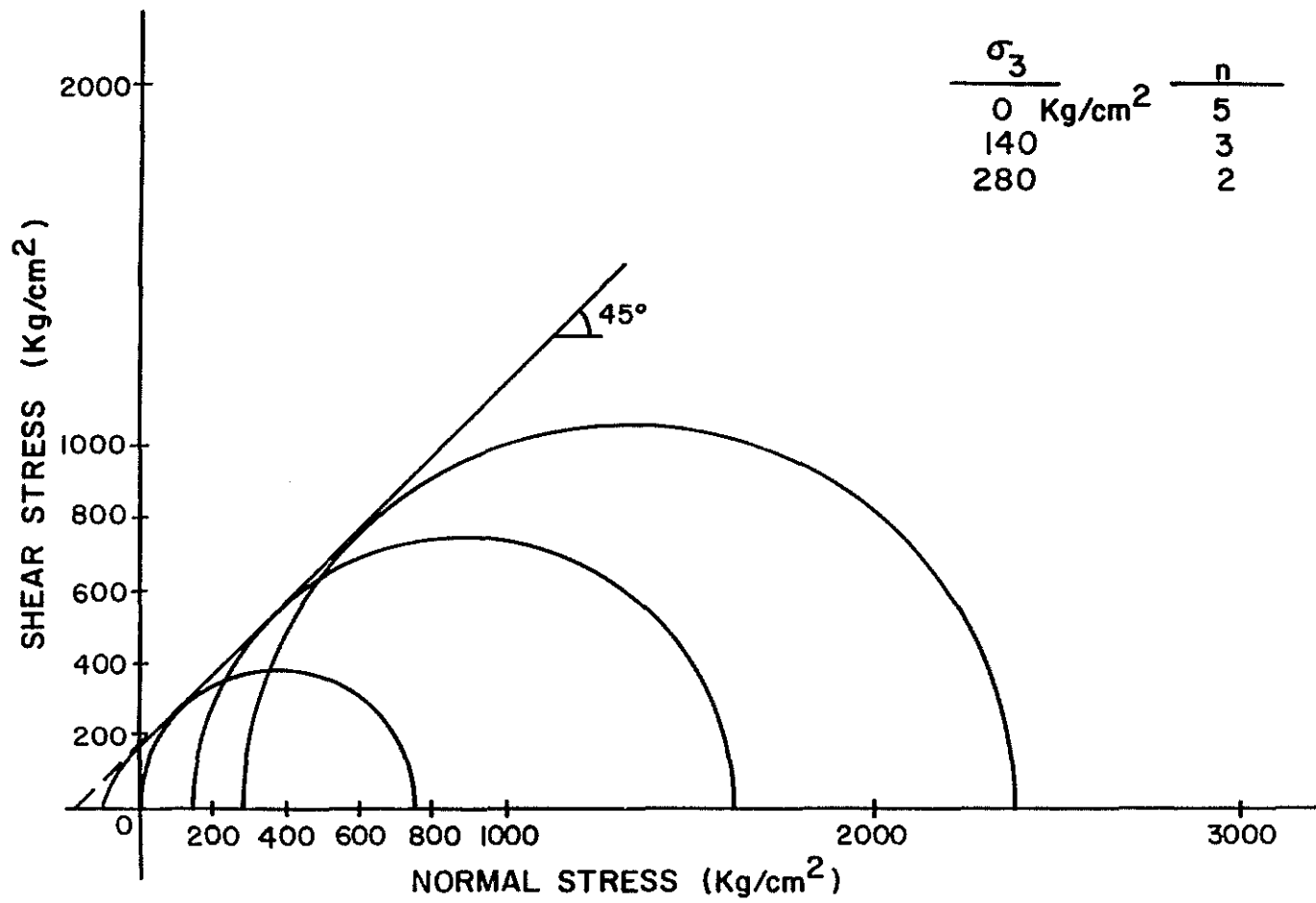


Figure 52. Hematite Ore Mohr Diagram.

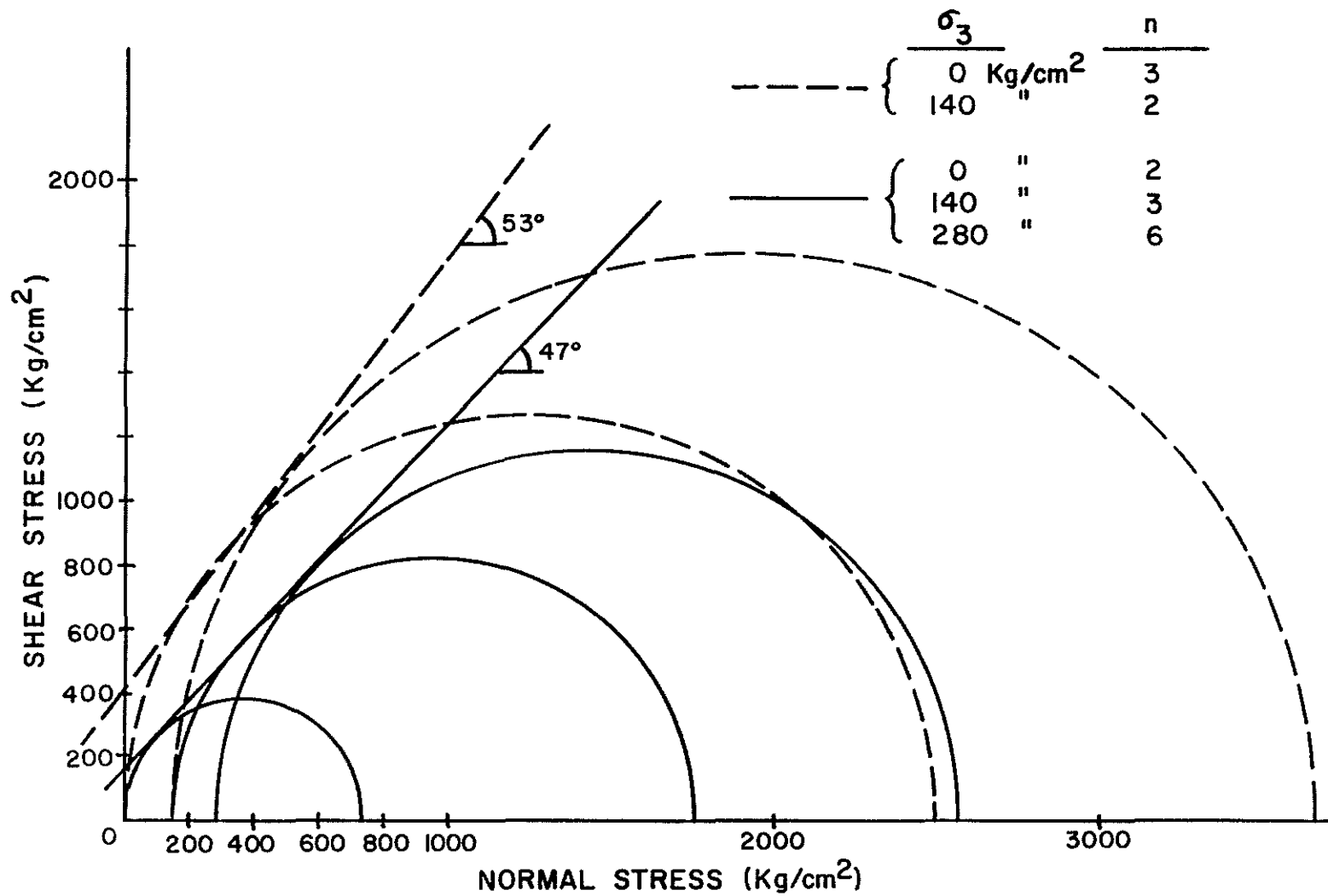


Figure 53. Quartzite Mohr Diagram.

envelope for the quartzite. In Figure 53 two Mohr envelopes have been drawn for the combined quartzite and micaceous quartzite. The specimens which failed at high stress levels are shown with dashed lines and give a Mohr envelope with a slope of 53° and a cohesion intercept of 400 kg/cm^2 . The specimens which failed at lower stress levels give an envelope with a slope of 47° and a cohesion intercept of 160 kg/cm^2 .

There was an insufficient number of samples of schist to develop a Mohr envelope for the schist.

Elastic Properties

The results of the physical testing indicate that the intact BHQ and the quartzite will behave as an elastic material within the stress ranges to be expected in the slopes of the Tazadit pit.

The sample of quartzite tested in the University of Arizona laboratory showed a linear reversible stress-strain curve with no appreciable hysteresis up to 400 kg/cm^2 . With the high elastic modulus and low Poisson's ratio, the intact rock will fail brittley rather than being preceded by yielding (Figure 54).

The hematite ore had an appreciably lower modulus of elasticity than the BHQ or quartzite but should still behave elastically unless subject to very high stress levels.

Although the schist showed a compressive strength in the same order of magnitude as the ore and a slightly lower elastic modulus, these samples represent the upper limit of the strength and elastic properties of the schist because of the problems of obtaining samples; the schist is very friable and tends to deteriorate when exposed to air.

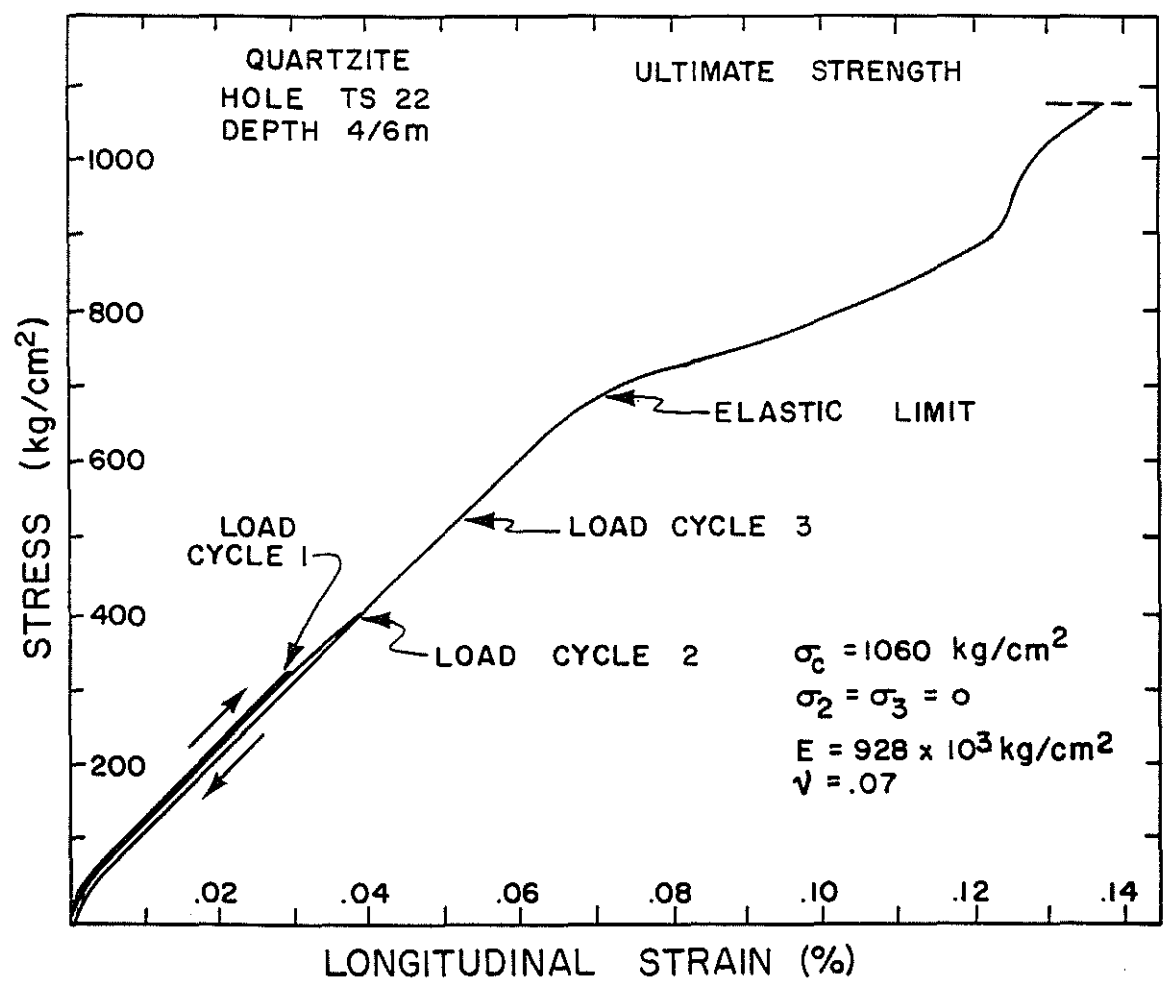


Figure 54. Stress Strain Curve for Quartzite.

There was also appreciable core loss experienced during drilling of the schist beds, therefore the possibility of the schist beds yielding nonelastically must be considered in the design of the Tazadit slopes.

For all of the rocks tested a small but significant increase in Poisson's ratio was noted for the confined tests as opposed to the unconfined tests. This effect was particularly noticeable for the iron ore which showed an increased rate of transverse strain at about 50% of the failure strength indicating a prefailure nonelastic yielding.

No clear-cut relationship between confinement and modulus of elasticity was shown by the test samples indicating the elastic modulus is relatively insensitive to confinement.

Rock Mass Classification

A general classification system for the rock mass (Coates 1964) includes a modifier describing the rock formation and the geologic name. According to this system, modified to use the strength categories defined by Deere (1968), the rocks of the Tazadit pit would be:

blocky, very strong, elastic banded hematite quartzite (BHQ)

broken and layered, very strong, elastic quartzite

layered, low strength, elastic schist (or phyllite)

blocky, medium strength, elastic hematite ore

The descriptive term "blocky" indicates a fracture spacing from one foot to six feet, and the term "broken" indicates a fracture spacing less than one foot.

Fracture Strength

In the case of a rock mass with a strong rock substance, the strength of the fractures is more important than the rock substance. Since the fractures are essentially two-dimensional features, failure takes place as tensile failure or opening of the fractures and as shear or slip along the fractures.

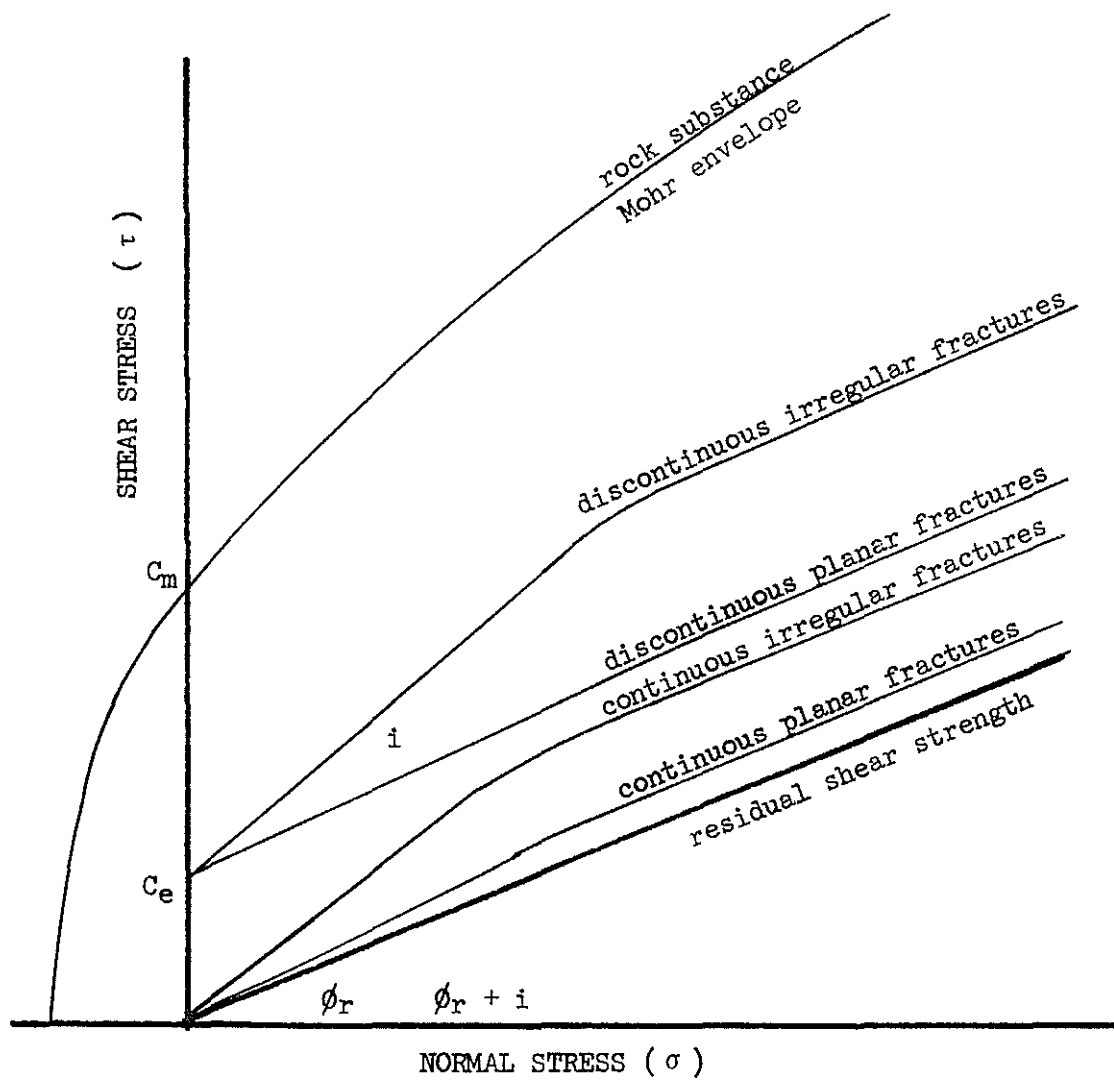
Tensile Strength

Although the Brazilian tension tests on the rock substance indicate tensile strengths ranging from 15 kg/cm² to 200 kg/cm², the fractures (jointing and bedding) are sufficiently intense and multi-directional to assume that the rocks of the Tazadit pit have little or no tensile strength in bulk.

Shear Strength

The shear strength of a fracture consists of two components: (1) the frictional resistance of the two surfaces sliding relative to one another and (2) the resistance to sliding resulting from the geometry of the fracture.

A convenient means of describing the shear strength of a rock is to plot the maximum shear stress at failure versus the normal stress as in the classic Mohr diagram (Figure 55). The maximum shear strength of a rock is that of the intact rock or rock substance with no fractures present. This is the Mohr envelope shown on the upper line of Figure 55. The minimum shear strength of a rock is the residual shearing strength of a smooth planar fracture after considerable displacement has occurred.



ϕ_r = Residual Friction Angle

i = Angle of Irregularities

$\phi_r + i$ = Effective Friction Angle

C_e = Effective Cohesion

C_m = Cohesion Intercept of Mohr Envelope

Figure 55. Shear Strength Envelopes for Fractures.

The shearing resistance of natural fractures lies between these two limiting envelopes. For a continuous fracture surface, the shearing resistance is a function of the irregularities of the surface. Patton (1966) has found that for low normal stresses the irregularities remain intact and the upper block slides up the irregularities as on an inclined plane. In this case the sliding resistance can be expressed by the relationship:

$$\tau = \sigma \tan (\phi_r + i)$$

where

i = inclination of the irregularities relative to the average plane of the fracture.

Field studies by Patton have shown that the first order irregularities, irregularities on the scale of one meter or greater, are more significant than the second order irregularities, which are irregularities less than ten centimeters.

At high normal stresses it has been found that the irregularities shear off and the strength envelope assumes the relationship:

$$\tau = c_e + \sigma \tan \phi_r$$

where

c_e = the effective cohesion mobilized in shearing the irregularities.

The more numerous the irregularities and the larger the i angle, the larger the effective cohesion will be.

For a failure to occur along a discontinuous fracture, some intact rock must be broken which will result in an effective cohesion. The amount of the effective cohesion will be a function of the amount of intact rock present along the fracture surface.

Because of the scale factor, only the intact rock envelope and the residual shear envelope can be determined with any certainty by laboratory testing. The contribution of the geometric aspects of the fracture to the shearing resistance is best determined by field observations of continuity and planarity.

Residual Shear Strength. It was originally intended to obtain samples for direct shear testing by coring 9 inch diameter samples oriented such that fractures would lie on the axis of the core. In spite of a great deal of effort by the Drilling Department in constructing drilling equipment and in test drilling, it was not possible to obtain suitable samples. Attempts were made to drill the schists in the footwall; however, water flow through the core barrel eroded the core so badly that the sample could not be obtained. In the quartzite and in the BHQ, the rock was fractured and broke up in the core barrel, then the fragments rolled around the core barrel damaging the bit and the core catcher.

As an alternate to coring, eight samples were obtained for direct shear tests by cutting rectangular specimens from blocks of rock obtained from the pit face. These samples consisted of schist, schist with thin interbeds of quartzite, and one sample of schistose BHQ. An attempt was made to obtain samples of quartzite and BHQ, but the

rocks at the pit face tended to be too fragmented to obtain a specimen containing suitable fracture planes. With the limited time available it was not possible to obtain samples. As the schists are the weakest rock in the Tazadit pit area and contain the most likely failure planes, the data from these samples is more valuable than data obtained from samples of quartzite and BHQ. There is information in the literature of the shear strength of sandstone and quartz minerals from which estimates can be made as to the shear strength of the quartzites and the BHQ (Coulson 1970).

The results and a description of the direct shear testing are given in a report by H. Kutter (1970). The procedure for the direct shear tests was to mount a sample, which was 9 inches by 9 inches by 12 inches, in the Imperial College direct shear machine. A normal stress was applied to the sample and a shear stress applied across the surface of sliding. The resulting displacement-stress curve shows a rapid rise in stress with displacement, reaching a peak, then dropping off asymptotically to a residual value. Usually a series of samples of the same rock type are tested at different normal stresses to develop peak and residual shear strength values for a range of normal stresses. Because of the limited number of samples from the Tazadit pit, each sample was displaced through a distance of 1 inch to develop the peak and residual strength, then the normal stress level was changed and displacement was continued (Figure 56). The normal stress was changed as much as five times through the displacement range of the testing machine, which is five inches. In this way, it was possible to

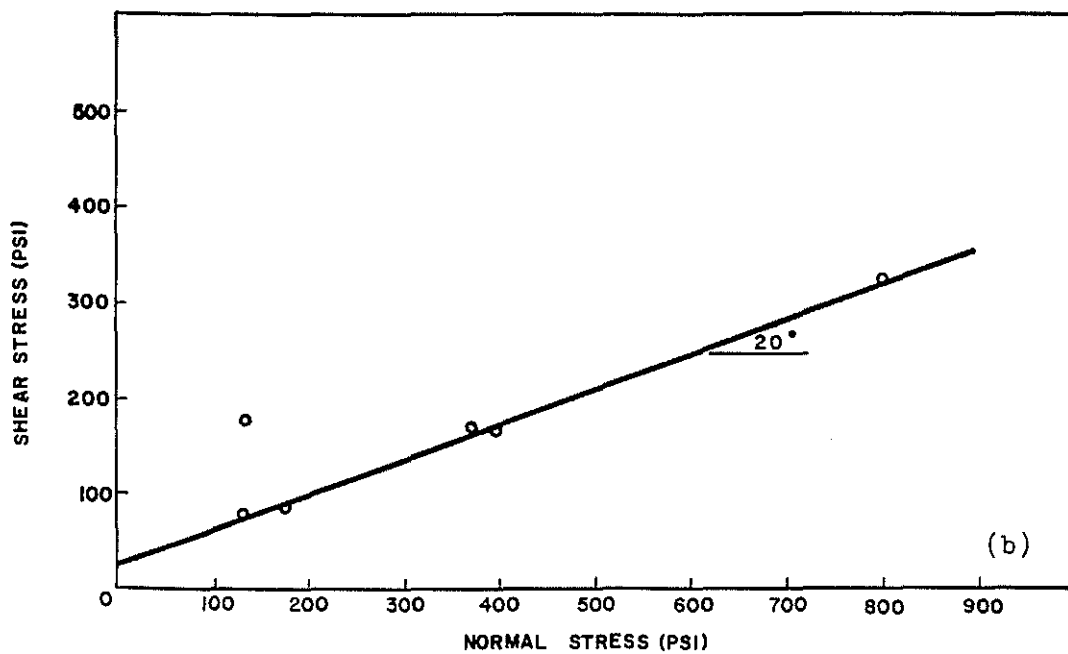
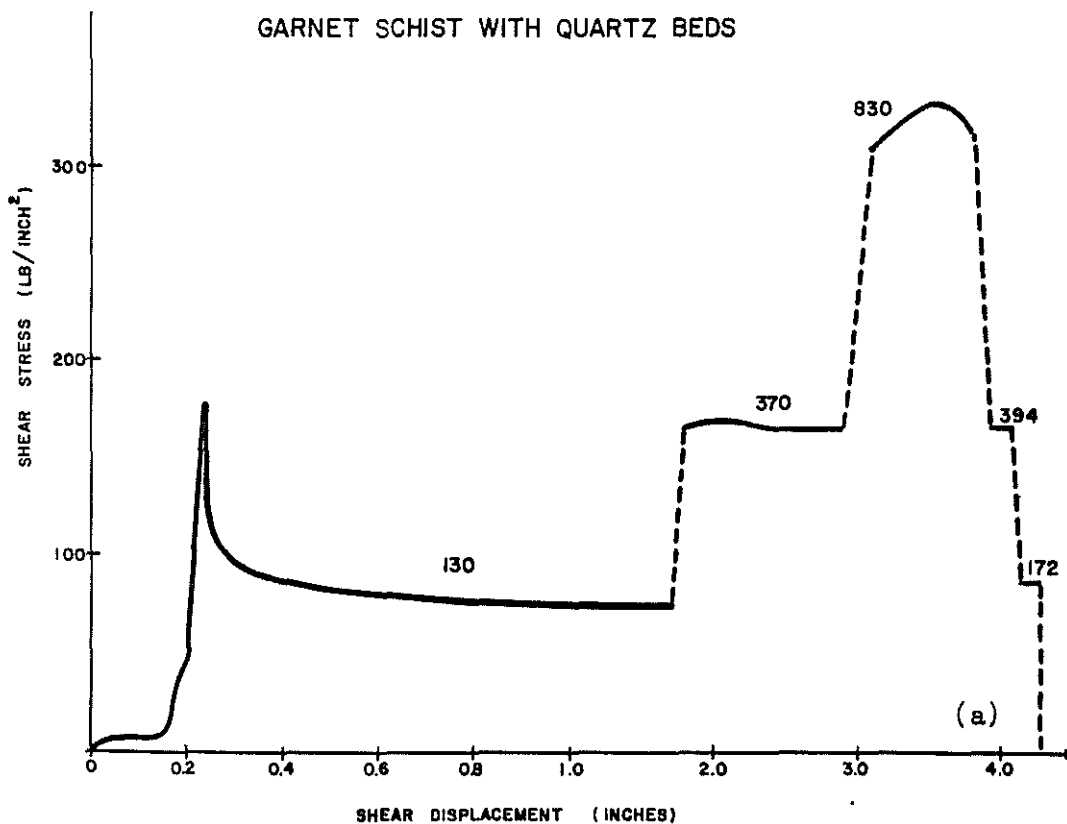


Figure 56. Direct Shear Test Results for Sample 1.

obtain a residual shear strength curve for each sample as shown in Figure 56.

The shear stress versus normal stress plot for each sample showed the linear relationship in agreement with the Coulomb equation

$$\tau = c + \sigma \tan \phi$$

where

τ = shear stress

σ = normal stress

$\tan \phi$ = coefficient of sliding friction

ϕ = friction angle

A linear regression analysis was used to obtain a least squares fit of the residual strength curve to the data points. The results of these tests are attached as Appendix A. The results are also shown on Table 8. Since the residual strength curve should go through the origin, the apparent cohesion intercepts are probably a machine constant which would have a mean value of 19.8 psi. This does not affect the residual friction angle, however.

In addition to the direct shear tests, slip tests were made on core specimens under triaxial conditions at the Elliot Lake Research Laboratory. The surfaces tested consisted of both natural fractures and surfaces cut with a diamond saw. The results of these tests agreed quite closely with the direct shear tests.

Table 8. Friction Angle Test Results

<u>Direct Shear Tests</u>			
Rock Type	Sample Number	Tan ϕ	ϕ
Schistose BHQ	3	0.622	31.9
Schist with Quartz beds	1	0.369	24.4 ^a
	4	0.451	24.4
	5	0.598	30.5
Mica Schist	7	0.503	26.7
	8	0.532	28.0
	2	0.501	26.6
Altered Mica Schist	6	0.416	22.6

<u>Triaxial Slip Tests</u>			
Rock Type	Sample Number	ϕ	
Ore	C 2, C 6	25	
	C 5, C 9	32	
Quartzite	C 17	26	
Micaceous Quartzite	C 154	26	
	C 155	27	
	C 147	27	
Schist	C 93	26	
	C 168	36	
Altered Schist	C 53	21	

^a = corrected for an inclination of the failure plane of -4°

Banded Hematite Quartzite. Since no shear tests were conducted on the banded hematite quartzite (BHQ), it is necessary to estimate the residual friction angle from data on the quartzite, the ore, and information from the literature on the sliding friction of quartz and sandstone. Figure 57 shows the results of the slip tests on the quartzite and on the ore, as well as direct shear tests on pure quartz and sandstone. (From Coulson 1970, p. 16.) The slip tests on the quartzite grouped quite closely between 26° and 27° and lay between the values obtained for dry quartzite, 24.5° , and dry sandstone, 29.5° . There were two slip tests for the hematite ore: one gave a value of 25° , the other a value of 32° , therefore the ore brackets the values for the quartzite. On the basis of these tests, the friction angle for the hanging wall BHQ will be assumed to be between 26° and 28° .

It has been demonstrated (Horn and Deere 1962) that water has little effect on the friction angle of rough surfaces of quartz. As can be seen in Figure 3.19, for ground surfaces of quartz mineral the friction angle actually is increased when water is added. For the two sandstones tested the difference between the wet and the dry tests were minimal, 0.5° or less. Thus, the same value for residual friction for the BHQ can be used for both the wet and the dry conditions.

Footwall Schist. A direct shear test on the footwall schist gave a range of friction angles from 22.5° to 31° . These values lie above those obtained for shear tests on pure mica and shales and are slightly below those obtained for a schistose gneiss which is comparable to the Tazadit schist in composition (Coulson 1970). The slip tests

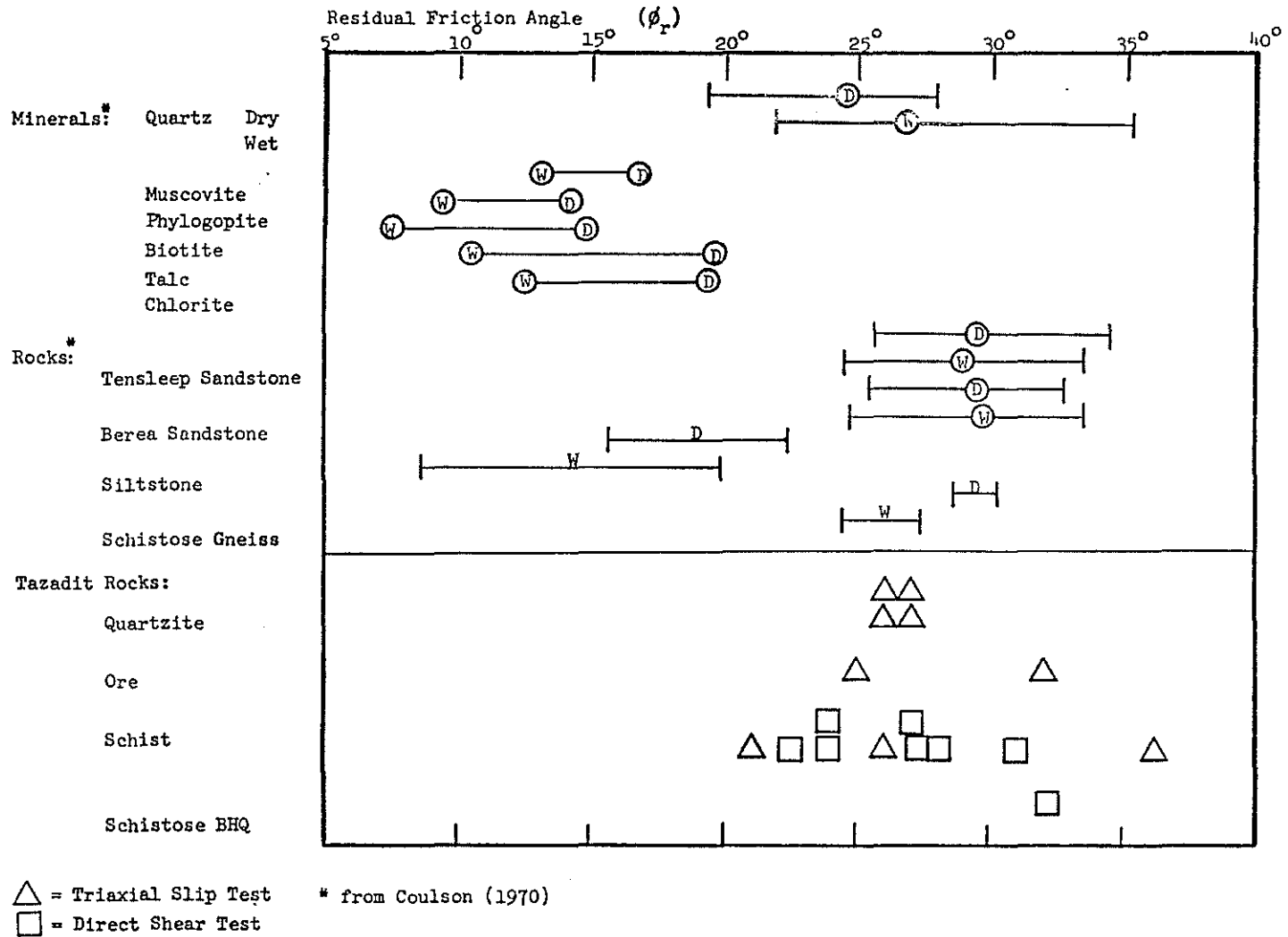


Figure 57. Friction Angles for Rocks and Minerals.

performed at Elliot Lake Laboratory gave three values, one at 21° , one at 26° and one at 36° , which bracket the values from the direct shear testing. For design purposes, an angle of 23° should be used rather than the mean value of 25.9° . On this basis only two samples, one slip test and one direct shear test, would have lower friction angles than the design value.

Water has a definite effect upon the friction angle of micaceous minerals. For example, for biotite the saturated sliding friction is 9° less than the oven-dried sliding friction and 7° less than the air-equilibrated sample (Horn and Deere 1962). Schistose gneiss tested by Coulson (1970) had a 4° lower angle of sliding friction when wet than when dry. Since the micaceous mineral of the footwall schist is predominately biotite and the direct shear tests performed at Imperial College were air-equilibrium tests rather than oven-dried, a 7° reduction in shear strength should be used for the saturated conditions for the footwall schist; i.e., an angle of 16° .

Footwall Quartzite. The slip tests performed at Elliot Lake Laboratory gave a residual friction angle of 26° to 27° for the footwall quartzite. This would be a representative value for joints which cut across the bedding. However, because of the presence of many thin schist beds within the quartzites, the shearing resistance of the quartzite would be governed more by the schist beds; thus, for the bedding within the quartzite, the 23° friction angle of the schist would be more appropriate.

Footwall Schistose Banded Hematite Quartzite (BHQ). Although the one direct shear test of the schistose BHQ gave a friction angle of 32° , the presence of many small beds of schist would make the 24° angle of friction for the schist itself more appropriate for the bedding planes in the schistose BHQ. For jointing, where the fracture plane breaks across the bedding, the 26° angle of friction for the quartzite would be more appropriate.

Effective Friction Angle. As mentioned above, the effective ϕ angle of a natural fracture is the ϕ angle of the residual shear plus the angle of irregularities measured relative to the mean surface of the plane. Although no specific measurements were made of the angles of the irregularities in the Tazadit pit, the fracture observations included a measurement of planarity. In the hanging wall, mapped by detail line, the joint distribution was 51% planar, 33% wavey, and 16% irregular (Table 9). In the footwall fracture set mapping, the jointing was 46% planar, 34% wavey, and 20% irregular.

An indirect measure of the i angle of a fracture set is the dispersion of the attitude measurements of that fracture set taken along a detail line. Although it is not the same as measuring the i angle of individual fractures, it is reasonable to assume that a potential failure plane following a joint set would have an effective i angle similar to the deviations of the individual joints from the mean attitude of the joint set.

To obtain dispersion values for the jointing of the footwall, 18 fracture sets were chosen on the basis of clustering on the scatter

Table 9. Planarity and Continuity Measurements

	Jointing				Bedding				
	Planar	Wavy	Irregular	Total	Planar	Wavy	Irregular	Total	
Footwall Fracture Set Data									
Continuous	6%	20%	2%	28%	17%	60%	4%	80%	
Micontinuous	19	8	7	34	5	10	1	16	
Discontinuous	21	6	11	38	0	1	2	4	
Total	46	34	20		22	71	7		

Hanging Wall Detail Line Data									
Continuous	21%	17%	4%	42%	28%	46%	1%	75%	
Micontinuous	22	10	5	37	10	11	1	22	
Discontinuous	8	6	7	21	0	3	0	3	
Total	51	33	16		38	60	2		

diagrams of the detail line samples. Since the potential movement would be primarily down-dip, the standard deviation of the dip was chosen as one estimate of the effective i angle (Table 10). The standard deviation of the dip for the 18 fractures varied from 2.2° to 11.2° with an average of 6.4° . As another estimate of effective i angle the maximum negative deviation from the mean for each set was determined. The negative deviation was chosen as it represents the irregularities the sliding block would have to ride over or shear off. The average maximum deviation for the 18 fracture sets is 10.4° .

The dispersion of the field measurements includes the measurement error. A test of operator variance for measurements (by eight trained men) of an ideal plane surface (a drafting table) gave a standard deviation of 0.5° . For field conditions, minimum operator variance of 1° would be more realistic. Removing this operator variance from the above dispersion values gives an estimate of the effective i angle for jointing in the footwall of the Tazadit pit of 5.4° to 9.4° .

In the footwall the bedding is unfavorably oriented and would constitute the most probable failure surface. Only 6% of the planarity observations for the footwall bedding were irregular, 71% were wavey, and 22% were planar. Although the majority of the bedding planes were recorded as wavey, this waviness is parallel to the fold axes and the lineation which are directed almost down-dip into the pit. Thus, for plane shear analysis, the bedding can be considered to be planar and the i angle for stability analysis should not be more than 1° or 2° .

Table 10. Tazadit Hanging Wall Joint Set Dispersion Values

Detail line	Joint set	n	<u>Dip</u>			<u>Strike</u>	
			s	R	d _n	s	R
1	1	23	6.4°	20°	7.1°	13.2°	45°
1	2	9	9.4	27	8.0	13.0	38
1	3	6	2.3	5	3.3	5.2	16
2	1	9	3.4	10	5.7	8.2	25
2	2	6	10.5	20	17.0	6.8	20
2	3	4	2.2	4	3.5	10.5	15
3	1	7	2.5	6	2.1	9.0	25
3	2	21	8.6	29	13.0	6.8	23
3	3	6	5.2	16	9.3	4.3	11
4	1	31	11.6	38	20.9	8.0	35
6	1	35	7.3	30	13.1	10.4	40
6	2	10	6.7	15	4.1	8.2	25
7	1	25	6.0	21	12.3	5.6	25
8	1	15	5.7	22	11.7	6.3	21
9	1	13	5.9	18	9.2	5.5	10
9	2	9	6.4	22	11.7	7.0	25
9	3	34	8.9	32	12.5	10.3	44
10	1	10	5.9	20	11.6	8.2	28

n = number of observations

s = standard deviation

R = range

d_n = maximum negative deviation

With a residual shear value of 24° for the schistose bedding planes in the footwall, the effective friction angle would be 25° to 26° .

Effective Cohesion. The effective cohesion of a natural fracture surface is a function of two things: (1) the amount of intact rock along the plane of the fracture surface and (2) the number of second order irregularities present on the fracture surface. As a rough approximation, the effective cohesion would be a percentage of the cohesion intercept of the Mohr circle for the intact rock. In the case of the BHQ, with a cohesion intercept of 350 kg/cm^2 , an estimate of 10% intact rock along the fracture plane (which is a conservative estimate) would give an effective cohesion for joint surfaces of 35 kg/cm^2 .

In the footwall, where potential failure surfaces would be primarily the bedding planes within the schist which are relatively continuous, no effective cohesion can be assumed for design purposes.

CHAPTER 7

DESIGN APPLICATIONS

Plane Shear Analysis

The plane shear analysis assumes that a volume of rock bounded by planar geologic structural features is free to slide into the pit. The driving force is the weight of the mass of rock and the resistance to sliding is determined by the Coulomb relationship.

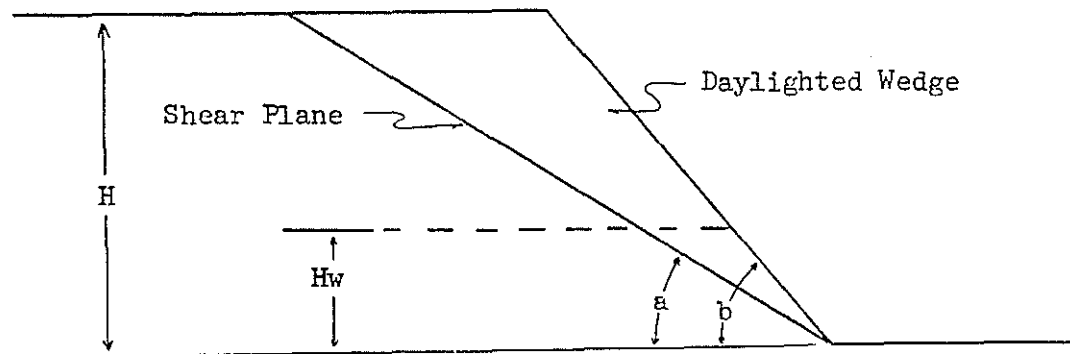
Where the failure surface is parallel to the pit slope a two-dimensional analysis can be used. For this analysis to apply, the potential failure surface must be parallel to the pit face and dip into the pit at an angle less than the pit slope angle. This is referred to as "daylighting," and the block between the potential failure surface and the pit face is called the daylighted wedge (Patton 1966). If the failure plane dips steeper than the pit slope, it does not intersect the face and a sliding block is not defined. If the failure surface is flatter than the angle of friction, the resisting force is greater than the driving force and the block will not slide unless high ground water pressures exist or the block is acted on by external forces such as earthquakes. Between these two limits, the stability is determined by the contribution to resisting forces made by the effective cohesion of discontinuities in the failure plane and the increase in the friction angle resulting from deviations from a true plane.

The method of calculating the stability is given in Figure 58 for two cases: (1) where the dip angle of the potential failure plane is specified, and (2) where the failure plane is not specified and the plane with the most unfavorable combination of driving forces and resisting forces is assumed.

The hydrostatic influence of ground water is included, assuming a horizontal water table.

The equations shown in Figure 58 were incorporated in the computer program "cohesion" which was used for making stability calculations. The program was designed to print out a tabular array (Figure 59) of effective cohesion values at limiting equilibrium for a range of slope angles and effective friction values when the slope height, rock density, dip of the potential failure plane, and hydrostatic water level are specified. A similar array (Figure 60) is also printed out for the maximum shear plane, in which case the dip of the maximum shear plane is computed (Figure 61).

This approach differs somewhat from the conventional computation of the safety factor of a slope although the same limiting equilibrium relationship is used. The safety factor is a dimension-less ratio of the resisting forces versus the driving forces and is therefore a function of the assumed values for cohesion and friction angles of the failure surface. The approach of relating the slope angle to the strength of the potential failure surface required for limiting equilibrium allows a determination of the maximum slope angle directly in terms of the strength of the rock rather than via a dimension-less ratio.



SHEAR PLANE SPECIFIED

$$\frac{\gamma H}{C} = \frac{2 \sin b \cos \phi}{\sin (b-a) [\sin (a-\phi) + K \sin \phi \sec a]}$$

$$K = \frac{\gamma_w \left(\frac{H_w}{H} \right)^2}{\gamma \left(\frac{H}{H} \right)}$$

MAXIMUM SHEAR PLANE

$$\frac{\gamma H}{C} = \frac{2 \sin b \cos \phi}{\sin \frac{1}{2}(b-(1-K) \phi) \left[\sin \frac{1}{2}(b-(1-K) \phi) + K \sin \phi \sec \frac{1}{2}(b+(1-K) \phi) \right]}$$

- H = slope height
- b = slope angle
- a = dip of shear plane
- H_w = height of water table above pit bottom
- γ = unit weight of rock
- γ_w = unit weight of water
- φ = friction angle of shear plane
- C = cohesion of failure surface

Figure 56. Limiting Equilibrium for a Planar Surface Parallel to the Pit Face.

LIMITING EQUILIBRIUM ON SPECIFIC PLANE

HEIGHT = 304.8 WATER LEVEL = 91.4 DENSITY OF ROCK = 3.40 ANGLE A=45.0
 COHESION AT LIMITING EQUILIBRIUM IN KG/CM²

D	F R I C T I O N										A N G L E															
	16	18	20	22	24	26	28	30	32	34	36	38	40	16	18	20	22	24	26	28	30	32	34	36	38	40
45	0.00	0.00	0.00	0.00	0.00	0.00	0.00	0.00	0.00	0.00	0.00	0.00	0.00	0.00	0.00	0.00	0.00	0.00	0.00	0.00	0.00	0.00	0.00	0.00	0.00	
50	3.04	2.99	2.73	2.57	2.41	2.24	2.07	1.89	1.70	1.51	1.30	1.08	.86	3.04	2.99	2.73	2.57	2.41	2.24	2.07	1.89	1.70	1.51	1.30	1.08	.86
55	5.66	5.33	5.09	4.79	4.49	4.18	3.86	3.52	3.17	2.81	2.42	2.02	1.59	5.66	5.33	5.09	4.79	4.49	4.18	3.86	3.52	3.17	2.81	2.42	2.02	1.59
60	7.93	7.58	7.16	6.76	6.33	5.89	5.44	4.96	4.47	3.95	3.42	2.85	2.25	7.93	7.58	7.16	6.76	6.33	5.89	5.44	4.96	4.47	3.95	3.42	2.85	2.25
65	10.07	9.57	9.05	8.54	8.00	7.44	6.86	6.27	5.64	4.99	4.31	3.60	2.84	10.07	9.57	9.05	8.54	8.00	7.44	6.86	6.27	5.64	4.99	4.31	3.60	2.84
70	12.05	11.41	10.80	10.17	9.53	8.87	8.18	7.47	6.73	5.95	5.14	4.29	3.38	12.05	11.41	10.80	10.17	9.53	8.87	8.18	7.47	6.73	5.95	5.14	4.29	3.38
75	13.82	13.13	12.43	11.71	10.97	10.20	9.41	8.60	7.74	6.85	5.92	4.93	3.89	13.82	13.13	12.43	11.71	10.97	10.20	9.41	8.60	7.74	6.85	5.92	4.93	3.89
80	15.54	14.77	13.98	13.17	12.34	11.48	10.59	9.67	8.71	7.71	6.66	5.55	4.38	15.54	14.77	13.98	13.17	12.34	11.48	10.59	9.67	8.71	7.71	6.66	5.55	4.38
85	17.22	16.37	15.49	14.59	13.67	12.72	11.74	10.71	9.65	8.54	7.37	6.15	4.85	17.22	16.37	15.49	14.59	13.67	12.72	11.74	10.71	9.65	8.54	7.37	6.15	4.85
90	18.87	17.94	16.96	15.99	14.98	13.94	12.86	11.74	10.58	9.36	8.08	6.74	5.32	18.87	17.94	16.96	15.99	14.98	13.94	12.86	11.74	10.58	9.36	8.08	6.74	5.32
95	20.52	19.51	18.46	17.39	16.29	15.16	13.99	12.77	11.50	10.18	8.79	7.33	5.78	20.52	19.51	18.46	17.39	16.29	15.16	13.99	12.77	11.50	10.18	8.79	7.33	5.78
96	22.21	21.19	19.97	18.81	17.63	16.40	15.13	13.81	12.44	11.01	9.51	7.93	6.26	22.21	21.19	19.97	18.81	17.63	16.40	15.13	13.81	12.44	11.01	9.51	7.93	6.26
95	23.93	22.74	21.53	20.28	19.00	17.68	16.31	14.89	13.41	11.86	10.25	8.54	6.74	23.93	22.74	21.53	20.28	19.00	17.68	16.31	14.89	13.41	11.86	10.25	8.54	6.74

Figure 59. Cohesion Required on Specified Failure Plane at Limiting Equilibrium.

LIMITING EQUILIBRIUM ON MAXIMUM SHEAR PLANE

HEIGHT = 304.8 WATER LEVEL = 91.4 DENSITY OF ROCK = 3.40
 COHESION AT LIMITING EQUILIBRIUM IN KG/CM²

θ	F R I C T I O N										A N G L E														
	16	18	20	22	24	26	28	30	32	34	36	38	40	16	18	20	22	24	26	28	30	32	34	36	38
20	.24	.28	.30	.32	.34	.36	.38	.40	.42	.44	.46	.48	.50	.52	.54	.56	.58	.60	.62	.64	.66	.68	.70	.72	.74
25	.46	.55	.61	.67	.73	.79	.85	.91	.97	1.03	1.09	1.15	1.21	1.27	1.33	1.39	1.45	1.51	1.57	1.63	1.69	1.75	1.81	1.87	1.93
30	1.71	1.29	.94	.63	.39	.20	.07	.01	.01	.09	.24	.47	.80	1.21	1.67	2.14	2.59	3.04	3.49	3.94	4.39	4.84	5.29	5.74	6.19
35	2.69	2.21	1.77	1.38	1.03	.73	.48	.28	.13	.03	-.00	.03	.13	.29	.50	.74	1.01	1.31	1.63	1.97	2.32	2.67	3.02	3.37	3.72
40	3.77	3.24	2.74	2.29	1.87	1.49	1.14	.84	.58	.37	.20	.08	.01	.11	.27	.47	.71	1.00	1.31	1.64	2.00	2.36	2.72	3.08	3.44
45	4.94	4.37	3.84	3.33	2.86	2.42	2.01	1.63	1.29	.98	.71	.48	.29	.34	.51	.71	1.00	1.31	1.64	2.00	2.36	2.72	3.08	3.44	3.80
50	6.19	5.63	5.03	4.49	3.97	3.49	3.03	2.59	2.19	1.81	1.47	1.15	.87	.92	1.10	1.31	1.54	1.80	2.09	2.39	2.69	2.99	3.29	3.59	3.89
55	7.53	6.91	6.32	5.75	5.20	4.68	4.18	3.71	3.26	2.83	2.42	2.04	1.69	1.74	1.93	2.15	2.39	2.65	2.93	3.21	3.49	3.77	4.05	4.33	4.61
60	8.95	8.32	7.71	7.12	6.55	6.00	5.47	4.97	4.48	4.01	3.56	3.13	2.72	2.77	2.97	3.20	3.45	3.71	3.97	4.23	4.49	4.75	5.01	5.27	5.53
65	10.47	9.82	9.20	8.59	8.01	7.44	6.89	6.36	5.85	5.35	4.87	4.40	3.95	3.99	4.20	4.44	4.69	4.94	5.19	5.44	5.69	5.94	6.19	6.44	6.69
70	12.08	11.43	10.80	10.18	9.59	9.01	8.45	7.90	7.37	6.85	6.34	5.86	5.38	5.42	5.64	5.88	6.13	6.38	6.63	6.88	7.13	7.38	7.63	7.88	8.13
75	13.82	13.16	12.52	11.91	11.30	10.72	10.14	9.59	9.04	8.51	8.00	7.49	7.00	7.03	7.26	7.51	7.76	8.01	8.26	8.51	8.76	9.01	9.26	9.51	9.76
80	15.69	15.03	14.39	13.77	13.17	12.58	12.00	11.44	10.90	10.36	9.84	9.33	8.83	8.85	9.08	9.33	9.58	9.83	10.08	10.33	10.58	10.83	11.08	11.33	11.58

Figure 60. Cohesion Required on Maximum Shear Plane at Limiting Equilibrium.

LIMITING EQUILIBRIUM ON MAXIMUM SHEAR PLANE

HEIGHT = 304.8 WATER LEVEL = 91.4 DENSITY OF ROCK = 3.40

ANGLE OF MAXIMUM SHEAR PLANE

	F R I C T I O N A N G L E												
	16	18	20	22	24	26	28	30	32	34	36	38	40
20	17.8	18.8	19.7	20.7	21.7	22.7	23.6	24.6	25.6	26.6	27.5	28.5	29.5
25	20.3	21.3	22.2	23.2	24.2	25.2	26.1	27.1	28.1	29.1	30.0	31.0	32.0
30	22.8	23.8	24.7	25.7	26.7	27.7	28.6	29.6	30.6	31.6	32.5	33.5	34.5
35	25.3	26.3	27.2	28.2	29.2	30.2	31.1	32.1	33.1	34.1	35.0	36.0	37.0
40	27.8	28.8	29.7	30.7	31.7	32.7	33.6	34.6	35.6	36.6	37.5	38.5	39.5
45	30.3	31.3	32.2	33.2	34.2	35.2	36.1	37.1	38.1	39.1	40.0	41.0	42.0
50	32.8	33.8	34.7	35.7	36.7	37.7	38.6	39.6	40.6	41.6	42.5	43.5	44.5
55	35.3	36.3	37.2	38.2	39.2	40.2	41.1	42.1	43.1	44.1	45.0	46.0	47.0
60	37.8	38.8	39.7	40.7	41.7	42.7	43.6	44.6	45.6	46.6	47.5	48.5	49.5
65	40.3	41.3	42.2	43.2	44.2	45.2	46.1	47.1	48.1	49.1	50.0	51.0	52.0
70	42.8	43.8	44.7	45.7	46.7	47.7	48.6	49.6	50.6	51.6	52.5	53.5	54.5
75	45.3	46.3	47.2	48.2	49.2	50.2	51.1	52.1	53.1	54.1	55.0	56.0	57.0
80	47.8	48.8	49.7	50.7	51.7	52.7	53.6	54.6	55.6	56.6	57.5	58.5	59.5

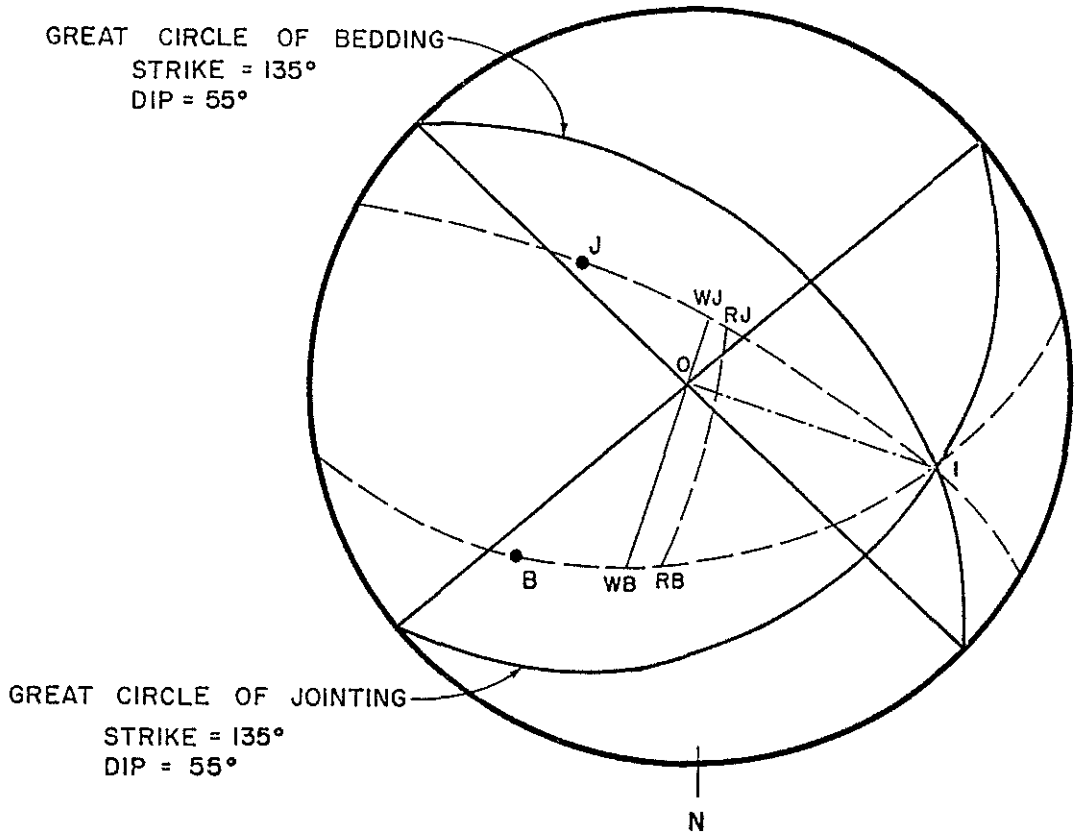
Figure 61. Dip of Maximum Shear Plane.

It is more realistic and easier to comprehend conceptually, to state that a slope angle of 65° , for example, will be stable if the potential failure surface has an angle of friction greater than 32° and a cohesion greater than 4 kg/cm^2 , than to state that a 65° slope would have a safety factor of 1.2. The computation of a safety factor implies a greater precision than is warranted and tends to divert one's thinking to consideration of what is the appropriate safety factor for a slope rather than evaluation of the assumptions which were used to make the calculations.

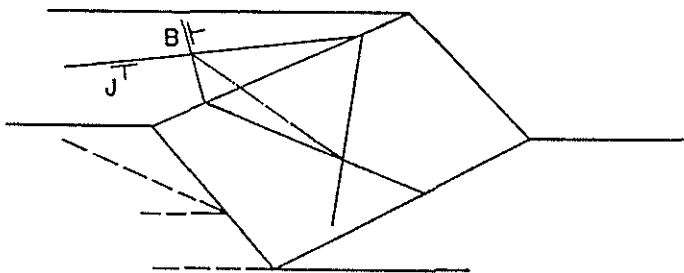
When there are no fractures parallel to the pit face, the potential failure geometry can be formed by the intersection of two fractures as shown in Figure 62a. If the line of intersection dips into the pit and is daylighted, the block bounded by the two fractures in the pit face is free to slide into the pit. Depending upon the relative orientations of the two fractures, motion can be sliding on one fracture surface and separation on the other, or sliding on both surfaces, in which case the direction of motion is along the line of the intersection.

In the case where the sliding occurs on one plane, the separation or opening occurs on the second plane, the two-dimensional plane shear analysis can be used as an approximate solution. The dip of the failure plane (angle a in Figure 58) would be replaced by the direction of movement which would be an apparent dip of the failure plane.

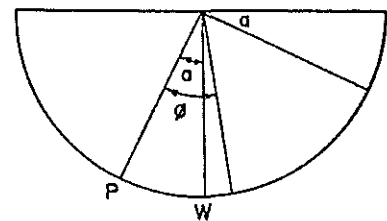
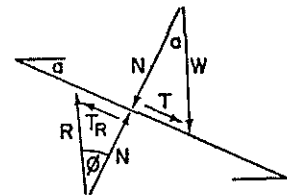
For the case of sliding on both planes, the limiting equilibrium condition is similar to the simple two-dimensional plane shear except



(b) Schmidt Diagram Graphic Analysis



(a) Isometric Diagram of Wedge



(c) Two-dimensional Analog

Figure 62. Graphic Stability Analysis of a Wedge Formed by the Intersection of Two Fractures

that the weight of the sliding block must be resolved into a normal force and a shear force on each plane.

A graphic analysis using a Schmidt diagram (John 1968) can be employed to assess the potential for sliding. In this method the great circles of the fractures are plotted to determine the direction and plunge of the line of intersection as shown in Figure 62b. The great circle through the intersection (I) and the pole of one of the fractures (B or J) represents the plane containing the direction of motion (OI) and the direction of the normal to the fracture (OB and OJ). The friction angles for the two surfaces (ϕ_b and ϕ_j) are measured along the great circles utilizing the friction cone concept of Talobre (1957). These points are shown in Figure 62b. If the great circle connecting points RB and RJ lies on the same side of the center of the diagram as the direction of motion (OI) the resisting forces will be greater than the driving forces and the block will be stable. When the RB-RJ great circle passes through the center (O), the block would be at limiting equilibrium. An RB-RJ great circle on the side of O (center) opposite from the direction of motion indicates instability.

This graphic solution is the three-dimensional analog to the simple two-dimensional plane shear model with no cohesion where the sliding block is stable if the failure plane has an inclination less than the friction angle of the failure plane. In the example shown in Figure 62b. the angle B,WB measured on the BI great circle is the equivalent of the inclination (a) of the failure plane in the two-dimensional model for sliding on the bedding plane (Figure 62c).

Thus, if B, WB is less than ϕ for the bedding and J, WJ is less than ϕ for the jointing, sliding will not occur.

The manner of plotting the angular relationships on the Schmidt diagram is independent of the position of the structures, thus the area and volume cannot be included in the graphic analysis which limits it to the no cohesion case. Numerical methods are available for computing the stability of an intersection type geometry (Lounde 1965) which includes effective cohesion and fluid pressures. The graphic method, however, is a rapid and inexpensive method of evaluating intersections where cohesion is not a critical factor. The two-dimensional plane shear solution using the line of intersection as the failure plane can be used to give conservative solutions including effective cohesion and hydrostatic pressure.

Analysis of the Tazadit Pit Hanging Wall

Planar Features Parallel to the Pit Slope

The simplest method of locating potential plane shear failure is by use of a Schmidt diagram. Figure 63 is a contoured plot of joint observations from the detail line mapping of the hanging wall. It can be seen on the diagram that the main joint concentration strikes between 60° and 140° with a complete range of dips from 0° to 90° . This indicates a potential plane shear type failure in the south and southwest quadrant of the pit. The main sector of the hanging wall, which has a strike of approximately 150° , is relatively free of structures parallel to the face dipping into the pit. The bulk of the bedding is parallel to the

hanging wall but dipping into the hanging wall, and therefore would not produce plane shear failure.

In the northwest quadrant of the pit there is a second high angle group of joints with strikes of 200° to 310° . Some of the bedding is in the same attitude, thus there is a potential second plane shear failure situation in the northwest quadrant of the pit.

For the main joint set with a potential failure in the southwest quadrant of the pit, the potential failure planes would lie above a minimum of 26° , assuming a minimum angle of friction of 26° . This limit is shown on Figure 63 . It can be seen on the diagram that the major concentration, the 5% per 1% area contour, lies between 40° and 45° . By limiting the maximum slope to 65° , a second concentration of 4% is eliminated because it is dipping steeper than the pit slope and would therefore not daylight.

For the jointing in the BHQ we have assumed a ϕ of 26° and an i of 5° , so the effective friction angle would be 31° to 36° ; thus limiting equilibrium would not be exceeded on any surface flatter than 31° . For daylighted surfaces with a dip greater than 31° , cohesion is required for limiting equilibrium. Since the joints are distributed fairly evenly between 40° dip and 65° dip (Figure 64), the maximum shear plane option of the cohesion program is most applicable. The cohesion required for stability at various slope angles is shown in Table 11 and plotted on Figure 63.

A slope of 65° would require a cohesion of 4 kg/cm^2 on a failure plane dipping 50° . This would be equivalent to 2% intact rock along the

Table 11. Limiting Equilibrium for Plane Shear Failure

Slope Height = 250 Meters Density = 3.40

Slope Angle	<u>Effective Friction Angle</u>							
	26°		30°		34°		38°	
	Ce	Pm	Ce	Pm	Ce	Pm	Ce	Pm
35	0.5	31°	0.2	33°	--	--	--	--
40	1.1	33°	0.6	35°	0.2	37°	0.1	39°
45	1.8	36°	1.2	38°	0.7	40°	0.3	42°
50	2.7	38°	1.9	40°	1.3	42°	0.8	44°
55	3.6	40°	2.8	43°	2.1	45°	1.4	47°
60	4.7	43°	3.8	45°	3.0	47°	2.3	49°
65	5.8	46°	4.9	48°	4.0	50°	3.2	52°
70	7.1	48°	6.1	50°	5.2	52°	4.4	54°
75	8.4	51°	7.4	53°	6.5	55°	5.6	57°
80	9.9	53°	8.9	55°	8.0	57°	7.0	59°

Ce = Effective Cohesion

Pm = Dip of Shear Plane

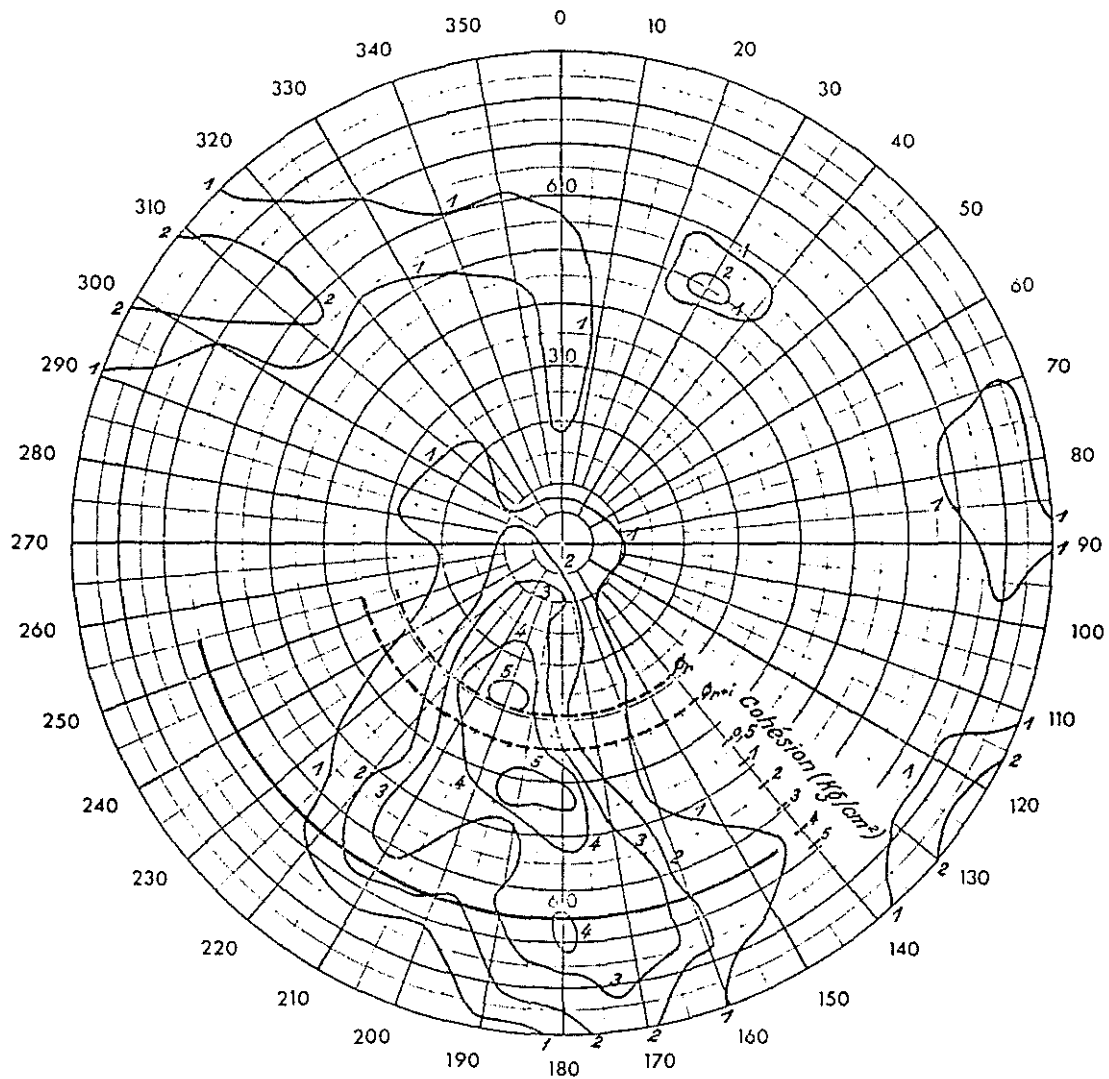
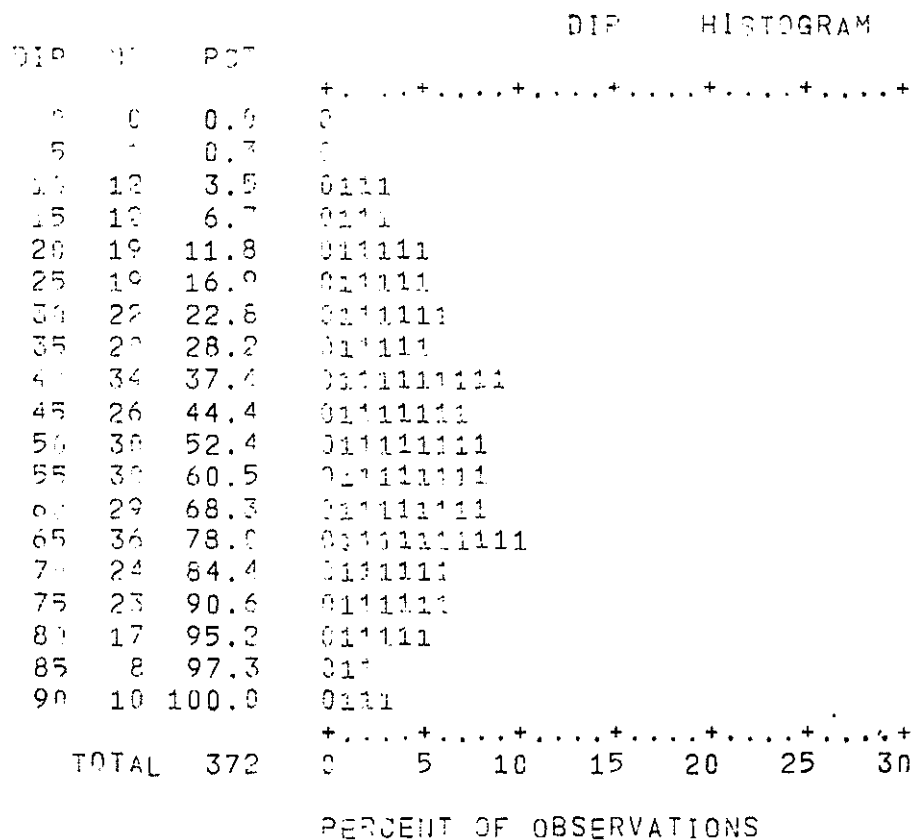


Figure 63. Schmidt Diagram of the Plane Shear Analysis of Hanging Wall Jointing.



STRIKE MINIMUM = 270. STRIKE MAXIMUM = 360.
 DIP MINIMUM = DIP MAXIMUM = 180.

Mean Dip = 50.1° Std. Dev. = 20.7°

Figure 64. Dip Histogram of Hanging Wall Critical Joint Set.

failure surface, well within the estimate of 10% minimum intact rock based on the continuity measurements of jointing in the hanging wall. Alternately, the 4 kg/cm^2 is less than the 7 kg/cm^2 difference between peak and residual strengths for the direct shear tests at 10 kg/cm^2 normal stress. Thus, a 65° slope would be stable with respect to plane shear failure along a surface dipping into the pit.

Intersections

The joint attitude data from the detail line mapping of the hanging wall was examined for possible failure composed of two joint surfaces not parallel to the pit face but whose intersection is directed into the pit.

For each line, the three or four most prominent joint sets were chosen by inspection of the Schmidt plot. These sets were grouped into pairs, and all the possible intersections for each pair were calculated and plotted on a Schmidt diagram using the Intersections, Intermean and Interschmidt Programs. Twenty-five pairs were analysed and a total of about 5000 intersections were computed.

Pairs of fracture sets for which 90% or more of the intersections dipped less than the effective friction angle of 31° were eliminated leaving fourteen pairs which were analysed by the graphic method of John (1968). Of these fourteen pairs, ten would involve sliding on surfaces striking about 310° and opening on other surfaces. This sliding surface is the same joint set as analysed with the two-dimensional approach and the same conclusions would apply.

The remaining four pairs are:

Line	Set 1		Set 2		Per Cent of Potential Failure Intersections For The Detail Line
	Strike	Dip	Strike	Dip	
1	310°	50°	240°	50°	2%
8	255°	70°	40°	70°	5%
9	267°	78°	40°	70°	15%
10	255°	70°	40°	85°	10%

For these cases the cohesion required for limiting equilibrium would be the same or less than for the two-dimensional analysis. Thus, they should present no problems for a 65° slope. Since they are local in nature involving only one detail line and only a small percentage of the total jointing, any failures which might occur would be small (one or two benches) and would be infrequent.

Analysis of the Tazadit Pit Footwall

Planar Features Parallel to the Pit Slope

The predominant fracture system in the footwall is the bedding which strikes 149° and dips 63° (Figure 65). Since the footwall of the ore body is in general concordant with the bedding, along most of the footwall side of the pit the bedding will be parallel to the pit face and dipping into the pit. Thus, any slope angle which is steeper than the dip of the bedding has a potential for plane shear failure as the bedding will be daylighted. The bedding is planar and continuous with a very small cohesion and an estimated friction angle of 23°. With this type of potential failure plane, any daylighted wedge would be unstable unless the failure plane (bedding) had a dip of 23°, which is not the case in the Tazadit footwall. Empirical evidence for this control of

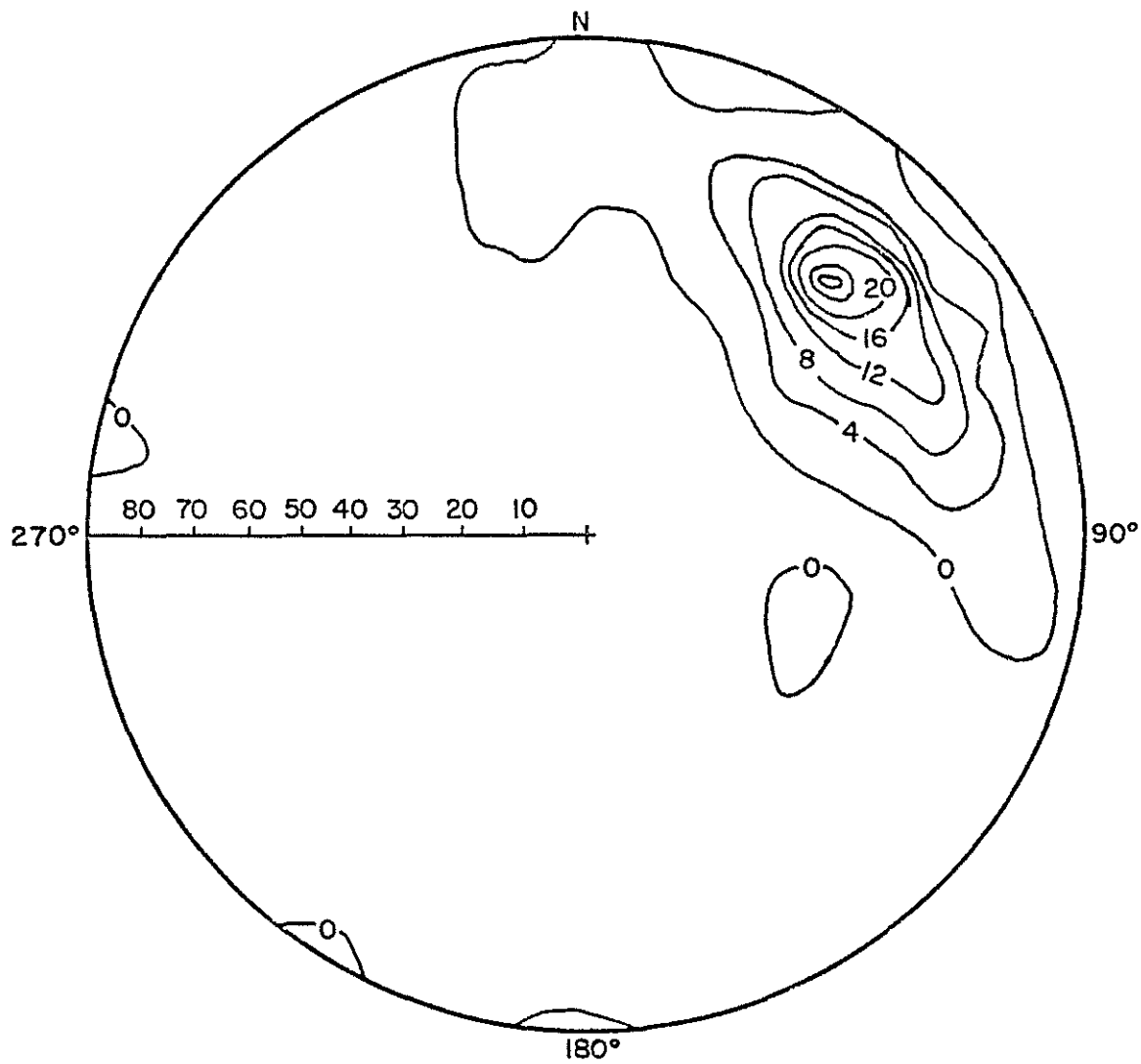


Figure 65. Schmidt Diagram of Footwall Bedding.

the slope angle by the bedding is the geometry of the existing bench faces. Even with vertical blast holes the bench face breaks back to the bedding plane that daylights at the toe of the bench.

Under these conditions, determining the maximum slope angle with respect to the plane shear analysis becomes a problem of determining the dip of the bedding. Since there are variations in the dip from location to location and an additional dispersion is introduced with a normal operator variance, the dip of the bedding is not a single number but is a distribution which must be analysed on a statistical basis.

A histogram of the fracture set measurements of dip is shown in Figure 66. The mean dip is 63.3 with a standard deviation of 9.5. The fracture set data were chosen for this analysis rather than the oriented core data or a combination of the two as the fracture set measurements are less influenced by minor local variations on the scale of several centimeters (as is the case with oriented core) and also have a lower measurement error than the indirect oriented core technique.

The mean dip of the bedding is not a satisfactory maximum slope angle as it would result in 50 per cent of the observed bedding planes flatter than the slope and thereby daylighted. Likewise the flattest observed bedding is not a satisfactory maximum slope angle as the low angle observations represent local folding and the cost of flattening the slope to eliminate all small local slides would be greater than the cost of the slides.

The dip histogram (Figure 66) shows a sharp increase in the percentage of observations between 50° and 55° . An overall pit slope

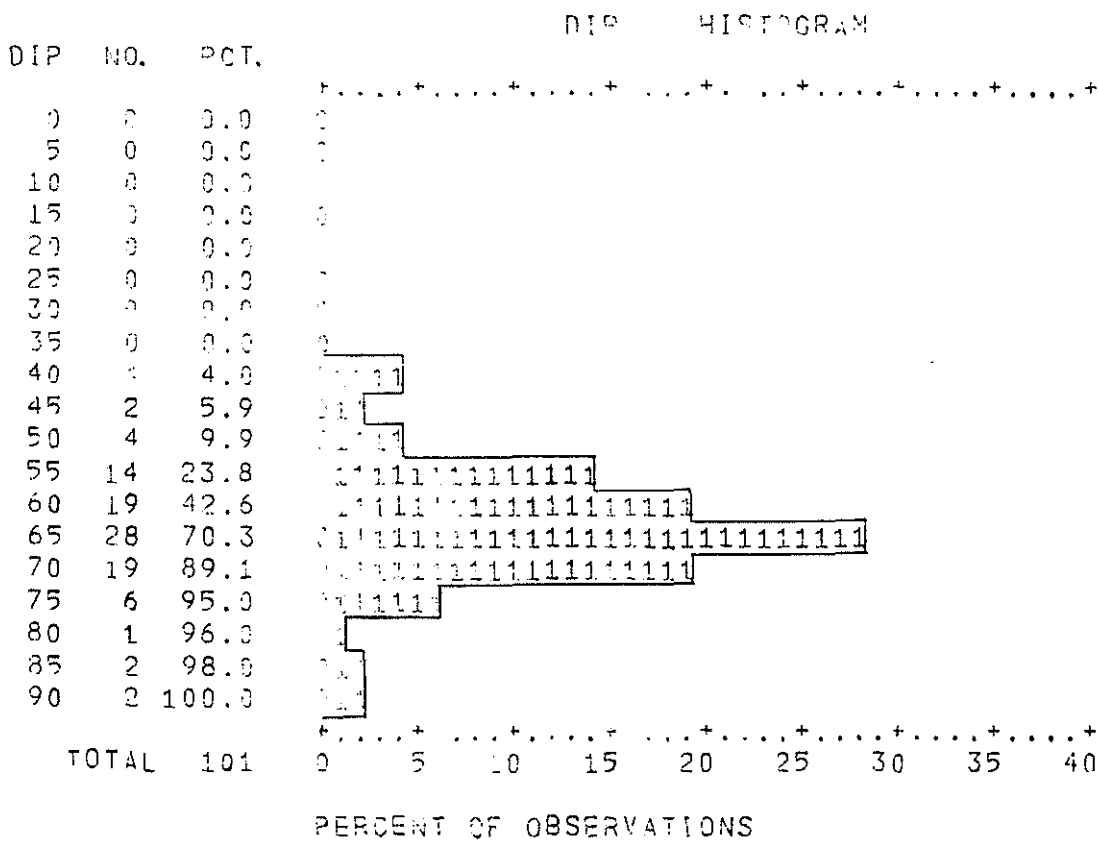


Figure 66. Dip Histogram of Footwall Bedding.

angle of 50° would therefore be a logical choice. Only six observations, which represent 6% of the total observations, are flatter than 50° . These observations are of bedding in areas of local folding and are not representative of the overall structure. The specific observations are described in Table 12. Since these observations do not all come from the same area, and the dips of less than 50° do not extend for more than one bench (12 meters), an overall slope of 50° would produce only a few daylighted wedges one or two benches high and of a similar extent. These observations were made on the present pit face and are, therefore, not the specific situations that will be encountered in the final pit; but they are representative of the type of deviation from the mean attitude that will be present in the final pit wall.

Intersections

To test for potential failure geometry, the intersection of all combinations of joints was computed. As can be seen on the Schmidt plot (Figure 67a), the predominant direction of the line of intersection is to the northeast with a plunge of 45° or less. Thus, the joint intersections are directed into the pit wall and would not constitute a potential failure geometry situation.

The intersections between jointing and bedding were also computed (Figure 67b). The predominant plunge of the intersections is 60° and the direction is 210° . These would appear as intersections dipping into the pit in the northeast corner of the pit where the strike is 120° . However, with a pit slope of 50° , these intersections would not be daylighted.

Table 12. Bedding Observations With Dips Less Than 50 Degrees

Number	Strike	Dip	Level	Coordinate	Description
1	200°	38°	634	759120 E	Overtured limb in a zone of repeated folding of the quartzite. A small scale feature extending less than one bench.
2	119°	42°	622	759147 E	A roll in the schist quartzite contact in the lower half of the bench. The same contact in the top of the bench dips 55° and in the bench below dips 60°, so only half a bench is involved.
3	138°	40°	610	2511384 N	A bedding plane in a schist bed. The same bed was intercepted by drill hole TS 28. Measuring from the pit surface to the drill hole the dip is 60°.
4	154°	45°	610	2511341 N	A shear plane in a section of contorted schist. Other observations in the same area range from 55° to 80°.
5	212°	39°	598	2511222 N	A limb of a small fold in schist just above TS 30. Oriented core from the same bed 20 meters below had a dip of 70°.
6	158°	47°	598	2511213 N	Same as Number 5.

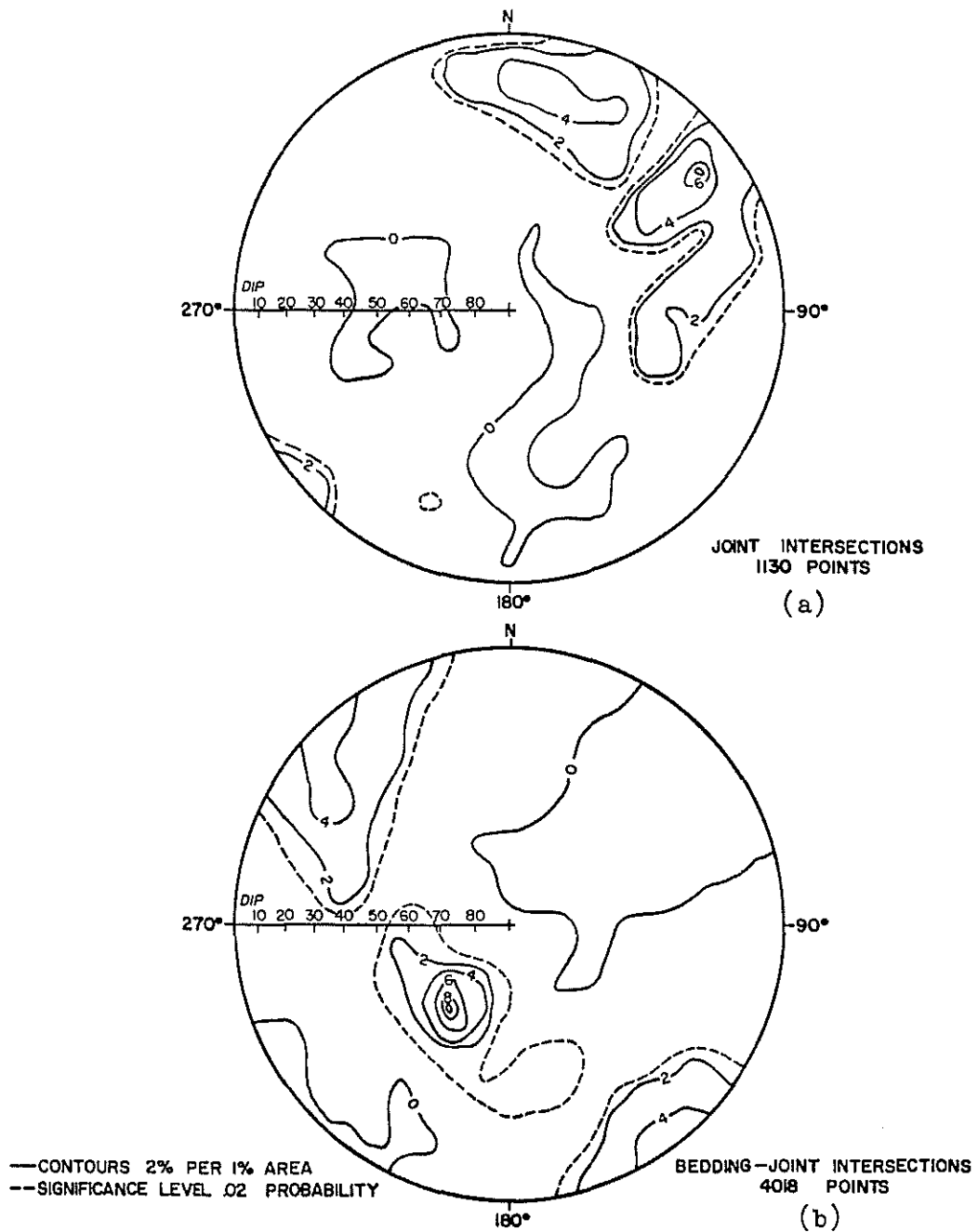


Figure 67. Footwall Fracture Intersections.

A second concentration of intersections is between bedding and jointing, is horizontal, and with a northwest-southeast direction. This does not constitute a probable failure geometry because of the low dip.

The most critical intersections between bedding and jointing are those plunging 30° to 50° with a direction of 280° . A typical intersection of this orientation is shown in Figure 62. Limiting equilibrium would exist for friction angles of 22° for the bedding and 30° for the jointing. The friction angles of 23° for the bedding and 31° to 36° for jointing (derived from the rock strength study) would make the potential sliding block stable but close to limiting equilibrium. Since the joints are discontinuous and therefore have cohesion (which is not included in this analysis), the potential failure planes would have sufficient strength to resist sliding.

Effect of Ground Water

Although the Tazadit Pit area, with an annual rainfall of less than 3 inches per year, is very dry by normal climatic standards, the proposed pit depth of 334 meters will intersect the static ground water table and the effect of water on the stability of the slope must be considered.

Water level measurements taken during the Person deep drilling and piezometers installed in TS 29 and TS 30 demonstrated that the static water level is almost horizontal at an elevation of 397 meters. Pumping of T0 13 during one month produced a drawdown of 0.4 meters in K10 at a distance of about 650 meters, which indicates that an open aquifer condition exists at least in the hanging wall.

Hydrostatic Uplift

The influence of hydrostatic uplift is included in the sliding block stability calculation (Program Cohesion) by a reduction in the effective normal stress equal to the weight of a column of water from the failure surface to the water table.

Calculations for the hanging wall at a pit depth of 334 meters, assuming maximum shear plane and a ϕ of 35° , showed an equilibrium cohesion of 5.12 kg/cm^2 for a slope of 65° without water, and 5.24 kg/cm^2 for the same slope with water. This change in cohesion is equivalent to a 0.4° change in slope angle. For the footwall slope of 50° and a ϕ of 26° , the difference (change in equilibrium cohesion) is from 2.61 kg/cm^2 to 2.65 kg/cm^2 , which is equivalent to a slope angle change of 0.2° . Thus, the effect of hydrostatic uplift alone is small.

Seepage Pressure

When large quantities of water flow into a pit, the seepage pressure exerts an adverse effect on the stability of the slope. Since there is little or no recharge of ground water in the Tazadit area, large continuous flows are not likely. Flow into the pit would probably be erratic, with large flows occurring as a fracture is intersected, diminishing quickly as the fracture is drained. With the present knowledge, it is difficult to assess the potential effect on slope stability.

If it is possible to lower the water table in the footwall so that the hydraulic gradient is away from the pit, the seepage pressure will improve rather than decrease the stability of the slope.

Reduction of Shear Strength

Laboratory tests have shown that the friction angle for wet quartz is the same or slightly higher than for dry quartz. Thus water in the BHQ of the hanging wall would not reduce the ϕ for the hanging wall.

Layered silicates do show a reduction in ϕ when wet, although the effect may be due more to the low permeability causing an undrained condition with resulting high pore pressure than to an actual reduction in ϕ . The effect is greater for clay minerals than for micas, which are the principal components of the footwall schists. As indicated in the chapter on rock strength, saturation of the footwall schist could reduce ϕ from 23° to 16° . However, in the plane shear analysis of the footwall, it is assumed that the bedding planes have a low strength and could not be daylighted. Thus a failure geometry would not be defined and the shear strength of the bedding would not enter directly in the stability analysis.

Finite Element Analysis

The stresses in a pit slope are affected by variations in the physical properties of the rock, the geometry of the slope, and regional tectonic stresses. In the Tazadit Pit, where the rock is anisotropic

and nonhomogeneous, the stress distribution could be expected to depart significantly from the simple vertical gravitational load mode.

To estimate the stresses in the walls of the final pit slope, a finite element analysis was conducted. D. F. Coates and his associates at the Canadian Mining Research Center (Ottawa) were chosen to perform the analysis because of their experience with the method. Since the Tazadit pit geology and geometry resulted in a much larger and more complex finite element model for a pit than had been attempted previously, the analysis was, in part, experimental.

The first set of analyses (Yu, Coates, and Toews, 1970) were run with preliminary information, as the scheduling of the project required that the finite element model construction be started before the geologic investigations were completed. Subsequent to these analyses, revised estimates of the physical properties of the rocks were developed. Since the revised values are significantly different from the preliminary estimates, additional computer runs will be required to assess the effect of the changes. Thus, it would be premature to present the results at this time. Therefore the following discussion is restricted primarily to the development of the finite element model and the estimation of the physical properties of the rock mass for use in the finite element mode.

The data required for finite element modeling are

1. The original ground surface topography
2. The shape of the proposed pit

3. The geology with the rock types and the location of contacts
4. The physical properties of the lithologic units

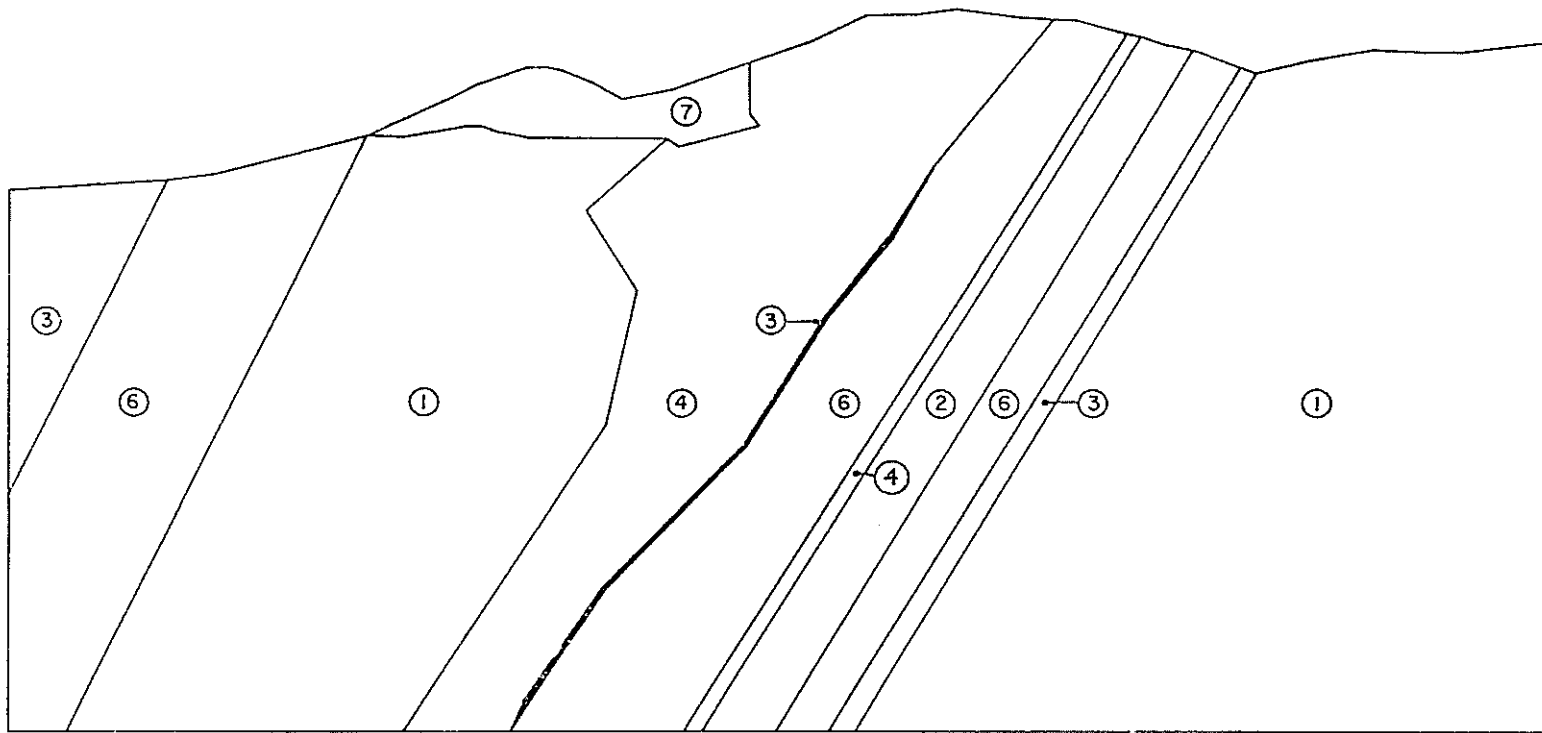
Geologic Section

Because of the tabular geometry of the ore body, a two-dimensional plane strain analysis of a vertical section at right angles to the pit wall was chosen. The geologic Cross Sections A through LL, developed for ore estimation, were suitable sections for analysis.

Section D (Figure 33) was chosen for the following reasons:

1. It is representative of the geology between Section A and Section H.
2. More geologic information was available for Section D than for the other sections.
3. The crusher is located on Section D. The footwall slope angle in the area of Section D is more critical than other parts of the pit.

The geology of section D was simplified as shown on Figure 68 to facilitate construction of the finite element mesh. This figure shows only the inner core of the total model which is 1200 meters high and 2500 meters wide. This model size is dictated by the requirement that the distance from the boundary to the center of the pit opening is four times the pit size in order to minimize the effect of boundary conditions on the stresses around the pit. The geology of Figure 68 was projected to the boundaries of the model, since local variations in geology outside the core of the model would have little effect on



LEGEND: ① BHQ (W), ② QUARTZITE (U), ③ SCHIST (S), ④ ORE (R), ⑥ BHQ (W_S), ⑦ BHQ (W_A).

Figure 68. Simplified Geology of Section D for Finite Element Analysis.

the stresses around the pit itself. Even with this simplification of the geology, the model consists of approximately 1500 elements and 1300 nodal points.

This simplified geology is a reasonable representation of the geology of Section D with three exceptions; (1) below the schist at the footwall ore contact, there is a section of quartzite, (2) between the bed of ore in the footwall and the underlying quartzite, there is a thin bed of schistose BHQ, and (3) between the easternmost schist and the BHQ, there is a quartzite bed. The effect of these modifications in the model would be minor, however, compared with changes in the elastic properties of the rock.

Density

The values for the density of the rock used in the finite element study were obtained from weight and volume measurements of the core samples tested at the Elliot Lake Laboratory. These values are in good agreement with the apparent specific weight of the rock substance obtained in a study conducted at Zouerate (Table 13).

Large scale (3.5 m^3 to 6.4 m^3) in-place density tests gave densities from 7% to 16% less than the rock substance density. This difference would be the effective porosity of fractures. Since these tests were made on benches in the pit, where the rock had been disturbed by blasting, the effective porosity of the fractures would be appreciably greater than that of undisturbed rock. On the basis of observation of the drill core and the rock exposed in the pit face, the

Table 13. Revised Physical Properties for Finite Element Analysis

Code No.	Rock Type	RQD	Density	E (kg/cm ² x 10 ⁵)			Poisson's Ratio		
				Laboratory	In Situ		Laboratory	In Situ	
					Revised Estimate	Prelim. Estimate		Revised Estimate	Prelim. Estimate
1	BHQ	84	3.30	9.66	7.05		.19	.20	
6	Schistose BHQ	64	3.33	8.97	.89	.91	.26	.26	.20
2	Quartzite	70	2.55	8.81	.88	4.57	.16	.16	.13
3	Schist	51	2.86	6.31	.40	0.56	.20	.35	.13
4	Ore	66	4.00	6.39	.64	3.31	.32	.32	.24

effective porosity of the fractures in the undisturbed rock mass would be less than 5%.

Modulus of Deformation

The modulus of deformation values used in the finite element analysis was derived from laboratory testing of drill core samples. To obtain the in situ rock mass deformation moduli, the laboratory values were reduced utilizing an empirical relationship based on the RQD from drill core logs. This relationship can be expressed as follows:

$$E_{rm} = (4.5 \text{ RQD} - 3.05) E_s \quad \text{For RQD} \quad 70\%$$

$$E_{rm} = 0.1 E_s \quad \text{For RQD} \quad 70\%$$

where E_{rm} and E_s are the deformation moduli for the rock mass and the rock substance respectively. (Yu et al. 1970)

The RQD values from the drilling have a high dispersion, as can be seen on the histograms in Figure 69, because of fracture zones and differences between individual units of a particular rock type. The median value was chosen as the estimated RQD shown on Table 13. The empirical equation used to estimate the modulus of deformation of the rock mass is very sensitive to changes in RQD above 70%. For all RQD values below 70%, the rock mass deformation is taken as 10% of the laboratory value. Since the median RQD for all the rock types, except the hanging wall BHQ, is below 70%, the in situ values are estimated to be 10% of the laboratory values. The test results of the schist core samples represent the upper limit of the strength of the schist, as the core of lower strength schist was too broken to prepare

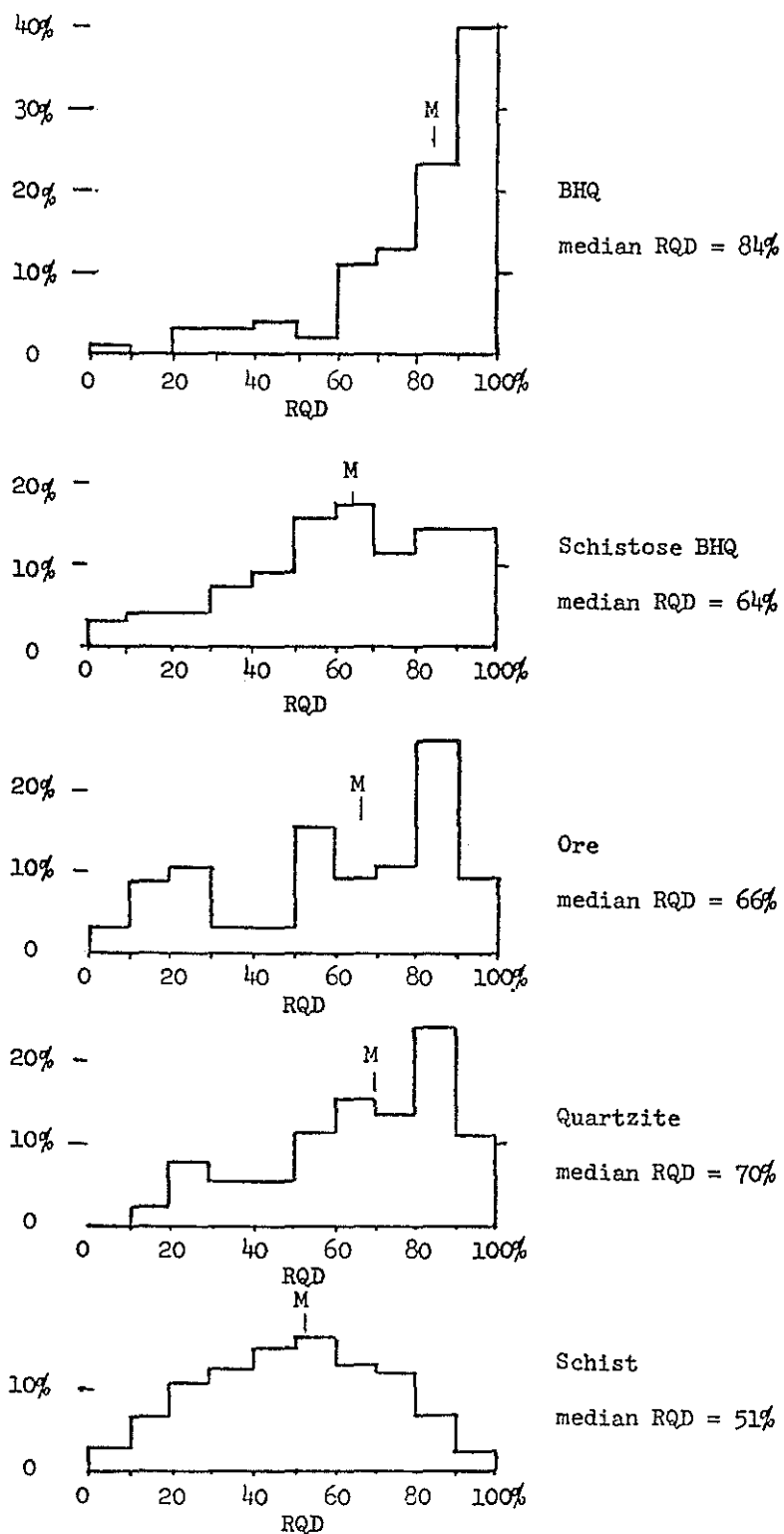


Figure 69. Histograms of RQD Measurements.

a sample. Thus, the modulus of the schist was reduced an additional 30% and the Poisson's ratio increased from 0.20 to 0.35. The hanging wall BHQ, which had a median RQD of 84%, was only reduced 26%.

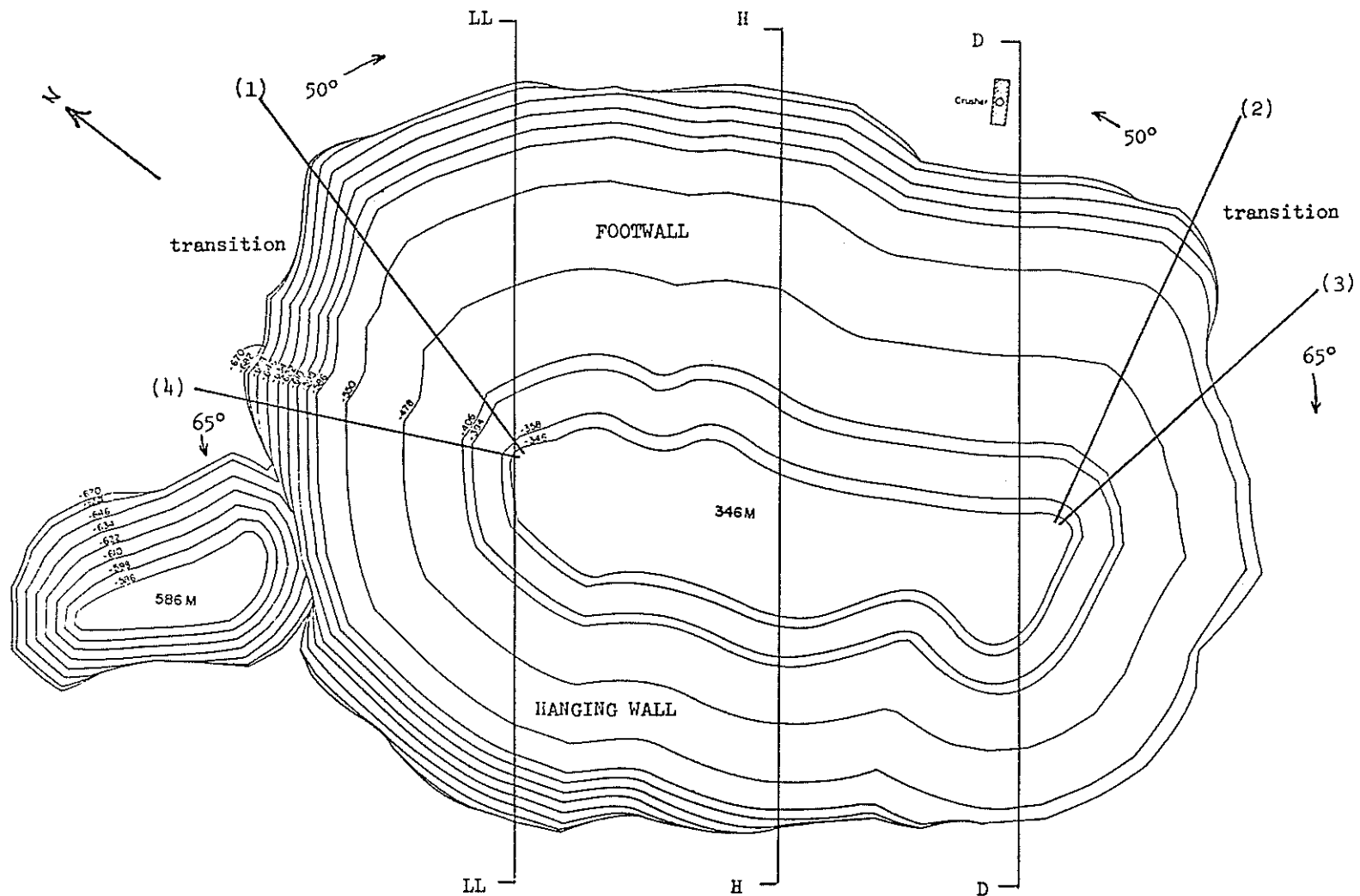
Final Pit Slope Angles

On the basis of the geologic structural data, the optimum slope angles for the final wall of the Tazadit Pit are 65° for the hanging wall and 50° for the footwall, with transition zones as shown in Figure 70. These transition zones are included for a gradual change in slope from 50° to 65°, as abrupt changes in the slope angle produce irregularities which can result in unfavorable stress concentrations. The slope angles are plotted on a Schmidt diagram of the critical geologic features (Figure 71) to show the relationship between the pit slope and the controlling geologic features. The basis for the recommended slope angles is as follows.

Hanging Wall

The rock of the Tazadit hanging wall is a very high strength elastic material, thus the rotational shear failure typical of soil slopes would not be a probable type of failure for the hanging wall.

The plane shear analysis of the hanging wall indicates that the daylighted joints shown on Figure 71 have sufficient shear strength to allow a stable slope in excess of 65°. Even if the relaxation of the tensile zones within the hanging wall destroy the effective cohesion of the joint surfaces, the peak shear strength of the joints is greater than the shearing stresses developed in a 65° slope.



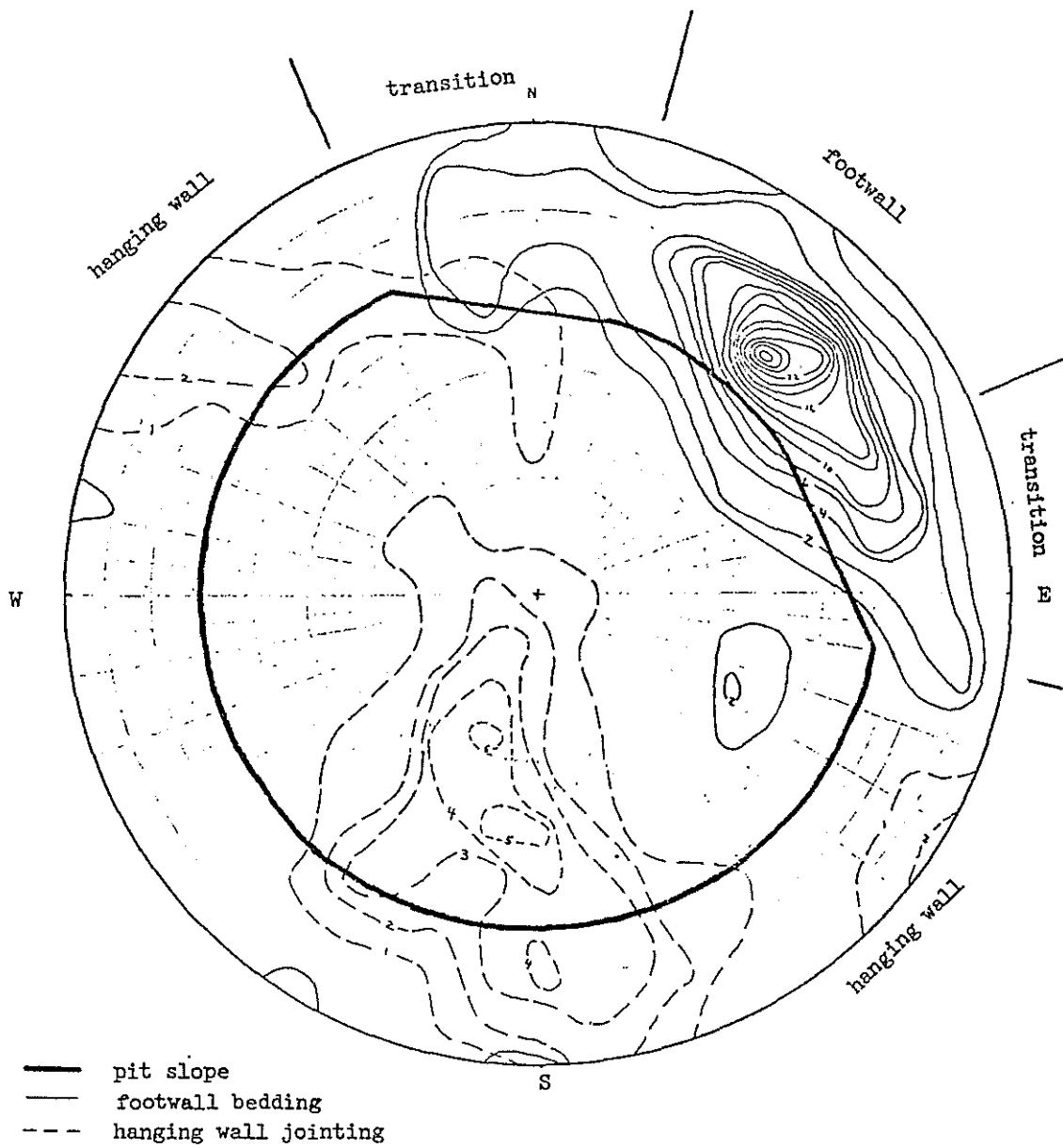


Figure 71. Schmidt Diagram of Tazadit Final Pit Slope Angles and Critical Structures.

The slope of 65° is based primarily on consideration of raveling type failure. If no catch benches are left on the final pit face, any loose boulder will roll into the mining area and present a hazard. If a catch bench is left every second level and the resulting 24 meter face is cut by smooth-wall blasting to an 80° angle, the catch bench will be 8 meters wide. Steepening the slope above 65° would require expensive pre-splitting, which would tend to offset the economic advantage of the steeper slope.

Footwall

The primary basis for recommending the 50° slope for the footwall is the plane shear analysis. As can be seen in the dip histogram of the footwall bedding (Figure 72), a slope of 50° would daylight an insignificant number of bedding planes. The bench faces on the footwall side of the pit tend to break to the bedding. If a catch bench is left every second level, the final slope will have 24 meter high faces with an average dip of 63° and an average bench width of 8 meters, as shown in Figure 72 and in the schematic section of the typical footwall final slope (Figure 73).

This slope configuration is shown on the detailed Geologic Sections LL, H, and D in Figures 74, 75 and 76. The position of the toe of the slope is approximate and will have to be determined by break-even stripping ratio calculations. The slopes in the diagrams are representative, however, and lateral shifts in the slope will have little effect on the stability.

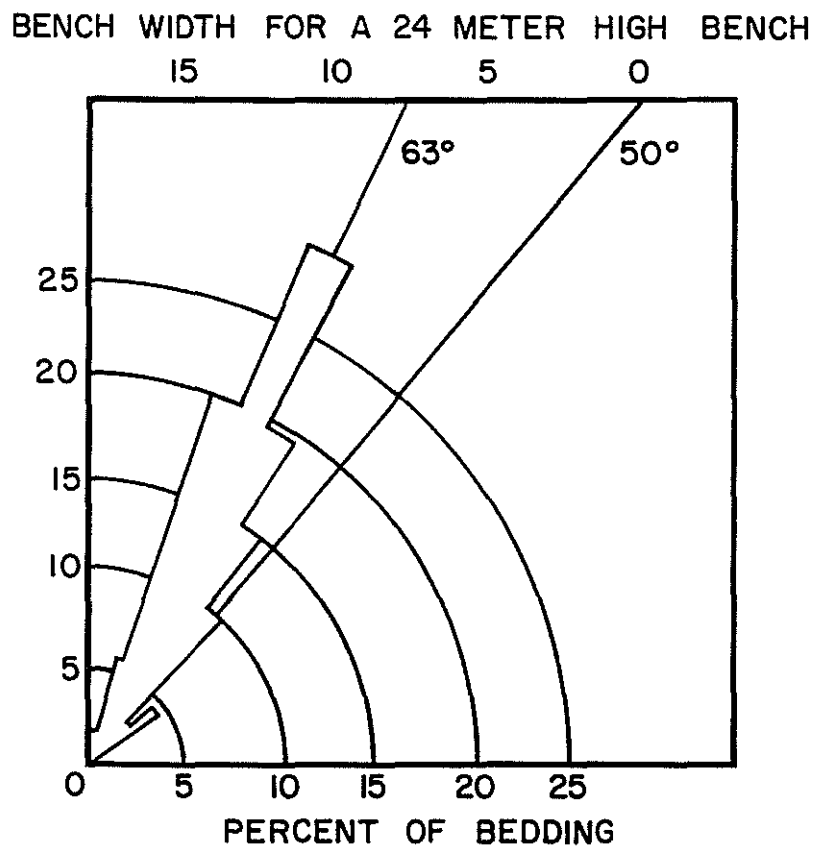


Figure 72. Dip Histogram of Footwall Bedding Observations

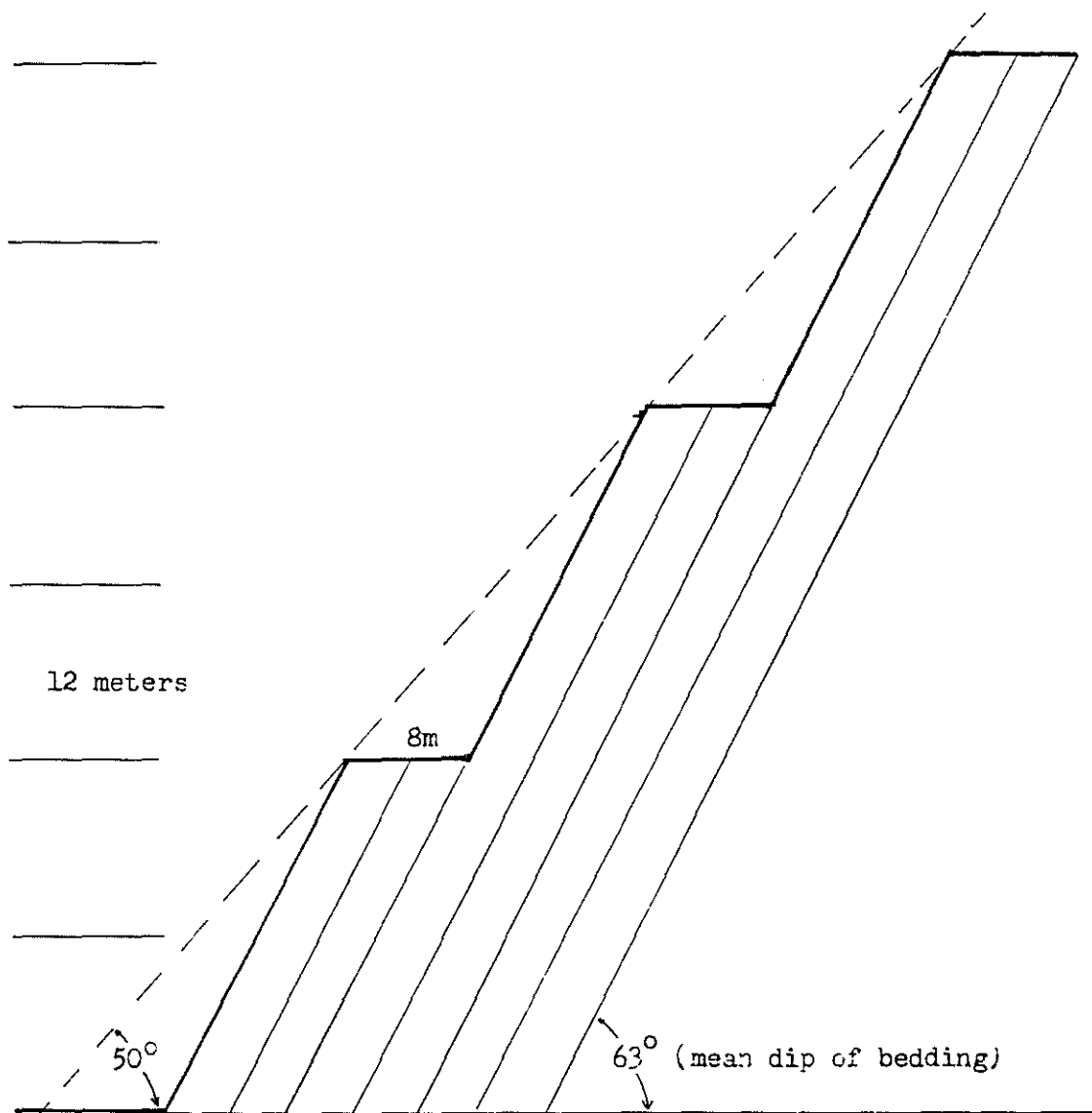


Figure 73. Schematic Cross Section of the Proposed Footwall Final Slope.

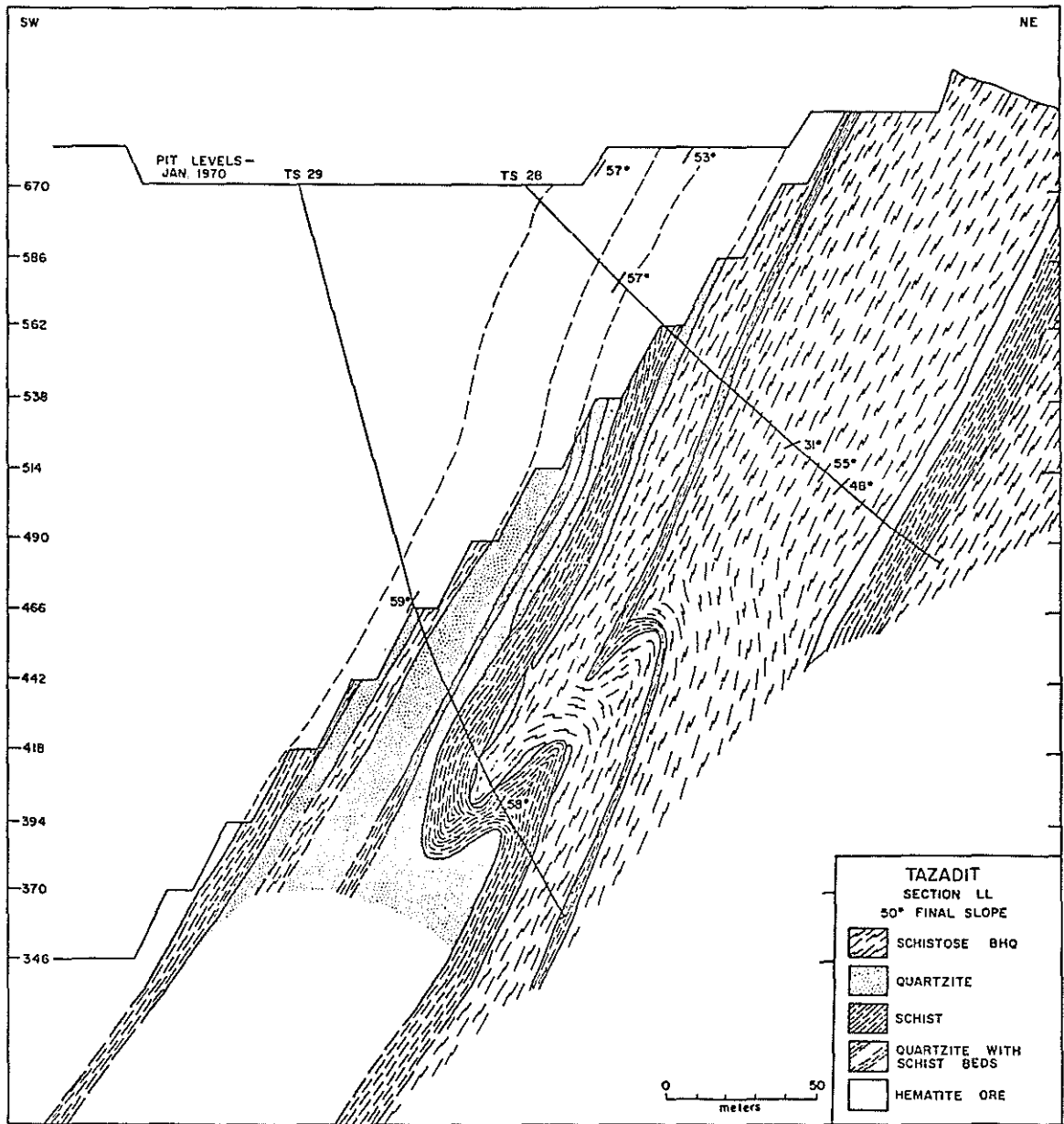


Figure 74. Footwall 50° Final Slope -- Section LL.

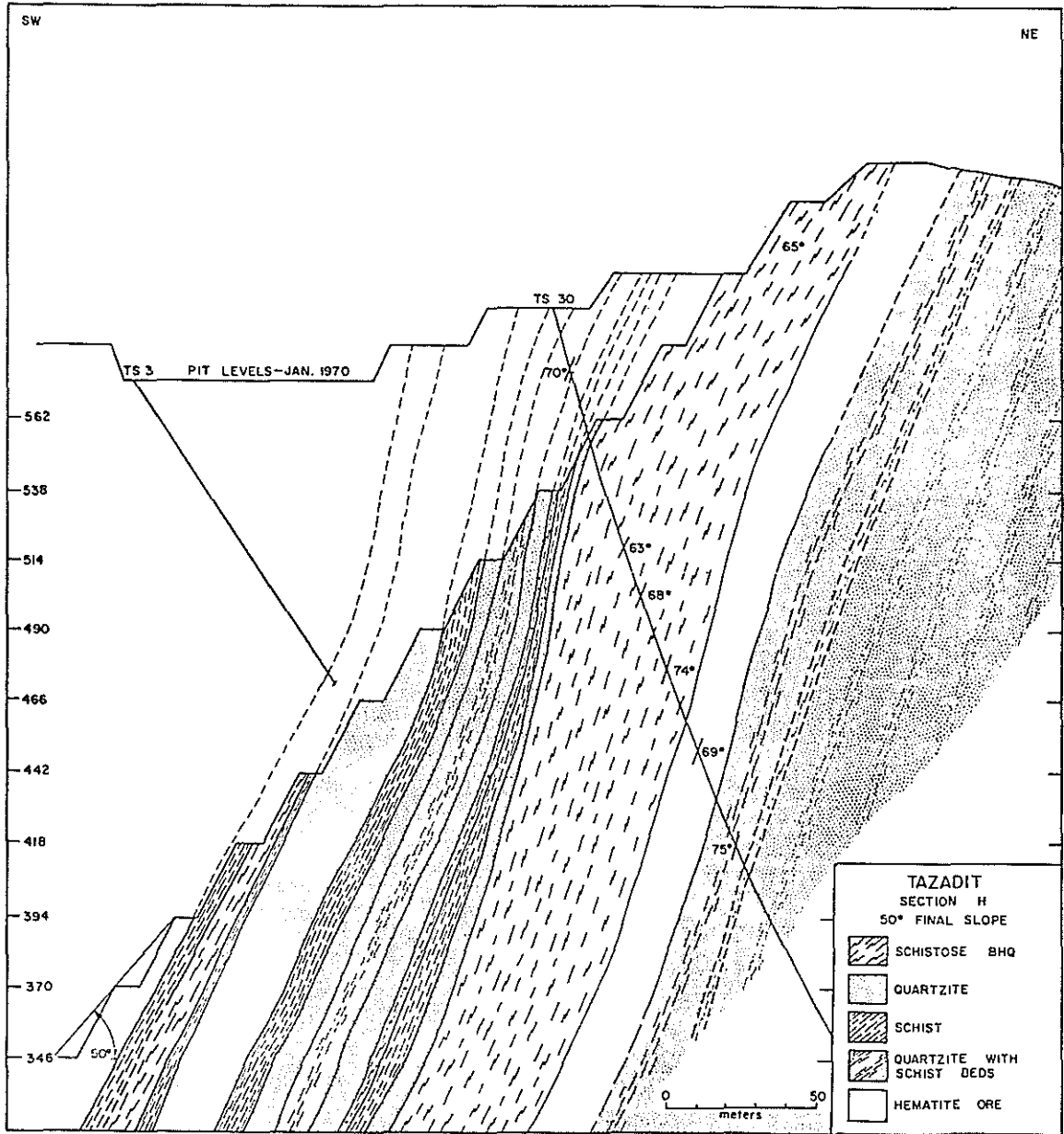


Figure 75. Footwall 50° Final Slope -- Section H.

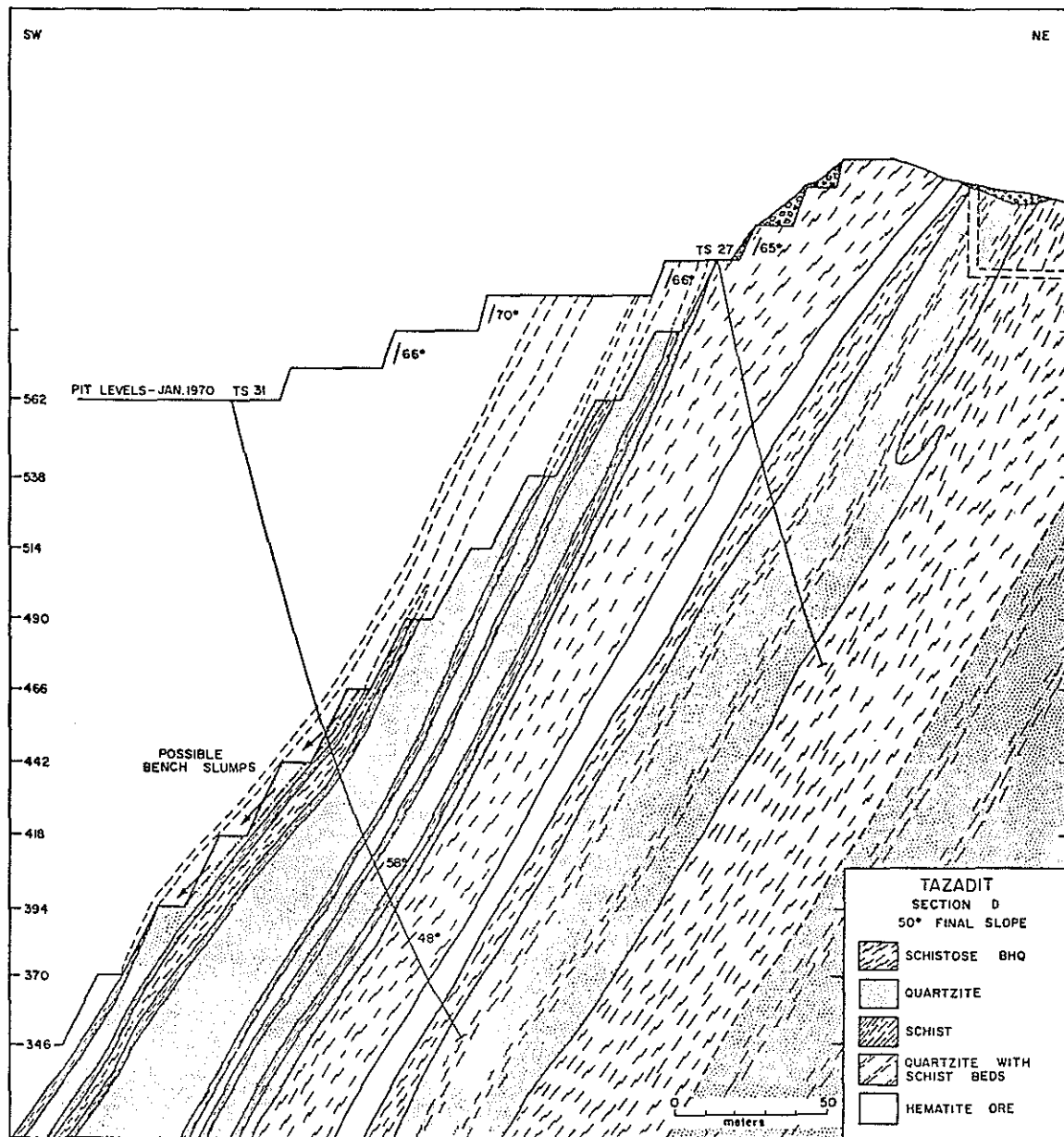


Figure 76. Footwall 50° Final Slope -- Section D.

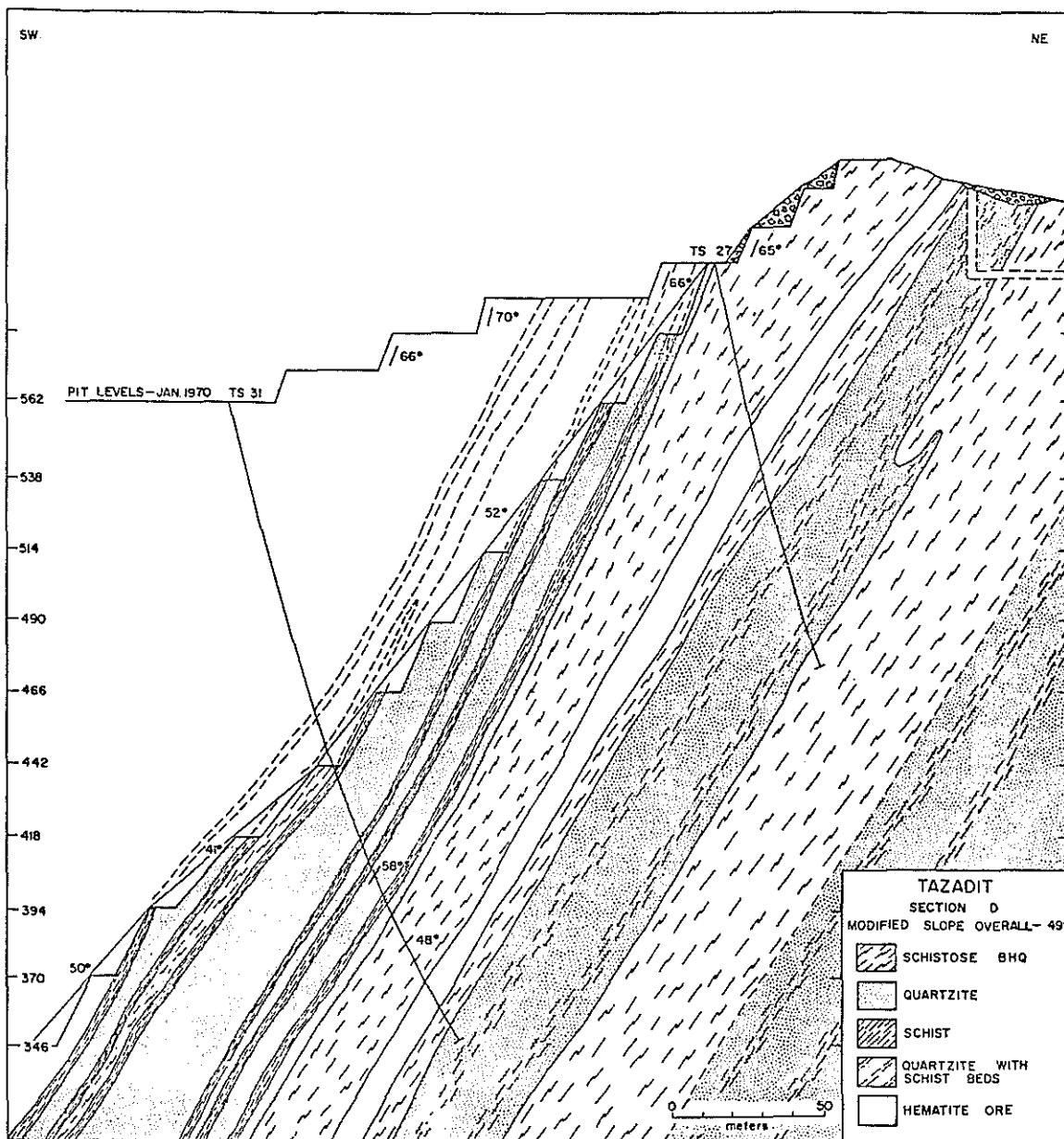


Figure 77. Variable Angle Slope, Section D.

As can be seen on the Sections, a 50° overall slope will not daylight any bedding, except for three benches between the 394 Level and the 466 Level on Section D. Even here, major sliding will not occur as the slope will be parallel to the bedding. All that might occur is a loss of catch benches during mining. To avoid this, the slope could be mined with variable angles as shown in Figure 77, which would give an overall slope angle of 49° . To determine the exact location of areas where the bedding flattens would require an extensive drilling program which would not be warranted. Rather than attempting to predetermine all the local variations in the bedding, the footwall slope can be designed at 50° and local adjustments in the slope angle can be made during the mining as required.

CHAPTER 8

CONCLUSIONS AND SUGGESTIONS FOR FURTHER RESEARCH

On the basis of the geologic investigations of the Tazadit pit and laboratory testing of rock samples, the following conclusions can be drawn.

Rock Fabric

The four methods of collecting data on fracture orientations (pre-mining surface mapping, fracture set mapping, detail line mapping, and oriented core logging) all give the same basic orientations for the bedding, lineation and jointing. These attitudes can be utilized to define potential failure geometry for stability analysis. The Schmidt diagram is a convenient method of summarizing the rock fabric and determining critical failure geometry (Figure 71).

In the case of the Tazadit pit, the critical structural control for the footwall slope is the bedding which strikes parallel to the proposed final pit slope and dips 63° into the pit. Slope angles steeper than the bedding will result in "daylighted" wedges with a high probability of failure.

Mapping Methods

The detail line method is the least subjective method and gives the most precise data on fracture orientations. It is a point sampling

method, however, and is not suitable for mapping major structural features.

The fracture set mapping is a more rapid method and can be combined with lithologic and major structure mapping. It is more subjective than detail line mapping as the geologist "chooses" fracture sets by eye.

Oriented core is a less precise method as it is affected by errors in the method of orientation. The small cross section of rock sampled by the core makes the interpretation of the type of fracture more difficult and results in a "blind zone" bias as fractures parallel to the drill hole are rarely intersected. The outstanding advantage of oriented core is that it samples directly the rock in the pit wall and does not require projection of the data.

Data from pre-mining surface geologic mapping depends on the rock exposures and the objective of the mapping, thus it is difficult to make a general conclusion. The mapping of the Tazadit pit surface was detailed and many observations of bedding attitude were made which proved useful for slope design.

Rock Strength

Rock Mass

The strength and deformation characteristics of the rock substance can be determined by laboratory testing. Extrapolation of these values to the in situ properties of the rock mass requires a correction factor based on the fracturing of the rock. The RQD measurements from diamond drilling were used in this study as an

estimate of the degree of fracturing. The empirical relationship between RQD and the ratio of the field deformation modulus (Yu, Coates and Toews, 1970) is very sensitive to changes in RQD. The RQD measurements from the Tazadit pit drill holes have a high dispersion and a non-normal distribution. Thus, the field modulus can vary widely depending on the interpretation of the RQD measurements.

More research on methods of estimating the in situ modulus of deformation of rock is needed.

Fracture Strength

Assuming the shear strength along the plane of a fracture can be approximately expressed by the relationship:

$$\tau = C + \sigma \tan (\phi_r + i)$$

values for C , ϕ and i must be determined from physical testing and fracture description.

The residual shear strength ϕ_r can be obtained from direct shear tests or triaxial slip tests. The Tazadit pit rocks have values of 26° for the hanging wall BHQ and 23° for the footwall schist.

An estimate of the angle or irregularities (i) of a fracture set can be obtained from the dispersion of the dip observations of that set taken by the detail line method. The jointing of the Tazadit hanging wall BHQ has an estimated i between 5° and 10° determined by this method. The ranking of the planarity of fractures in three categories as planar, wavy or irregular is useful in comparing the degree of irregularity but is inadequate for determining an i value.

The orientation of the irregularities is important. Although the footwall bedding is described as wavy, the curvature is parallel to the fold axis which is directed down-dip into the pit. Thus, the effective i for a block sliding into the pit along the bedding would be very small.

The cohesion (C) is the most difficult parameter to determine. As an approximation, the cohesion can be estimated by the percent of intact rock along the plane of the fracture multiplied by the cohesion intercept of the Mohr diagram of the rock substance. Although the continuity observations give an indication of the amount of intact rock on the plane of the fracture, they are difficult to quantify. Also, blasting affects the continuity of fractures exposed in a pit wall.

Final Pit Slope Angles

Slope angles can be selected on a rational basis which considers the rock fabric and rock strength characteristics. It cannot be said, however, that a precise analysis of the stability of a slope can be achieved at the present time. The inherent complexity of the geologic environment may well preclude the exact determination of the maximum stable slope angle. Even though slope design falls short of an exact analytical technique, the effect of the slope angle on the economics of a pit justifies the best possible determination of slope angle.

Suggestions for Further Research

Fracture Spacing

There is need for suitable methods of describing the spacing of fracture sets. The spacing of any given fracture set usually has

a wide variation and is a function of position in that a fracture set may be closely spaced in one part of a pit face and widely spaced fifty feet away. Thus, the mean and the dispersion are inadequate to describe the spacing. If the spacing of a fracture set is considered analogous to the wave length of a periodic function, it may be possible to describe fracture spacing with a Fourier series.

Core Orientation

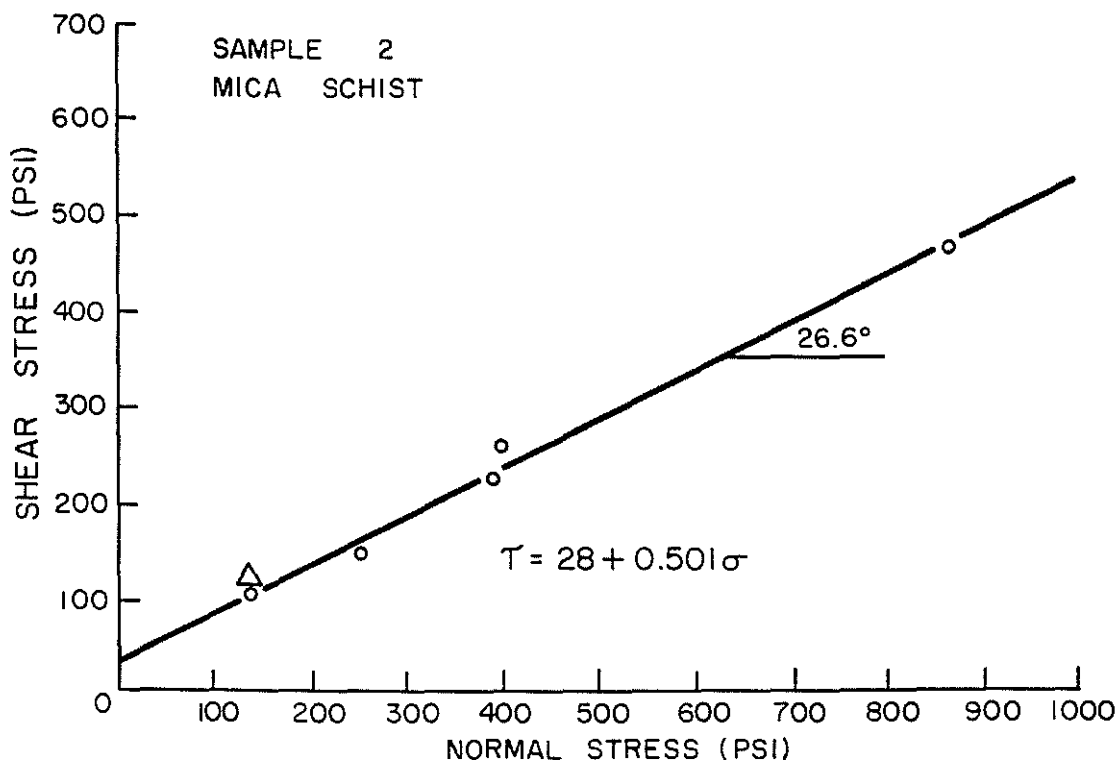
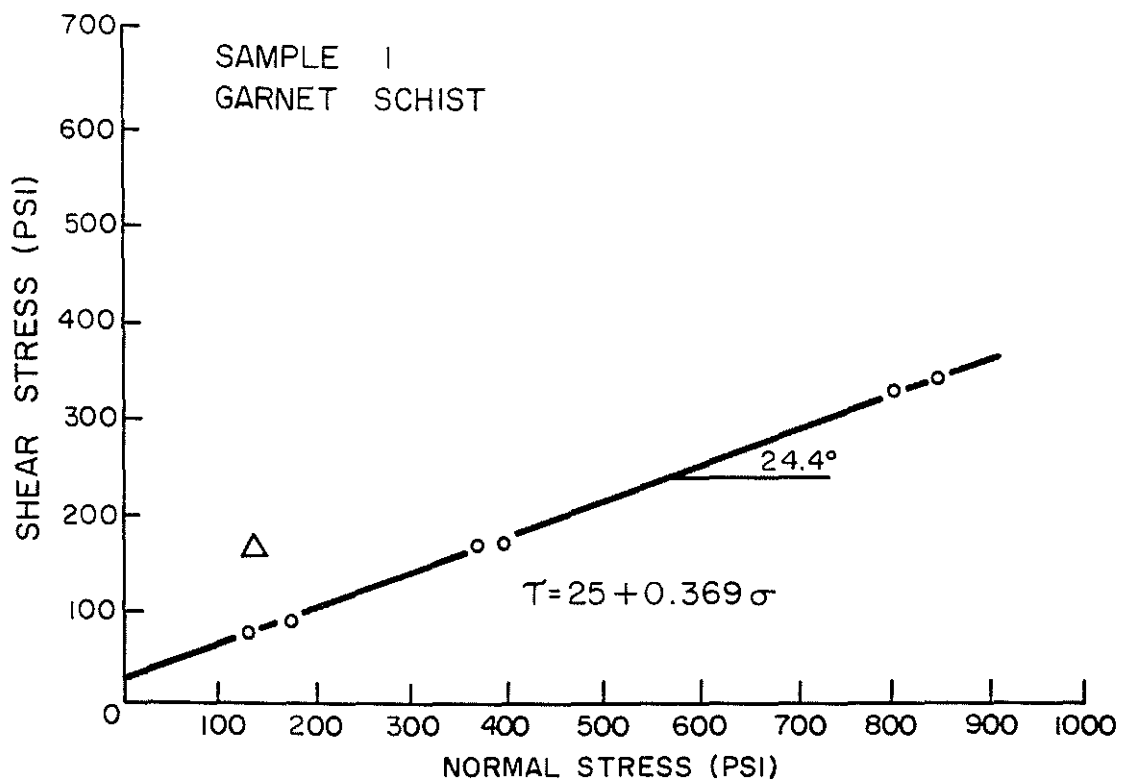
Since the failure of a slope takes place back in the wall of the pit rather than at the face, drilling can provide the most direct information on the rock of the final pit slope. In the case of a new ore discovery, there may be no surface exposures available for mapping. Thus there is a need for reliable methods of obtaining geologic structural data from drill holes. Improvement in the methods of obtaining oriented core would aid in fulfilling this need. Oriented core has advantages over indirect methods, such as the bore hole camera or sonic logging, in that a sample of the rock is obtained which can be subjected to strength testing.

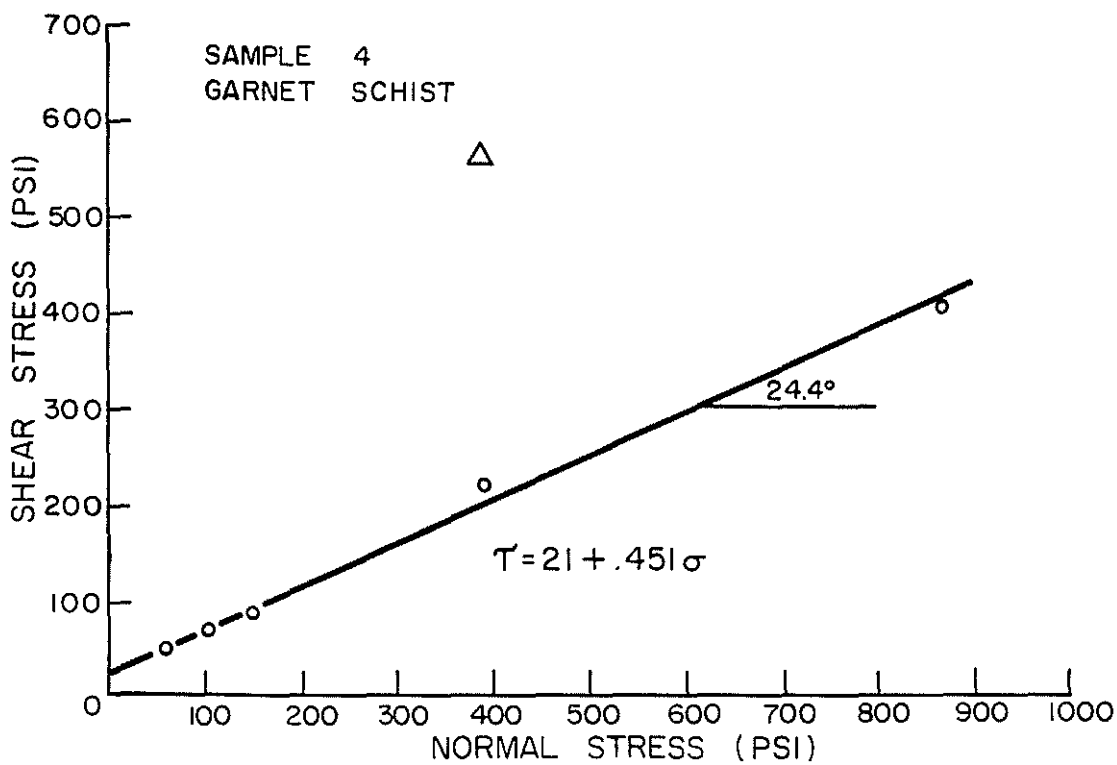
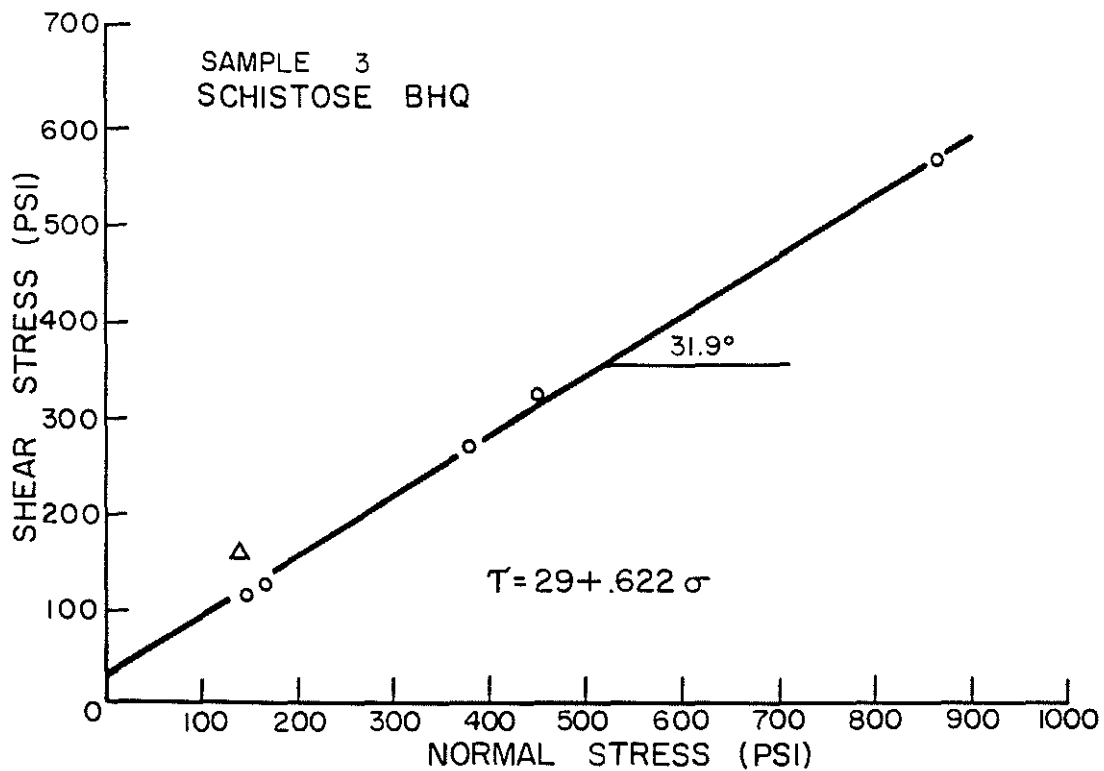
Application to Existing Slopes

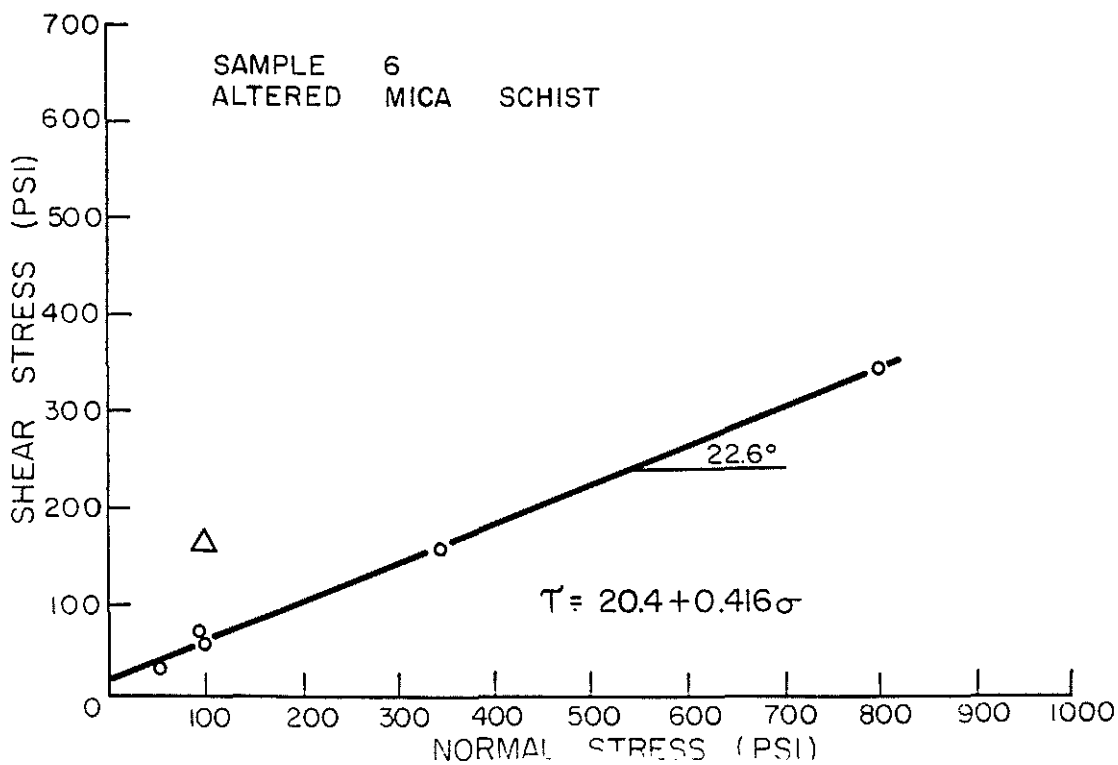
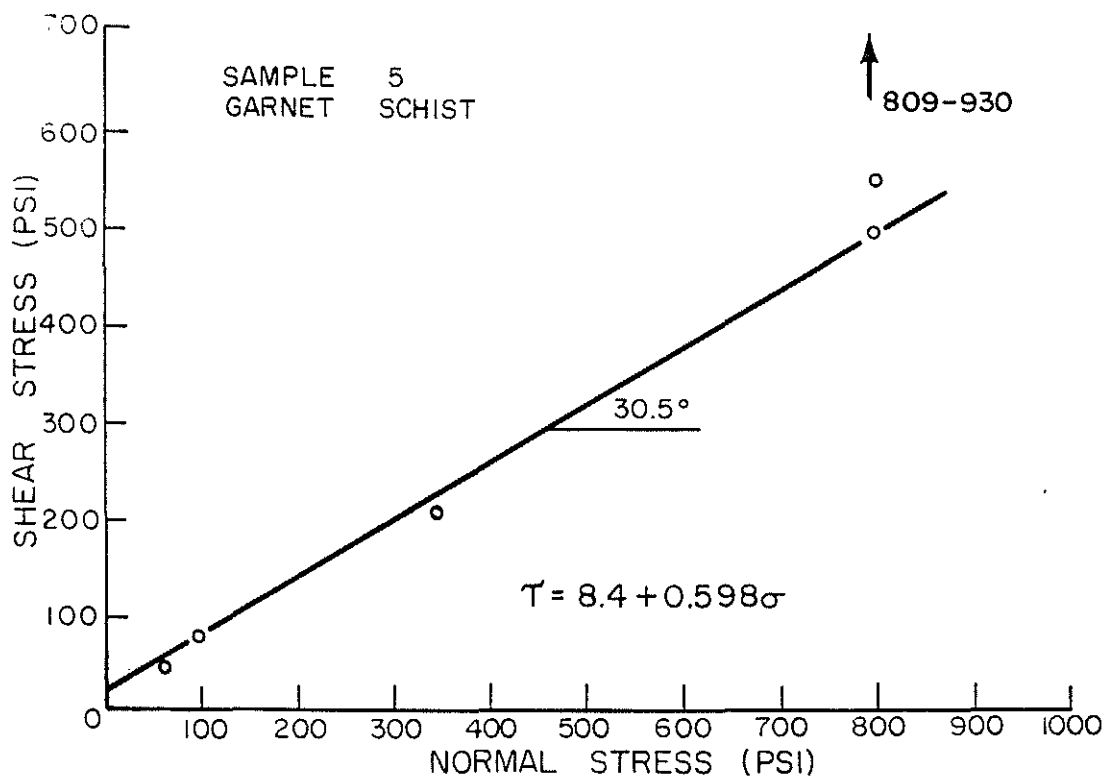
The final test of any design method is the actual application of the method. Thus the most suitable test of geologic investigations for slope design is to map a pit slope and to correlate the behavior of the slope with the geologic data. With the cooperation and support of mining companies, the slopes in existing pits could be utilized for such a study.

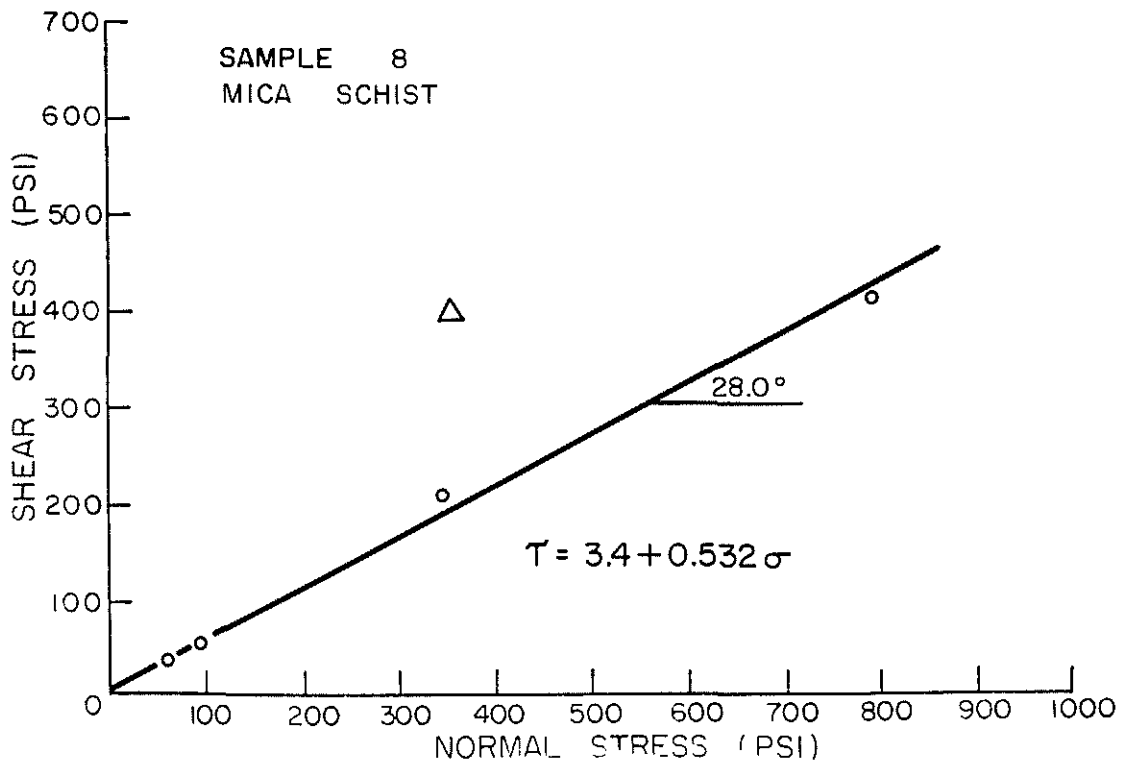
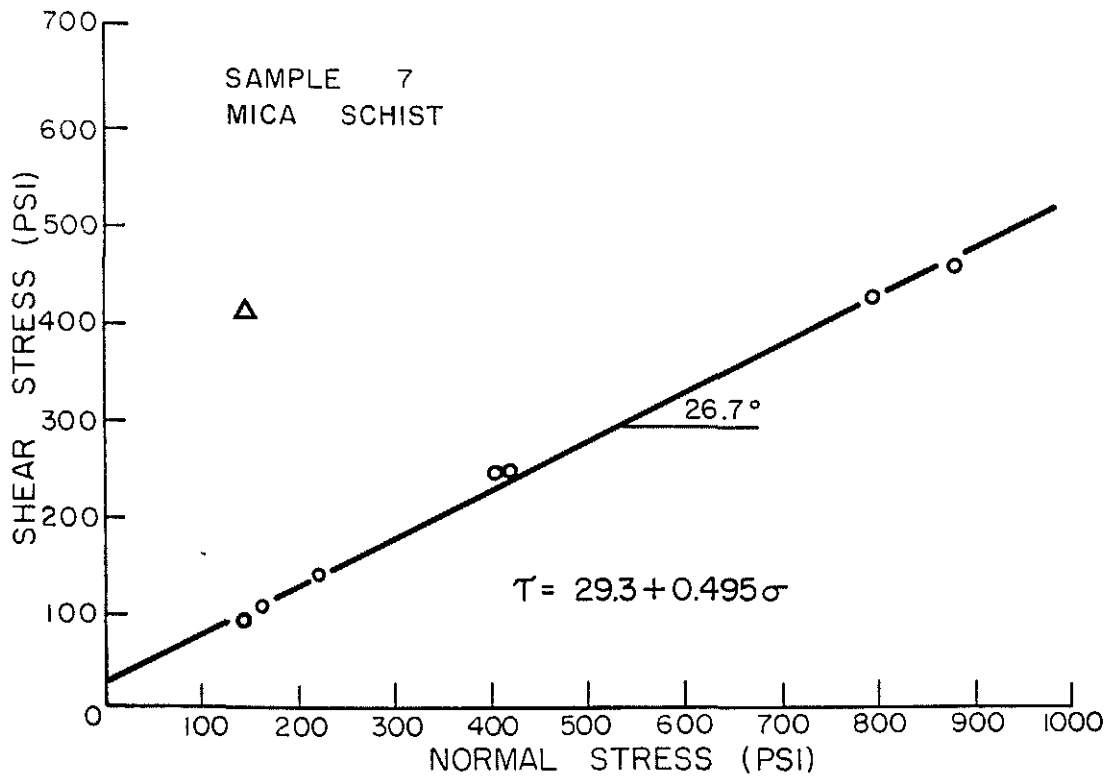
APPENDIX A

DIRECT SHEAR TEST RESULTS









REFERENCES

- Agterberg, F. P., 1961, Tectonics of the crystalline basement of the Dolomites in North Italy, *Geologica Ultraject.*, no. 8, p. 1-232.
- American Geological Institute, 1960, *Glossary of Geology and Related Sciences*, Washington.
- Barron, K., Coates, D. F., and Gyenge, M., 1970, Artificial support of rock slopes, Research Report R 228, Mining Research Centre, Dept. Energy, Mines and Resources, Mines Branch, Ottawa.
- Bishop, A. W., and Morgenstern, N., 1960, Stability coefficients for earth slopes, *Geotechnique*, v. 10, no. 4, p. 129-150.
- Bjerrum, L. and Jorstad, F., 1964, Rockfalls in Norway, Norwegian Geotechnical Institute, Oslo.
- Black, R. A. L., 1964, Economic and engineering design problems in open pit mining, *Mine and Quarry Engineering*, Jan., p. 13-15.
- Blanchot, A., 1951, The iron deposits of Fort Gouraud, Mauritania, *Chron. Miners Colon.*, vol. 19, p. 187-188, Paris
- Bronner, G., 1970, Etude petrographique et microstructurale des formations du mur de la mine de Tazadit, *Travaux des Laboratoires des Sciences de la Terre, Serie X*, no. 3, Saint Jerome, Marseille.
- Chayes, Felix, 1946, Application of the coefficient of correlation to fabric diagrams, *Transactions, Am. Geophysical Union*, vol. 27, no. 111, p. 400-406.
- Coates, D. F., 1964, Classification of rocks for rock mechanics, *Int. Journal Rock Mechanics Mining Sci.*, vol 1, Pergamon Press, Great Britain, p. 421-429.
- Coates, D. F., 1970, *Rock mechanics principles*, Mines Branch Monograph 874, Revised, Queen's Printer, Ottawa.
- Coates, D. F. and Brown, A., 1961, Stability of rock slopes at mines, *Canadian Mining and Metallurgical Bull.*, vol. 54, no. 591, p. 514-521.
- Coates, D. F. and Grant, F., 1966, Stress measurements at Elliot Lake, *Canadian Institute Mining and Metallurgy Bull.*, vol. 59, p. 603-613.

- Coulson, James H., 1970, The effects of surface roughness on the shear strength of joints in rocks, Technical Report MRD 2-70, Missouri River Division, Corps of Engineers; Omaha, Nebraska.
- Crane, W. R., 1931, Essential factors influencing subsidence and ground movement, U. S. Dept. Interior, Bureau of Mines, I. C. no. 6501, 20 pp.
- Deere, D. U., 1964, Technical description of rock cores for engineering purposes, Rock Mechanics and Engr. Geol., vol. 1, no. 1, p. 17-22.
- Deere, D. U., 1968, Geological considerations in Stagg, K. G. and Zienkiewicz, O. C., Rock Mechanics in Engineering Practice, John Wiley and Sons, Inc., New York, p. 1-20.
- Emery, Charles L., 1966, Rock mechanics in open-pit mining, Canadian Mining and Metallurgical Bull., Oct., p. 1184-1188.
- Fellenius, W., 1936, Calculation of the stability of earth dams, Transactions Second Congress on Large Dams, Washington, D. C., vol. 4, p. 445-462.
- Fisher, R., 1953, Dispersion on a sphere, Proc. Royal Society, London, Ser. A., vol. 217, p. 295-305.
- Fox, William T., 1967, Fortran IV program for vector trend analysis of directional data, in Computer Contributions 11, Kansas State Geological Survey.
- Friedman, M., 1964, Petrofabric techniques for the determination of principle stress directions in rock in International Conference on State of Stress in the Earth's Crust, Memo RM-3583, compiled by W. R. Judd, the Rand Corporation, chap. 10, p. 1-128.
- Hammel, D. J., 1967, Evaluation of factors in an unstable open-pit slope: University of Arizona, Tucson, Unpublished M. S. Thesis.
- Hammel, D. J., 1970, An application of the finite element method for rock slope stability analysis: University of Arizona, Tucson, Unpublished Ph.D. Dissertation, 124 pp.
- Heim, A., 1882, Uber bergsturze, Naturf. Gesell. Zurich, Neujahrsblatt 84, 31 pp.
- Hergot, G., 1970, Determination of properties of rocks exposed in an iron mine in Zouerate, Mauritania, Mining Research Centre Internal Report MR 70/70-D, Canadian Dept. of Energy, Mines and Resources, 14 pp.

- Hoek, Evert, 1970, Influence of structure upon the stability of rock slopes, Preprint: Symposium on Stability for Open Pit Mining, University of British Columbia, 13 pp.
- Horn, H. M. and Deere, D. U., 1962, Frictional characteristics of minerals, Geotechnique, vol. XII, p. 319-335.
- Janbu, N., 1954, Stability analysis of slopes with dimensionless parameters, Harvard Soil Mechanics Series, no. 46.
- Jennings, J. G., 1968, A preliminary theory for the stability of rock slopes based on the wedge theory and using the results of joint surveys, To Be Published.
- Jennings, J. G., 1970, A mathematical theory for the calculation of the stability of slopes in open cast mines, Open-pit Mining Symp., 1970, South African Institute of Mining and Metallurgy, Johannesburg, p. 87-102.
- John, Klaus W., 1962, An approach to rock mechanics, Proc. Amer. Soc. Civil Engrs., vol. 88, no. SM4, p. 1-30.
- John, Klaus W., 1968, Graphical stability analysis of slopes in jointed rock, Proc. Amer. Soc. Civil Engrs., vol. 94, no. SM2. paper no. 5865, p. 497-526.
- Kempe, Walter F., 1967, Core orientation, 12th Exploration Drilling Symp., University of Minnesota, Minneapolis.
- Kennedy, Bruce A. and Niermyer, K. E., 1970, Slope monitoring systems used in the prediction of a major slope failure at the Chuquicamata mine, Chile; Open-pit Mining Symp., 1970, South African Institute of Mining and Metallurgy, Johannesburg, 11 pp.
- Komarnitskii, N.I., 1968, Zones and planes of weakness in rocks and slope stability, F. P. Savarenskii Laboratory of Hydrological Problems, Academy of Sciences of the USSR; translated by: Consultants Bureau, New York.
- Kutter, H. K., 1970, Report on the results of a direct shear test program, Imperial College, London, Interdepartmental Rock Mechanics Project Report to MIFERMA, 26 pp.
- Lacy, Willard C., 1963, Quantitizing geological parameters for the prediction of stable slopes, Trans. SME, Sept., p. 1-5.
- Ladd, G. E., 1935, Landslides subsidences and rock falls, Am. Railroad Engrs. Assoc. Proceedings, vol. 36, p. 1091-1162.
- Long, Albert E., 1963, Open-pit slope stability research by the Bureau of Mines, Mining Congress Journal, June, p. 68-71.

- Louis, C., 1967, A study of groundwater flow in jointed rock and its influence on the stability of rock masses: Universitat (Th) Karlsruhe, Ph.D. Thesis.
- Lounde, P., 1965, Une methode d'analyse a trois dimensions de la stabilite d'une rive rocheuse, Annales des Ponts et Chaussees, vol. I, p. 37-60.
- MacDonald, D. F., 1913, Excavation deformation, 12th International Geol. Congress, p. 779-793.
- McMahon, B. K., 1967, Indices related to the mechanical properties of rocks, 9th Symp. Rock Mechanics; Colorado School of Mines, April.
- Michaelson, S. D. and Hammes, J. K., 1968, Copper ore mining, *in* Surface Mining, E. P. Pfleider, ed., published by American Institute Mining, Metallurgical and Petroleum Engineers, Inc., New York, p. 874-895.
- Mitcham, T. W., 1963, Fractures, joints, faults and fissures, Economic Geology, vol. 58, p. 1157-1158.
- Morgenstern, N. R. and Price, V. E., 1965, The analysis of the stability of general slip surfaces, Geotechnique, vol. 15, no. 1, p. 79-93.
- Mueller, L., 1964, Application of rock mechanics in the design of rock slopes, *in* State of Stress in the Earth's Crust, W. R. Judd, ed., American Elsevier Publishing Co., Inc., New York, p. 595-596.
- Mueller, L. and John, Klaus, 1963, Recent development of stability studies of steep rock slopes in Europe, Trans. American Institute Mining, Metall., Petrol. Engrs., vol 226, Sept., p. 326-331.
- Patton, R., 1966, Multiple modes of shear failure in rock and related materials, University of Illinois, Ph.D. Thesis, 281 pp.
- Pincus, H. J., 1951, Statistical methods applied to the study of rock fractures, G.S.A. Bull., vol. 62, p. 81-129.
- Pincus, H. J., 1953, The analysis of aggregates of orientation data in the earth sciences, Jour. Geol., vol 61, p. 482-509.
- Piteau, D. R., 1970, Geological factors significant to the stability of slopes cut in rock, Open Pit Mining Symp., 1970, South African Institute of Mining and Metallurgy, Johannesburg, p. 33-53.
- Price, N. J., 1966, Fault and joint development in brittle and semi-brittle rock, Pergamon Press, New York.
- Ramsey, John G., 1967, Folding and fracturing of rocks, McGraw-Hill Book Co., Inc., New York.

- Reibell, Henri V., 1969, Deep open-pit optimization in A Decade of Digital Computing in the Mineral Industry, Alfred Weiss, ed., published by American Institute Mining, Metallurgical and Petroleum Engineers, Inc., New York, p. 359-372.
- Sander, B., 1930, Gefugekunde der gesteine, Springer, Wien.
- Sander, B., 1942, Uber flachen-und achsengefuge (Westende der Hohen Tauern, III Bericht) Geologie des Tauern-Westendes I, Mitt. Reichsamts Bodenforsch. Zweigst. Wien, vol. 4, p. 1-94.
- Schottler, G. R., 1962, The economics of open-pit slope angle variation, University of Arizona, Tucson, Unpublished M. S. Thesis.
- Sharp, John C., 1970, Fluid flow through fissured media, University of London, Imperial College Science and Technology, Ph. D. Thesis.
- Sharpe, C. F. S., 1938, Landslides and related phenomena, Columbia University Press, New York. Reprinted 1960, Pageant Books, Inc., Patterson, N. J., 137 pp.
- Spencer, E. W., 1959, Geologic evolution of the Beartooth Mountains, Montana and Wyoming, Part 2, Fracture Patterns, G.S.A. Bull., vol. 70, no. 4, p. 467-508.
- Stacey, T. R., 1968, Stability of rock slopes in open pit mines, MEG 737, Council for Scientific and Industrial Research, Pretoria, South Africa, 50 pp.
- Talobre, J. A., 1957, La mecanique des roches, Paris, Dunod.
- Terzaghi, Karl, 1925, Erdbaumechanik, Franz Deuticke, Wien, 399 pp.
- Terzaghi, Karl, 1950, Mechanism of landslides in Application of Geology to Engineering Practice, Berkey Volume, Sidney Paige, ed., published by Geol. Soc. America, p. 83-123.
- Terzaghi, Karl, 1962, Stability of steep slopes on hard unweathered rock, Geotechnique, vol. 12, no. 4, p. 251-271.
- Terzaghi, Ruth D., 1965, Sources of error in joint surveys, Geotechnique, vol. 15, no. 3, p. 287-304.
- Turner, F. J., 1948, Mineralogical and structural evolution of the metamorphic rocks, G.S.A. Memoir 30.
- Varnes, D. J., 1958, Landslide types and processes, in Landslides and Engineering Practice, E. B. Eckel, ed., U. S. Highway Research Board, Special Rept. 29, p. 20-47.

- Watson, G., 1966, The statistics of orientation data, Jour. Geol., vol. 74, no. 5, part 2, p. 786-797.
- Weaver, R. C. and Call, R. D., 1965, Computer estimation of oriented fracture set intensity, Symp. on Computers in Mining and Exploration, Tucson, Arizona.
- Whitten, E. H. Timothy, 1966, Structural geology of folded rocks, Rand McNally and Co., Chicago, 623 pp.
- Winchell, Horace, 1937, A new method of interpretation of petrofabric diagrams, Am. Mineralogist, vol. 22, p. 15-36.
- Yu, Y. S. and Coates, D. F., 1970, Analysis of rock slopes using the finite element method, Mines Branch Research Report R229, Canadian Dept. of Energy, Mines and Resources, Ottawa.
- Yu, Y. S., Coates, D. F. and Toews, N. A., 1970, Finite element modelling of an open pit mine, Canadian Dept. of Energy, Mines and Resources, Mining Research Centre, Internal Report MR 70/116-ID, Ottawa.